HIGH RESOLUTION SEPARATIONS OF NANOPARTICLES WITH IMPROVED ELECTRICAL AND MAGNETIC FIELD FLOW FRACTIONATION

by

Tonguc Onur Tasci

A dissertation submitted to the faculty of
The University of Utah
in partial fulfillment of the requirements for the degree of

Doctor of Philosophy

Department of Bioengineering

The University of Utah

May 2013

The University of Utah Graduate School

STATEMENT OF DISSERTATION APPROVAL

The dissertation of **Tonguc Onur Tasci**

has been approved by the following supervisory committee members:

Bruce Kent Gale	, Chair	**10/23/2012** Date Approved
William Paul Johnson	, Member	**10/24/2012** Date Approved
Richard Rabbitt	, Member	**10/24/2013** Date Approved
Hamid Ghandehari	, Member	**10/24/2013** Date Approved
Florian Solzbacher	, Member	**01/31/2013** Date Approved

and by **Patrick A. Tresco**, Chair of the Department of **Bioengineering**

and by Donna M. White, Interim Dean of The Graduate School.

ABSTRACT

Electrical and Magnetic Field Flow Fractionation (ElFFF, MFFF) methods are two rapidly developing separation and characterization techniques using electrical and magnetic fields that have not been regularly applied to nanoparticle fractionation, separation, and characterization. Currently, several limitations characteristic of both techniques prevent them from being widely used tools in the separation of nanoparticles.

In this work, we address the main limitations of both techniques and develop methods to enhance their separation abilities, and particularly their application to nanoparticles. Specifically, one order of magnitude improvement is obtained in the separation capability of the Cyclical ElFFF systems. It is shown that high resolution separations of 15 and 40 nm gold nanoparticles can be achieved by Cyclical ElFFF, for which the separation of particles smaller than 100 nanometers was not demonstrated before.

In addition, the first particle based modeling of Electrical Field Flow Fractionation (ElFFF) systems is demonstrated for the first time. The developed particle based simulation code allows visualization of individual particles inside the separation channel, which leads to a better understanding of ElFFF operation and mechanisms. The outputs of the simulation code show good agreement with the experimental results.

We have also fabricated a new ElFFF system and tested it with four different channel heights to investigate the effect of channel height on the separation performance of the ElFFF systems.

It is also shown for the first time that ElFFF can be used for the separation of magnetic nanoparticles. In previously reported studies, magnetic field driven techniques were used for the separation of magnetic particles. However, in this study, it is revealed that an electrical field driven technique can also be used for the separation of these nanoparticles.

A new magnetic field flow fractionation (MFFF) system was designed and modeled using both finite element and particle based simulations. As a change from current magnetic FFF systems, which use static magnetic fields, the new system uses cyclical magnetic fields for the separation of the particles.

Finally, a novel passive magnetic microfluidic mixer is designed and fabricated which produces high efficiency mixing at the microscale, without need of an active actuation mechanism.

TABLE OF CONTENTS

LIST OF TABLES

LIST OF FIGURES

ACKNOWLEDGEMENTS

First of all, I would like thank my advisor, Dr. Bruce Gale, for his guidance and support throughout my PhD study. He has not only been an advisor to me with his immense knowledge, but also a great model as a person, who always has a friendly and encouraging attitude towards his students.

I am greatly thankful to Dr. William Johnson, with whom I had a chance to work during the last two years of my PhD study. His enthusiasm towards research has always impressed and motivated me through my PhD studies. By the support and research environment he provided, we have achieved significant productivity in our work.

I would like to thank Dr. Richard Rabbitt, especially for his support and guidance in the beginning of my PhD study. With his vast knowledge in many fields of bioengineering, he has always been an inspiration for a bioengineering researcher like me.

I would also like to thank my committee members Dr. Hamid Ghandehari and Dr. Florian Solzbacher, for their always helpful behavior and their insights and comments in this study. I am also thankful to Dr. Diego Fernandez for his valuable discussions about my research.

I thank to my lab friends Eliana Manangon, Himanshu Sant and Christopher Lambert, with whom working and producing in the lab has been always fun.

Additionally, I would like to thank all my colleagues at State of Utah Center of Excellence for Biomedical Microfluidics for their friendship throughout my PhD.

I am very thankful to all baroque music composers and especially to George Frideric Handel. Their music was always in the background during my PhD which made my work much easier and more enjoyable.

Finally, I would like to thank to my parents Yüksel and Kazım Taşcı, and my sister Arzu Taşcı. Their presence was the biggest motivation to me in everyday of this study.

CHAPTER 1

INTRODUCTION

Nanotechnology is one of the fastest grooving research fields, which involves production and use of substances at the nanoscale (i.e, between 1 and 100nm). Many nanotechnology-based consumer products are already available in the market, some of which are cosmetics, nano-medicines, sun screens, semiconductors, house cleaning items, paints and so forth. As the necessity of producing specialized nanoparticles increases, scientist have to use separation techniques that can sort particles according to their vast number of properties, such as size, shape, charge, internal structure, magnetic susceptibility and optical properties. Currently, several analytical methods are used to separate and characterize nanostructures. The names of the three main separation techniques are chromatography, electrophoresis and field flow fractionation.

Chromatography is a term given to the set of techniques used to separate and analyze mixtures. The components to be separated are distributed between two phases: stationary and mobile phase. When the mixture enters the chromatography system, different components of the mixture travel at different rates, causing them to separate. The variation in the migration rates stems from the differences in the interaction levels of the substances with the stationary phase[1, 2]. Based on the type of the mobile phase (gas

or liquid), chromotography methods are divided into two main classes. In gas chromatography, the mobile phase is a gas, and in liquid chromatography the mobile phase is a liquid. Gas chromatography is always carried out in a column (i.e., a porous packed bed or a capillary) and is widely used in analytical chemistry. Liquid chromatography (LC) can be carried out either in a column or a plane. The liquid chromatography technique is capable of producing high resolution separations and can be used for both analytical and sample preparation purposes.

Another major nanoparticle separation technique is electrophoresis. This separation technique is based on the differences in the electrophoretic mobilities and sizes of the particles. In electrophoresis, an electrical field is utilized as the driving force, which forces the particles to migrate from one electrode to other. Particles having discrepancies in their electrophoretic mobilities or sizes migrate at different rates, resulting in the separation. Electrophoresis is widely used in biochemistry for the separation of biological molecules such as amino acids[3, 4], proteins [5, 6], nucleic acids[7, 8], nucleotides [9, 10], etc.

The third major analytical separation technique is called Field Flow Fraction (FFF). In this technique, a separation field is applied perpendicular to the parabolic flow profile inside a ribbon-like channel [11]. Particles are separated according to their interaction strength with the field. Based on the type of the separation field applied, different kinds of FFF methods have been established, such as electrical [12], magnetic [13], gravitational [14], thermal [15] and flow FFF [16]. This broad range of available fields makes FFF a very versatile technique capable of sorting substances based on their their different particle properties.

In contrast to electrophoresis, where the direction of separation is the same as the direction of the field, in all FFF techniques the separation field is applied perpendicular to the carrier flow[11, 17-23]. Also, different from chromatography and electrophoresis, FFF is carried out in an open channel, which allows separation of larger particles (in the range of microns) besides the smaller particles (in the nanometer range). The open channel characteristic of the FFF systems also allows easy elution and collection of samples from the channel outlet. Furthermore, as a consequence of the open channel geometry, shear stresses in the FFF channels are low, which permits separation of fragile samples as well[11, 24].

Electrical Field Flow Fractionation (ElFFF) is one of the subtechniques of the FFF family, in which the separation field is an electrical field[12, 25]. This field is generated by applying potential difference on the top and bottom walls of the separating channel. The voltages used in the ElFFF are smaller than 20V, which is much lower than the voltages used in the electrophoresis (in the kV range). Accordingly, ElFFF is much gentler on the particles compared to the electrophoresis and biomolecules can be safely separated by much lower risk of denaturation.

Similar to electrophoresis, in ElFFF, particles are sorted according to their sizes and electrical properties (i.e., electrophoretic mobility). Since most of the bio-molecules are charged in nature, ElFFF can be used for the separation of these particles.

Two main types of ElFFF techniques exist. In traditional (normal) ElFFF [25], DC (static) voltages are used. On the other hand, in Cyclical Electrical Field Flow Fractionation (CyElFFF), AC (cyclical) voltages are employed[26]. Both techniques have their own advantages and disadvantages. Basically, the electrical double layer (EDL)

generation is an important drawback of the traditional ElFFF systems. As a consequence of the static field application, EDL is produced on the surfaces of the channel walls and electric field in the channel (effective field) drops to less than 3% of its nominal value[27]. In CyElFFF, full development of EDL is prevented by the application of cyclical fields. Since the polarities of the electrodes are changing in each cycle, insufficient time exists for the EDL to be fully formed on the electrode surfaces[27]. In cyclical ElFFF, as a consequence of the applied cyclical voltage, there are many more parameters to consider and the operation of the system is a more complex task compared to the traditional ElFFF. Consequently, CyElFFF needs further effort to determine the proper operating conditions to achieve particle separations.

Another subtype of FFF, which is even more immature than electrical FFF is Magnetic Field Flow Fractionation (MFFF) [13, 17]. Instead of electrical fields, this technique uses magnetic fields to separate and characterize magnetic nanoparticles. One of the biggest limitations of this technique is the particle trapping inside the channel as a result of the constant magnetic field [13, 28]. To achieve separations of magnetic nanoparticles, very high magnetic fields are needed and these high fields give rise to the sticking of the particles on the channel walls.

Motivation

Electrical and magnetic field flow fractionation methods have several limitations that prevent them from being widely used tools for the nanoparticle fractionation and characterization. In this study, we address the main limitations of both techniques so that

both methods will be used as much more effective tools for the separation and characterization of nanoparticles.

In electrical field flow fractionation many operating parameters should be selected correctly to achieve separations of nanoparticles. Some examples of these parameters are amplitude, frequency, shape, duty cycle and offset of the applied voltage. Furthermore, flow speed, ionic strength of the carrier, and dimensions of the separation channel have a significant effect on the separation efficiency. In order to achieve high resolution separations, all those parameters should be selected accurately. As a result, there is an immediate need for a modeling tool to determine the accurate operating conditions for each separation experiment.

Cyclical Electrical Field Flow Fractionation (CyElFFF) is a powerful separation method. But it shows limited performance in the fractionation of sub 100nm particles. Until now, only separations of particles with sizes bigger than 100nm have been achieved. The limitation of CyElFFF systems stems from the high diffusion rate of sub 100nm particles. As the sizes of the particles drop to nanometer range, diffusion of the particles become dominant and no separation can be achieved by the CyElFFF method. Thus, CyElFFF systems require an improvement in their operation and design so that they can also be used for the separation of particles smaller than 100nm.

The channel dimensions have a significant effect on the separation efficiency of ElFFF systems. It is still not clear which channel height gives the best separation results. Thus, the effect of channel height on the separation efficiency should be further investigated.

Magnetic nanoparticles have many biomedical applications, such as drug delivery, biomedical imaging, magnetic hyperthermia etc. Until now only magnetic field based systems (e.g., Magnetic FFF) have been used to separate and characterize those particles[13]. Since purification of magnetic nanoparticles still remains as a hard subject, other separation methods such as CyElFFF should also be tested in the separation of these particles.

The major drawback of the Magnetic Field Flow Fractionation (MFFF) technique is the trapping of the particles in the MFFF channel [13, 28]. This results in very low recoveries of the particles in the MFFF separations. This limitation should be addressed by proposing new magnetic separation methods other than the traditional MFFF.

Mixing in the microscale is a hard subject due to the laminar flow regime observed in the microfluidic devices. Currently, the micromixers that have high efficiencies are mostly active mixers, using moving parts or some other types of actuation. A high efficiency passive micromixer with very easy fabrication should be developed to be effectively used in the microfluidic systems.

Outline

This dissertation is structured such that each chapter is composed of a published work or a manuscript in preparation for publication.

Chapter 2. Computer Modeling of Electrical Field Flow Fractionation Systems

The first particle based simulation code for the Electrical Field Flow Fractionation systems is generated. This code allows visualization of individual particles inside the

separation channel, which leads to the better understanding of the ElFFF operation mechanisms. In addition, this simulation will help the researchers to determine optimum operating conditions prior to conducting ElFFF experiments.

Chapter 3. Utilization of High Duty Cycle Voltage Waveforms for High Resolution Electrical Field Flow Fractionation

Diffusion induced limitation of Cyclical ElFFF systems is resolved by utilization of high duty cycle voltage waveforms. By this method, separations of sub 50nm particles become possible in the CyElFFF systems. Chapter 3 explains the theory behind this novel method. In addition, the theoretical considerations are tested by many separation experiments conducted in different operating conditions.

Chapter 4. Circuit Modification in Electrical Field Flow Fractionation Systems for High Resolution Separations of Nanoparticles

To improve the separation capabilities of the CyElFFF systems, for the first time in the ElFFF literature, external circuit elements are used to modify the electrical circuitry of the system. This circuit modification allows high resolution separations of sub 50nm nanoparticles. The performance of this new method is tested by various separation experiments and presented in Chapter 4.

Chapter 5. The Effect of the Channel Height on the Separation Efficiency of an Electrical Field Flow Fractionation System

To investigate the effect of channel height on the separation efficiency, ElFFF systems with four different channel heights are fabricated. The separation performances

of these four systems are tested via separation experiments. Results are analyzed and optimum channel height that provides the highest separation resolution is determined.

Chapter 6. Separation of Magnetic Nanoparticles by Cyclical Electrical Field Flow Fractionation

CyElFFF systems are tested for the first time in the separation of magnetic nanoparticles. It is shown that magnetic nanoparticles can also be separated with the utilization of electrical fields other than the magnetic fields.

Chapter 7. Cyclical Magnetic Field Flow Fractionation

A new Magnetic Field Flow Fractionation (MFFF) system is designed and simulated, which uses cyclical magnetic fields instead of a constant magnetic field. By the help of alternating magnetic fields, we propose to overcome the particle trapping drawback of current MFFF systems. In this work, several simulation studies are conducted to test the performance of this new Cyclical Magnetic Field Flow Fractionation (CyMFFF) method as explained in Chapter 7.

Chapter 8. A Ferrofluidic Magnetic Micromixer

In all the previous chapters, electromagnetic fields are used for the separation of nanoparticles. Differently, in this chapter, magnetic field is used for the mixing of liquids and/or particles. A novel magnetic micromixer is designed, which does not need any active actuation. The micromixer can be fabricated very easily, and it is shown that it can enhance the mixing efficiency of a standard serpentine mixer more than three times. All the methods and experiments done in this study are presented in Chapter 8.

Chapter 9. Conclusion

Chapter 9 provides the summary of works completed in this thesis. In addition, possible future research directions are explained and discussed in this chapter.

References

[1] Q. Wang and L. Zhang, "Review of research on quantitative structure-retention relationships in thin-layer chromatography," *Journal of Liquid Chromatography & Related Technologies,* vol. 22, pp. 1-14, 1999.

[2] J. C. Giddings, *Dynamics of Chromatography: Principles and Theory* vol. 1: CRC, 2002.

[3] Y.-F. Cheng and N. J. Dovichi, "Subattomole amino acid analysis by capillary zone electrophoresis and laser-induced fluorescence," *Science (New York, NY),* vol. 242, p. 562, 1988.

[4] R. Bieleski and N. Turner, "Separation and estimation of amino acids in crude plant extracts by thin-layer electrophoresis and chromatography," *Analytical Biochemistry,* vol. 17, pp. 278-293, 1966.

[5] A. C. Peacock, S. L. Bunting, and K. G. Queen, "Serum protein electrophoresis in acrylamide gel: patterns from normal human subjects," *Science,* vol. 147, pp. 1451-1453, 1965.

[6] D. F. Hochstrasser, M. G. Harrington, A.-C. Hochstrasser, M. J. Miller, and C. R. Merril, "Methods for increasing the resolution of two-dimensional protein electrophoresis," *Analytical Biochemistry,* vol. 173, pp. 424-435, 1988.

[7] K. Kellings, N. Meyer, C. Mirenda, S. B. Prusiner, and D. Riesner, "Further analysis of nucleic acids in purified scrapie prion preparations by improved return refocusing gel electrophoresis," *The Journal of General Virology,* vol. 73, p. 1025, 1992.

[8] Y. Shi, P. C. Simpson, J. R. Scherer, D. Wexler, C. Skibola, M. T. Smith, and R. A. Mathies, "Radial capillary array electrophoresis microplate and scanner for high-performance nucleic acid analysis," *Analytical Chemistry,* vol. 71, pp. 5354-5361, 1999.

[9] W. A. Susor and W. J. Rutter, "Method for the detection of pyruvate kinase, aldolase, and other pyridine nucleotide linked enzyme activities after electrophoresis," *Analytical Biochemistry,* vol. 43, pp. 147-155, 1971.

[10] C. A. Pigge, J. Muth, E. Carrilho, and B. L. Karger, "Capillary electrophoresis for the detection of known point mutations by single-nucleotide primer extension and laser-induced fluorescence detection," *Journal of Chromatography A,* vol. 781, pp. 367-375, 1997.

[11] J. C. Giddings, "A new separation concept based on a coupling of concentration and flow nonuniformities," *Separation Science,* vol. 1, pp. 123-125, 1966.

[12] K. D. Caldwell, L. F. Kesner, M. N. Myers, and J. C. Giddings, "Electrical field-flow fractionation of proteins," *Science,* vol. 176, pp. 296-298, 1972.

[13] F. Carpino, L. R. Moore, M. Zborowski, J. J. Chalmers, and P. S. Williams, "Analysis of magnetic nanoparticles using quadrupole magnetic field-flow fractionation," *Journal of Magnetism and Magnetic Materials,* vol. 293, pp. 546-552, 2005.

[14] M. R. Park, D. Y. Kang, J. Chmelik, N. Kang, J. S. Kim, and S. Lee, "Different elution modes and field programming in gravitational field-flow fractionation: Effect of channel angle," *Journal of Chromatography A,* vol. 1209, pp. 206-211, 2008.

[15] T. L. Edwards, B. K. Gale, and A. B. Frazier, "A microfabricated thermal field-flow fractionation system," *Analytical Chemistry,* vol. 74, pp. 1211-1216, 2002.

[16] J. C. Giddings, F. J. Yang, and M. N. Myers, "Flow field-flow fractionation: new method for separating, purifying, and characterizing the diffusivity of viruses," *Journal of Virology,* vol. 21, pp. 131-138, 1977.

[17] T. Schunk, J. Gorse, and M. Burke, "Parameters affecting magnetic field-flow fractionation of metal oxide particles," *Separation Science and Technology,* vol. 19, pp. 653-666, 1984.

[18] J. C. Giddings, F. J. Yang, and M. N. Myers, "Sedimentation field-flow fractionation," *Analytical Chemistry,* vol. 46, pp. 1917-1924, 1974.

[19] K. D. Caldwell, G. Karaiskakis, and J. C. Giddings, "Characterization of liposomes by sedimentation field-flow fractionation," *Colloids and Surfaces,* vol. 3, pp. 233-238, 1981.

[20] G. H. Thompson, M. N. Myers, and J. C. Giddings, "Thermal field-flow fractionation of polystyrene samples," *Analytical Chemistry,* vol. 41, pp. 1219-1222, 1969.

[21] W. Cao, P. S. Williams, M. N. Myers, and J. C. Giddings, "Thermal field-flow fractionation universal calibration: Extension for consideration of variation of cold wall temperature," *Analytical Chemistry,* vol. 71, pp. 1597-1609, 1999.

[22] W. Fraunhofer and G. Winter, "The use of asymmetrical flow field-flow fractionation in pharmaceutics and biopharmaceutics," *European Journal of Pharmaceutics and Biopharmaceutics,* vol. 58, pp. 369-383, 2004.

[23] N. Tri, K. Caldwell, and R. Beckett, "Development of electrical field-flow fractionation," *Analytical Chemistry,* vol. 72, pp. 1823-1829, 2000.

[24] S. K. R. Williams, J. R. Runyon, and A. A. Ashames, "Field-flow fractionation: addressing the nano challenge," *Analytical Chemistry,* vol. 83, pp. 634-642, 2010.

[25] K. D. Caldwell and Y. S. Gao, "Electrical field-flow fractionation in particle separation. 1. Monodisperse standards," *Analytical Chemistry,* vol. 65, pp. 1764-1772, 1993.

[26] B. K. Gale and M. Srinivas, "Cyclical electrical field flow fractionation," *Electrophoresis,* vol. 26, pp. 1623-32, May 2005.

[27] A. I. Lao, D. Trau, and I.-M. Hsing, "Miniaturized flow fractionation device assisted by a pulsed electric field for nanoparticle separation," *Analytical Chemistry,* vol. 74, pp. 5364-5369, 2002.

[28] A. H. Latham, R. S. Freitas, P. Schiffer, and M. E. Williams, "Capillary magnetic field flow fractionation and analysis of magnetic nanoparticles," *Analytical Chemistry,* vol. 77, pp. 5055-5062, 2005.

CHAPTER 2

COMPUTER MODELING OF ELECTRICAL FIELD FLOW FRACTIONATION SYSTEMS

Introduction

Separation of nanoparticles can be effectively achieved by the family of separation techniques called Field Flow Fractionation (FFF) [1]. In this method, a separation field is applied perpendicular to the parabolic flow profile inside the ribbon-like channel. Particles are separated based on their interaction strength with the field. Electrical Field Flow Fractionation (ElFFF) is one of the members of the FFF family, in which the electrical field is utilized as the separation field [2]. This technique is very useful in separation of charged particles and the fractionation mainly depends on particle sizes and electrophoretic mobilities.

There are two main types of ElFFF techniques exist. In traditional (normal) ElFFF [3], DC (static) voltages are applied to the channel walls (electrodes). On the other hand, in Cyclical Electrical Field Flow Fractionation (CyElFFF), AC (cyclical) voltages are applied[4]. Both techniques have their own advantages and disadvantages. Basically, the electrical double layer (EDL) generation is an important drawback of the traditional ElFFF systems. As a consequence of the static field application, electric double layer is produced on the surfaces of the channel walls and electric field drops to 3% of its initial

value in the first couple of minutes. In CyElFFF, development of EDL is prevented by the application of cyclical fields. Since the polarity of the voltage changes in each cycle of the field, there is an insufficient time for the electric double layer to be fully formed[5]. Besides its advantage, CyElFFF method is a much more complex technique compared to the traditional ElFFF. Many parameters should be selected carefully for the accurate operation of a CyElFFF system. Some examples of these parameters are amplitude, frequency, shape, duty cycle and offset of the applied voltage. In addition to the electric parameters, flow speed, ionic strength of the carrier, and dimensions of the separation channel have a significant effect on the separation efficiency. In order to achieve an efficient separation with the ElFFF method, all those parameters should be accurately selected.

Several studies have been done to predict the correct operating conditions of the ElFFF systems. Electric circuit modeling of the system was studied for the proper estimation of the electric field (effective field) inside the channel [6-8]. Besides the electrical models, a few analytical and numerical models were also generated to estimate the separation efficiency of the system at different operating conditions [9-12]. Furthermore, several experimental studies have been done to analyze the effects of different experimental parameters on the separation performance [13-18].

Despite the high number of studies on electrical field flow fractionation, to date no method exists to predict the individual motions of particles in the separation channel. The motion paths of the particles should be accurately estimated to come up with a model that matches with the experimental data. For this purpose, in this study, a particle based computer model is generated for the ElFFF systems. This is the first particle based

simulation study made in the ElFFF literature, which will help for a better understanding of the physics of the system. In addition, by visualization of the individual particles in the separation channel, the selection of the operating parameters will be more precise. Furthermore, this simulation tool will help the researchers to estimate the separation results without conducting the actual experiments, which usually takes more time and effort. Moreover, the particle based simulation code generated in this study is capable of simulating systems with any geometry, which may lead to the design of new separation systems which can produce high resolution separations.

Theory and Methods

Operation principles of two main electrical field flow fractionation techniques (Normal and Cyclical ElFFF) are explained in Figure 2.1. In normal ElFFF, a constant (DC) voltage is applied to the channel walls and particles are attracted to one of the channel walls (i.e., bottom wall in this figure). After a certain period, equilibrium establishes between the electrically driven motion and the diffusion of the particles. Accordingly, particle clouds gain a steady state height (y-coordinate) in the channel. This height is directly proportional to the particle diffusion and inversely proportional to the particle electrophoretic mobility. As a result, particle clouds having different sizes or electrophoretic mobilities will achieve different heights in the channel and because of the parabolic velocity profile, particle clouds closer to the middle of the channel will elute earlier than the particle clouds closer to the channel wall. In Figure 2.1a, since the steady state height of the dotted particles is closer to the middle of the channel, these particles gain higher velocities throughout the channel and elute earlier than the circled particles.

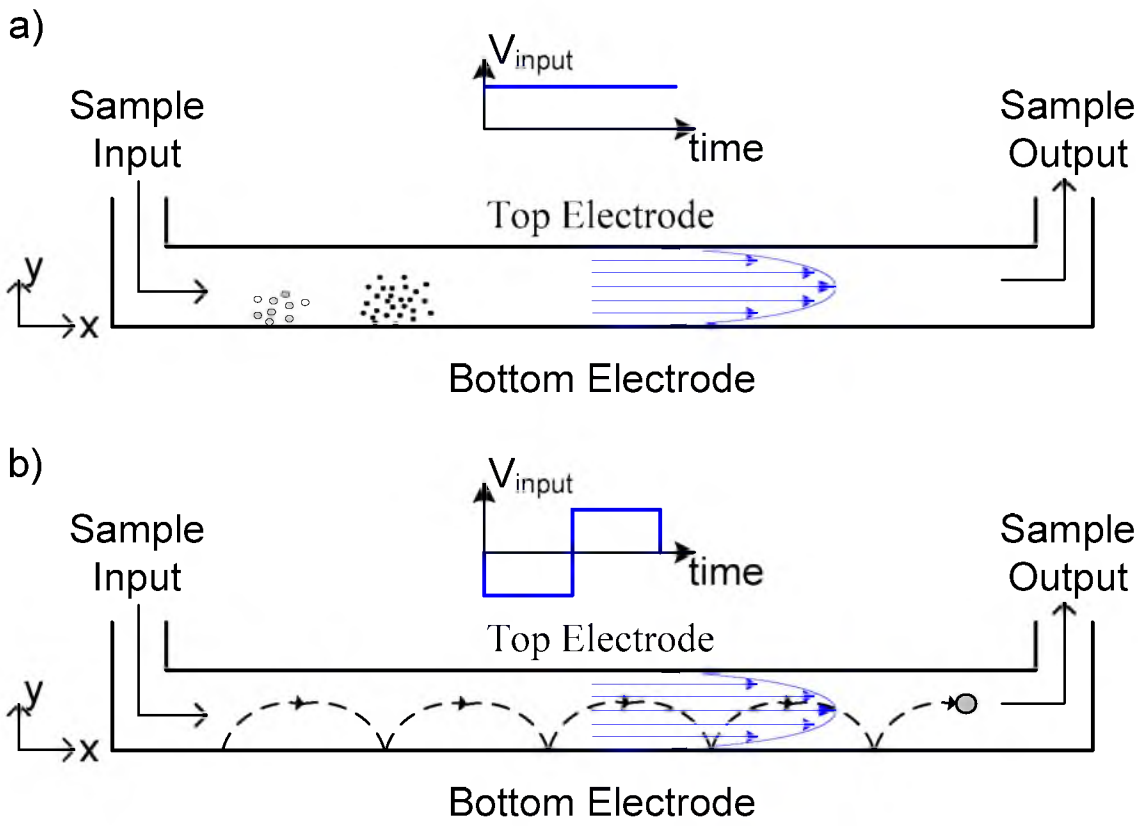

Figure 2.1. Operation principle of a) Normal ElFFF technique b) Cyclical ElFFF technique.

In CyElFFF, periodic square wave voltages are applied. Accordingly, particles move back and forth between the channel walls (as demonstrated by the dashed lines in Figure 2.1b. At the end of each voltage cycle, particles having different electrophoretic mobilities will achieve different heights. As a consequence of the parabolic velocity profile, particles with heights (y-coordinates) closer to the middle of the channel will gain higher speeds and elute earlier. Particles having heights closer to the channel wall will migrate slowly and elute later.

As can be deducted from the operation principles of the ElFFF techniques, particles have three main motions in the channel. First motion is the electrically driven movement of the particles, represented by the equation 2.1 below.

$$v_{py} = \mu_p \times E_{eff} \qquad (2.1)$$

where v_{py} *(m/s)* is the particle velocity in y-direction resulting from the electrical force, μ_p*(m²/Vs)* is the particle electrophoretic mobility and E_{eff}*(V/m)* is the electric field (effective field) inside the channel.

In addition to the electrical motion of a nanoparticle, the linear unidirectional diffusion length of the particle can be obtained from the random walk theory as follows.

$$l_d(\Delta t) = \sqrt{2D\Delta t} \qquad (2.2)$$

where $l_d(\Delta t)$ is the distance travelled by diffusion in Δt seconds, and D*(m²/s)* is the diffusion coefficient of the particle. The diffusion coefficient is a function of particle size, temperature and dynamic viscosity of the carrier liquid as denoted by Stokes-Einstein equation[19] below.

$$D = \frac{TK_b}{3\pi\eta d} \qquad (2.3)$$

where T (K) is temperature, K_b*(J/K)* is Boltzmann's constant, η *(Pa·s)* is the dynamic viscosity of the carrier liquid and d *(m)* is the particle diameter.

Finally, motion of the particles resulting from the parabolic velocity profile is represented by the following equation.

$$v_{px} = 6v\left(\frac{y}{w} - \frac{y^2}{w^2}\right) \qquad (2.4)$$

where v_{py}*(m/s)* is the x-velocity of the particle as a consequence of the parabolic flow profile. v*(m/s)* is the average x-velocity of the carrier in the channel. y*(m)* is the y coordinate of the particle and w*(m)* is the height of the channel.

By using these four equations, x and y coordinates of each particle are calculated in every time step, as demonstrated in equation 2.5.

$$x(t+\Delta t) = x(t) + n \cdot l_d(\Delta t) + v_{px} \cdot \Delta t$$
$$y(t+\Delta t) = y(t) + n \cdot l_d(\Delta t) + v_{py} \cdot \Delta t \quad (2.5)$$

Here, n is the random number with a mean of 0 and a standard deviation of 1. By multiplying the diffusion length (l_d) with n, random behavior of the particle diffusion is represented according to the random walk theory,

To visualize the particle trajectories, equation 2.5 is calculated for each time step by using the simulation code developed in Matlab® environment.

The channel geometry used in the simulation can be seen in Figure 2.2. The channel is rectangular in shape, in which the inlet is located at the upper left corner. The outlet is chosen as the right edge of the rectangle. All the walls have the bounce-back boundary condition (i.e., the particle coinciding with the boundary is reflected back with the same momentum) except the inlet and outlet sections, which have continuous flow boundary conditions.

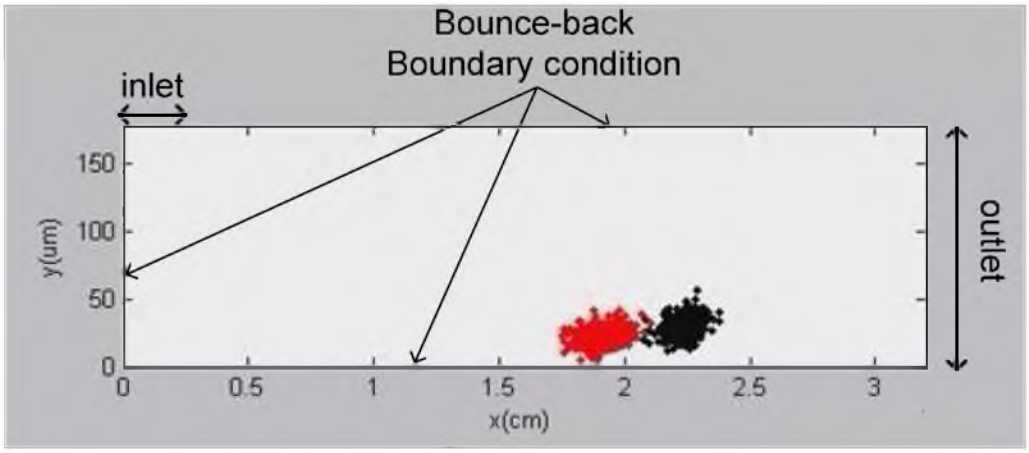

Figure 2.2. Channel geometry and boundary conditions used in the simulations.

In the simulation algorithm, at t=0, all the particles are uniformly distributed at the inlet (y=178μm, 0<x<0.75mm), and at t=Δt and on, x and y coordinates of each particle are updated as indicated by equation 2.5.

The location of each particle is represented by a dot in the channel. And after each time step (Δt), the snapshots of the particle distributions are taken, which are combined in to a movie file as the simulation is completed. By this way, all the history of the particle motions can be viewed at the end of the simulation.

The simulation code takes several inputs such as particle sizes R_1, R_2, ..., R_n and electrophoretic mobilities μ_{p1}, μ_{p2}, ..., μ_{pn} of n different type of particles. In addition, the number of particles can be given as an input as well. Electrical parameters, for instance, amplitude, frequency and shape of the applied voltage wave, duty cycle and offset voltage are the electrical inputs of the code. Furthermore, carrier flow speed and channel dimensions (height and length) are the remaining inputs entered before the simulation.

The outputs of the simulation are UV fractogram of the separation experiment, movie file showing the motion of the particles in the channel, histograms of the particles in the channel and effective voltage inside the channel with respect to time.

The extended output of the simulation can be seen in Figure 2.3. In this output, window a is assigned for particle tracing, which is used to visualize motions of the particles. The dots having different colors correspond to particles with different properties (such as electrophoretic mobility or size). Windows b and c show the histograms of the particles inside the channel. Window d represents the effective potential difference between the channel walls (which is produced according to the entered electrical inputs). Finally, window e corresponds to the resulting UV-fractogram

of the simulated separation experiment. In Figure 2.3, since particles haven't reached the outlet of the channel, UV signal is shown as zero at that time instant.

To test the prediction capabilities of the particle based simulation code, several experiments were conducted by using the experimental setup shown in Figure 2.4.

The ElFFF channel used in the experiments was the same as the one used in the earlier works [3, 4]. The channel had a length of 64cm, height of 178μm and a width of 2cm.

To facilitate the flow of the carrier liquid (de-ionized water, 18.2 MΩ/cm), HPLC pump (Alltech model 426, Alltech Associates, Inc., IL, USA) was used at a flow rate of 1ml/min. Application of AC and DC voltages was done by using Agilent signal generator (Model 33120A) and Agilent DC power supply (Model E3640A). For the detection of the nanoparticles UV/Vis detector (ESA -Model 520) was used at the wavelength of 520nm. The UV detector data was recorded by using LabView (National Instruments) data acquisition card.

In the ElFFF experiments, 10nm spherical gold nanoparticles (Nano-Composix, CA, USA) were injected by 100 μL Hamilton microliter syringe. The injection volume for each experiment was 50μL. The 10nm gold nanoparticles were tannic acid stabilized and their mass concentration was 0.05 mg/mL. The average electrophoretic mobility of the 10nm particles was measured by Zetasizer Nano ZS instrument (Malvern Instruments Ltd., UK), and the result was -4.2 μmcm/Vs.

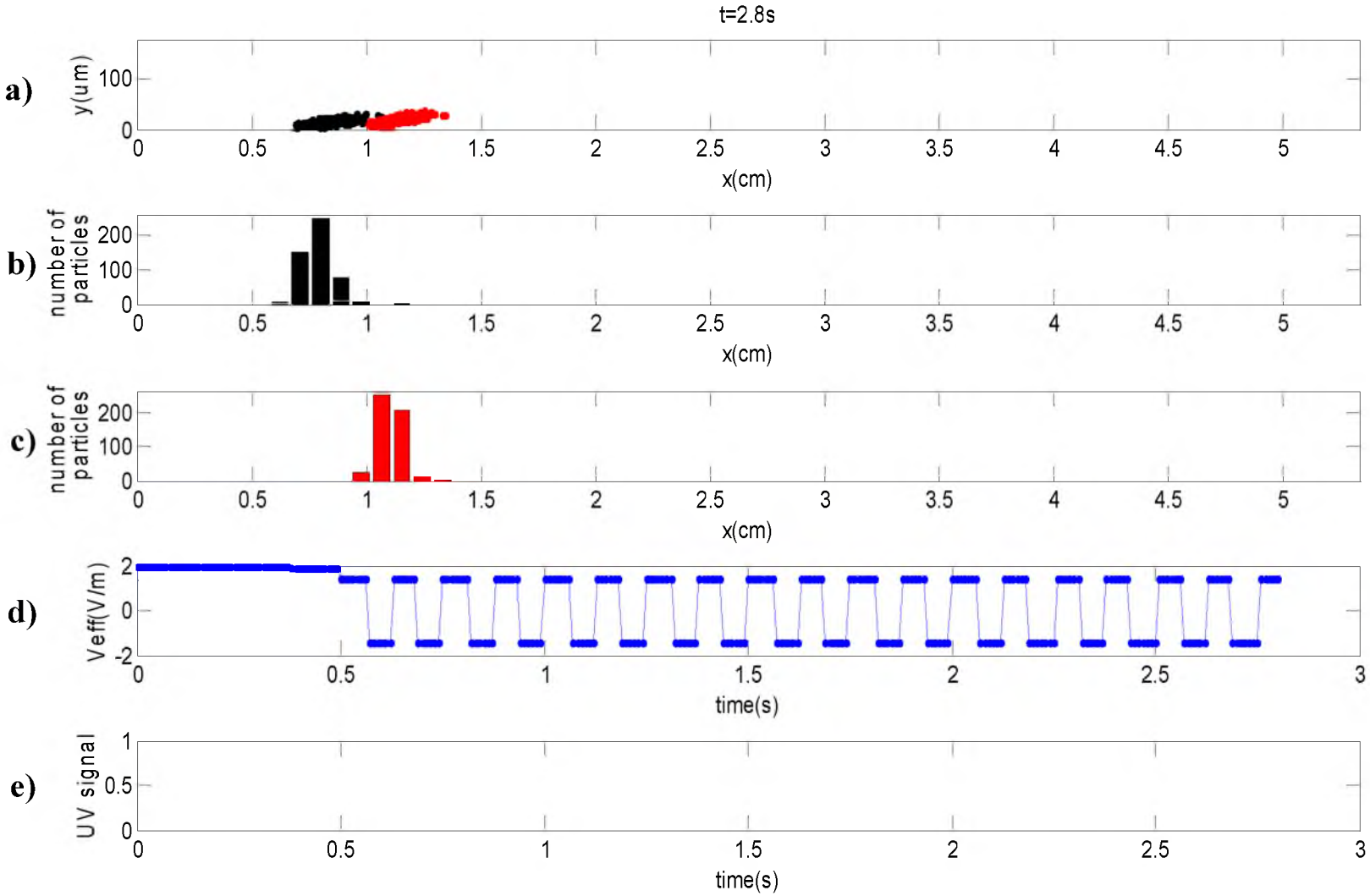

Figure 2.3. Typical extended output a) particle tracing, b & c) particle histograms, d) effective voltage, e) UV fractogram

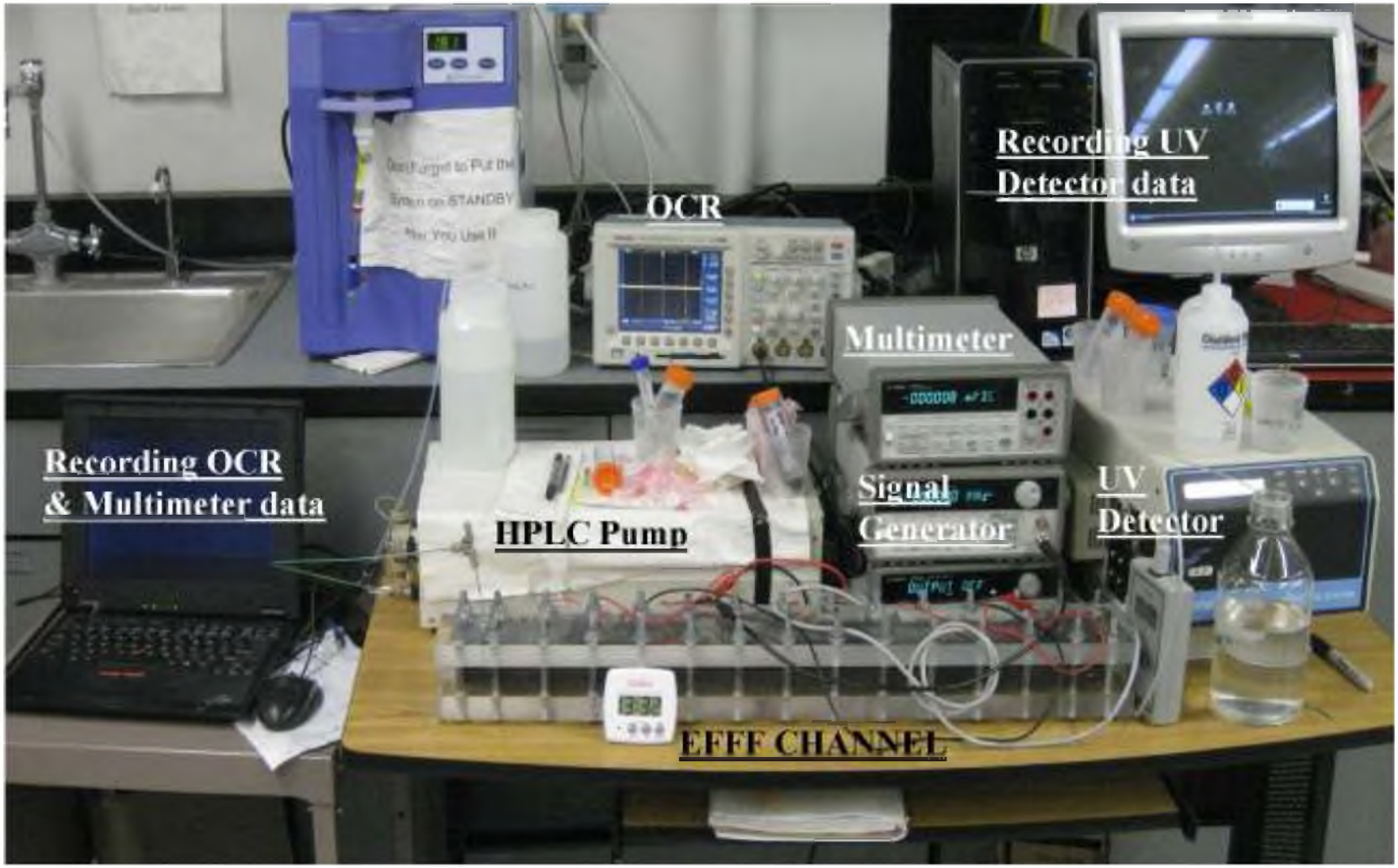

Figure 2.4. Experimental setup used in the separation experiments

The details of the simulations and experiments are summarized in the following section.

Simulation and Experiment 1 – Modeling of Normal ElFFF Operation

Experiments with traditional ElFFF method were conducted by using the 10nm gold particles. Different DC input voltages ranging from 1V to 1.7V were tested and resulting UV fractograms were compared with the simulation fractograms. In this experiment and simulation, particles are injected at t=0 and immediately following the injection at $t=0^{+}$, both input voltage and HPLC pump are turned on.

Simulation and Experiment 2 – Modeling of Cyclical ElFFF Operation

Cyclical ElFFF experiments were made with the injections of 10nm gold particles. 8Vpp square wave voltages were applied at different frequencies ranging from 1Hz to 20Hz. In order to analyze the estimation capability of the simulations, experimental UV fractograms were compared with the fractograms obtained from the simulations.

Simulation 3 – Detailed Modeling of the Channel Outlet

For more precise representation of the ElFFF system, channel outlet is modeled as shown in Figure 2.5. Instead of setting the right edge of the channel as the outlet, top right corner of the channel was selected as the new outlet. In addition, instead of modeling the flow profile in the channel by equation 2.4 (parabolic velocity equation),

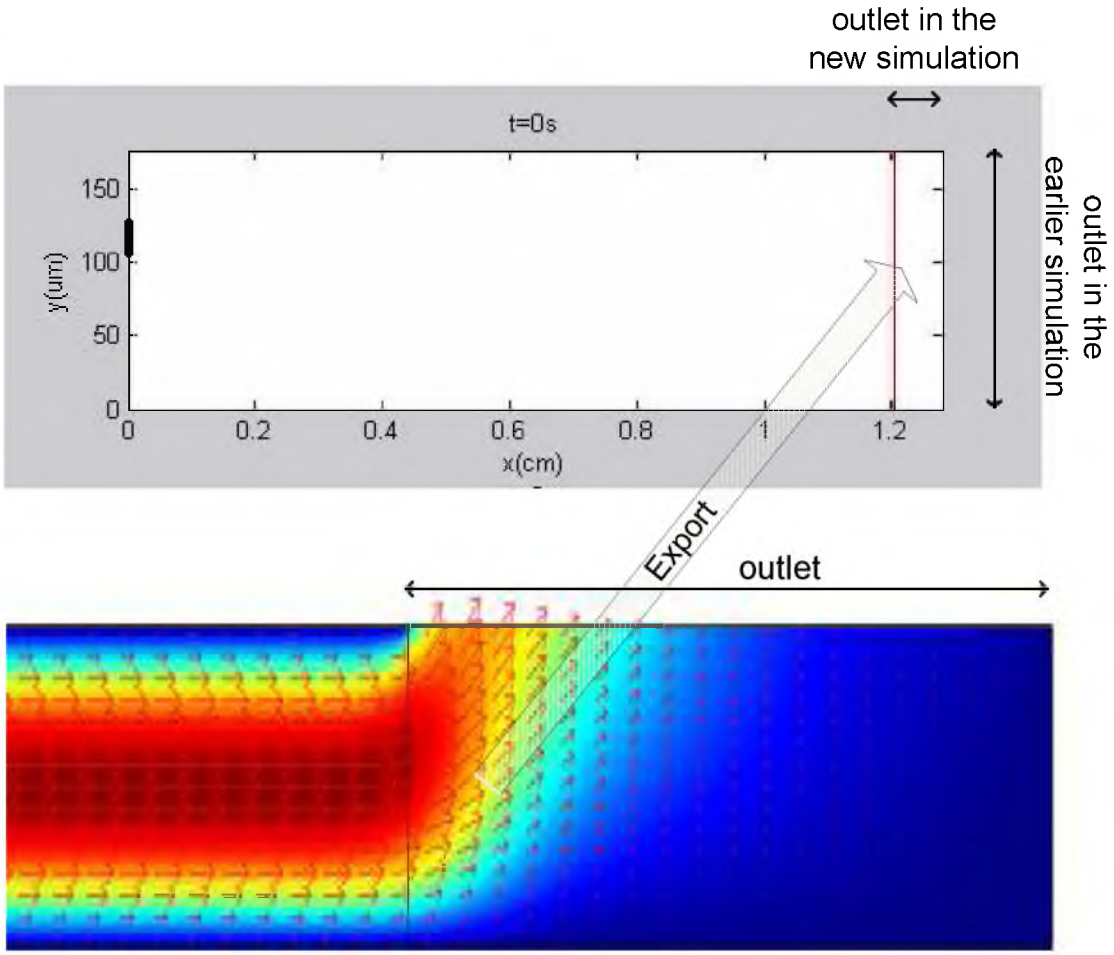

Figure 2.5. Improved outlet modeling of the ElFFF system. Outlet is selected as the top right corner of the channel. Flow profile obtained from the finite element simulation in Comsol is exported into the particle based simulation code in Matlab.

flow velocities in the channel were computed by finite element method in Comsol Multiphysics©. This is a more accurate representation of the outlet flow profile, since the parabolic flow profile is distorted at the outlet region of the channel. The flow velocity data at the outlet is exported from Comsol Multiphysics© to the particle based simulation code in Matlab®. Eventually, particle simulations are completed in Matlab.

In the outlet simulations, the last 1.28 cm of the channel was simulated to achieve results in comparably shorter durations. Similar to the earlier experiments, 10nm gold nanoparticles were used in the simulations and input voltage of 8.4Vpp, 1Hz square wave was applied. Simulations were made by selecting both top and bottom walls as the accumulation walls. In simulations 1 and 2, the bottom channel wall was selected as the accumulation wall. Therefore, the outcome of choosing the accumulation wall (top or bottom) was also investigated by this simulation.

Simulation 4 – Investigation of the Particle Retention Time for Even Duty and High Duty Cycle Input Voltages

In most of the CyElFFF studies, 50% duty cycle voltage waveforms were used as the input voltages[4, 12-15, 18, 20, 21]. In this simulation, both 50% and 70% duty cycle waveforms were used and corresponding retention times of the 10nm gold particles were analyzed. The input voltage used in the simulation was a 1Hz, 4Vpp square wave voltage.

Simulation 5 – Investigation of the Separation Efficiency for Even Duty and High Duty Cycle Input Voltages

In this simulation, separation of two different particles was visualized for 50% and 70% duty cycle conditions. The particles used in the simulation were same sized

particles with the diameter of 10nm.

The electrophoretic mobilities of the particles were -3μmcm/Vs and -4 μmcm/Vs. The input voltage used in the simulation was a 4Vpp, 1Hz square wave voltage.

Results and Discussion

The results of the normal ElFFF simulations and experiments can be seen in Figure 2.6. Experimental results in Figure 2.6a represents that as the input voltage increases, the retention time of the particles also increases. This trend is successfully predicted by the simulation as well (Figure 2.6b). The retention peak corresponding to 1.7 V is around 400s and the retention peak corresponding to 1V occurs just before 200 seconds. As shown in the experimental fractograms, the peaks having higher retention times are wider than the peaks with lower retention times, which can also be seen in the simulation fractograms (Figure 2.6b). In summary, it is shown that particle based simulation code is capable of predicting the outcome of the normal ElFFF experiments.

Figure 2.7 shows the results of the CyElFFF experiments and simulations. As shown in the plots, peak positions are very close between the experimental and simulation fractograms. One can observe that the retention time of the 10nm particles increases with the increasing frequency. In addition, larger peak widths are obtained for the higher frequencies. This trend in the retention times and peak widths is also predicted by the simulation code as shown in the simulation fractograms (Figure 2.7b).

Particle simulations made at the outlet of the channel can be viewed in Figure 2.8. Figure 2.8a represents the situation when the bottom channel wall is selected as the accumulation wall. In this case, since the outlet is located on the top wall, particles

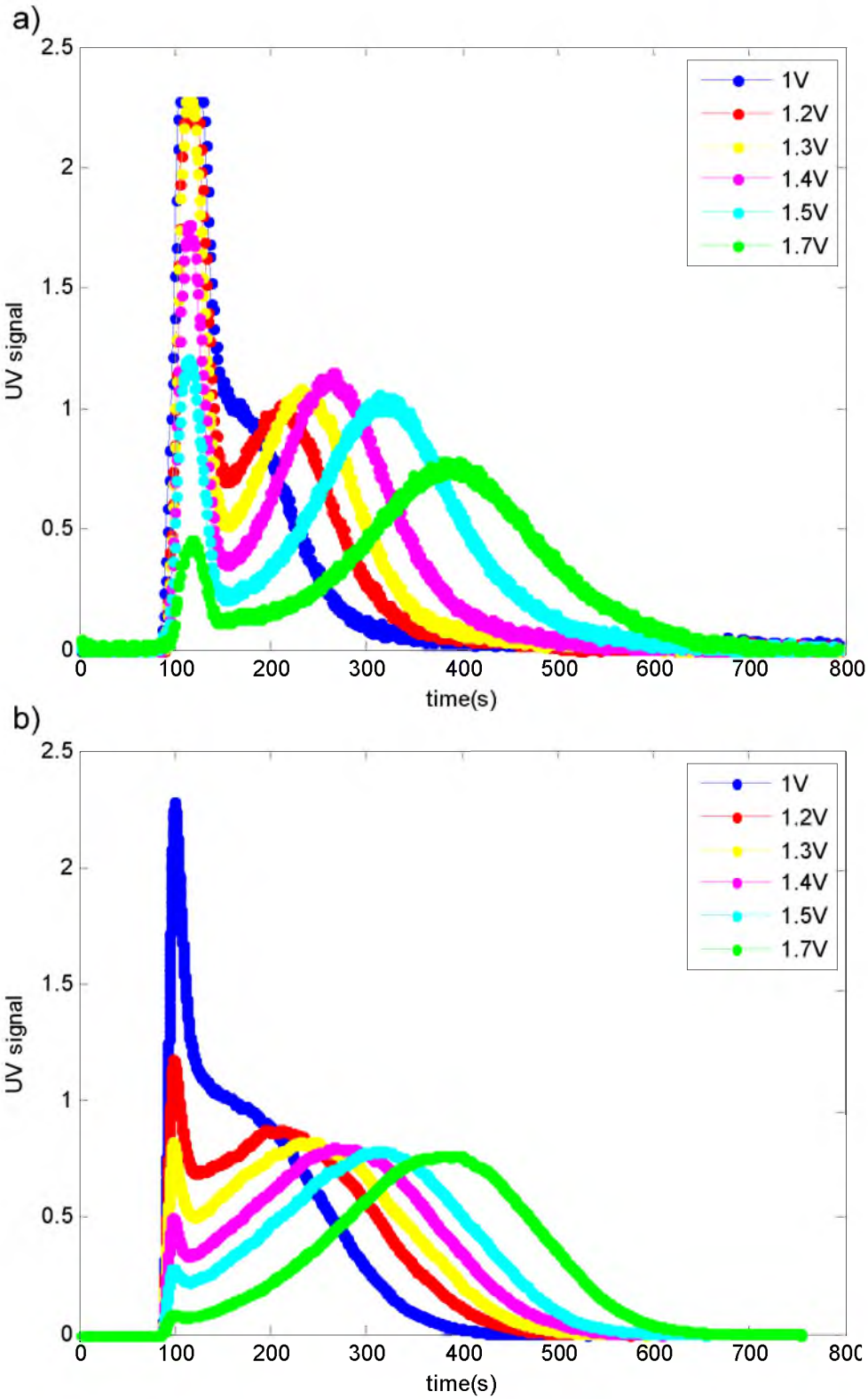

Figure 2.6. UV fractograms of 10nm gold nanoparticles obtained with the application of different input voltages. a) Results of the Normal ElFFF experiments b) Results of the Normal ElFFF simulations.

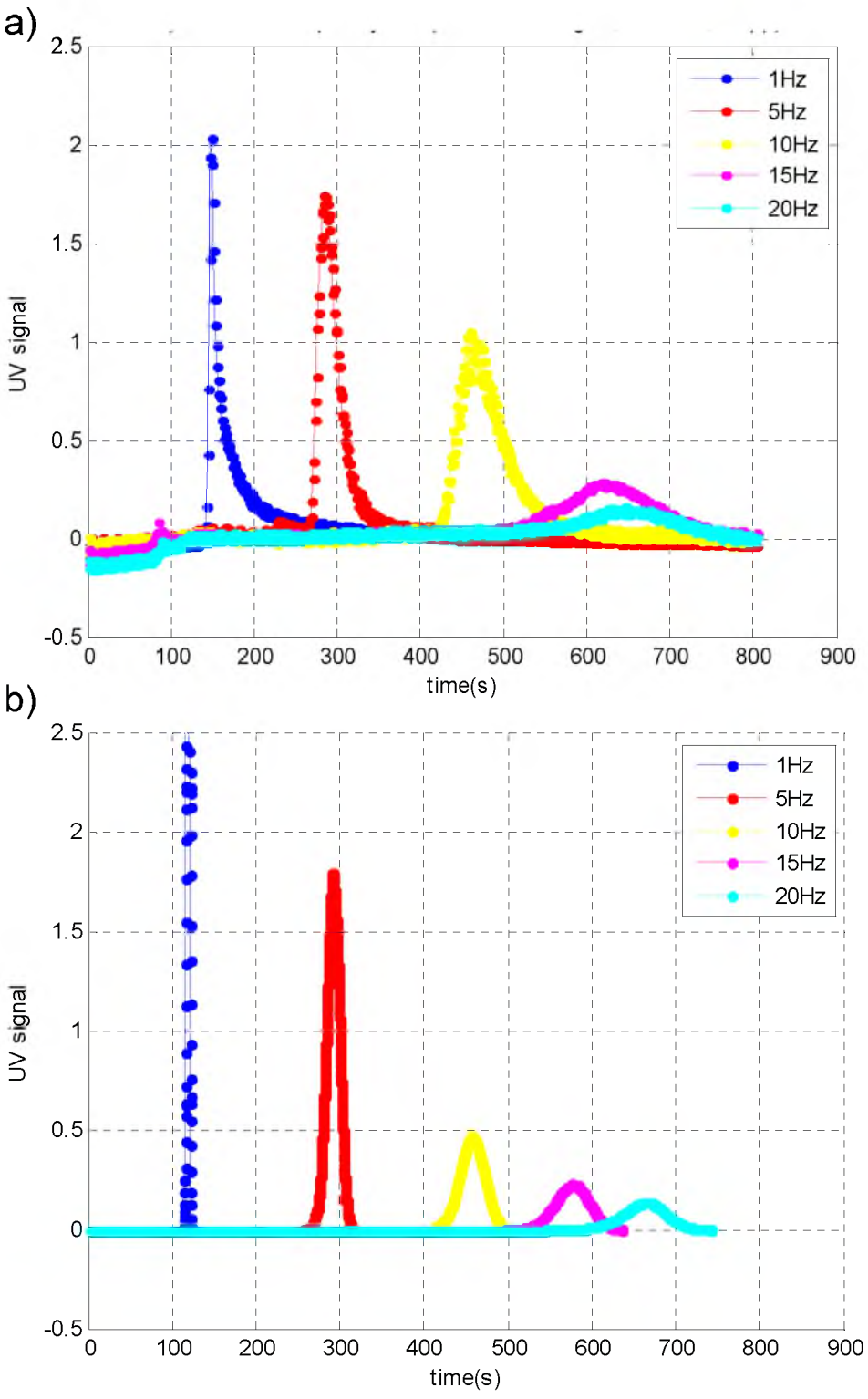

Figure 2.7. UV fractograms of 10nm gold nanoparticles which were obtained at different input frequencies. Other electrical parameters were Vamp=8Vpp, duty cycle=50%.
a) CyElFFF experimental results, b) CyElFFF simulation results.

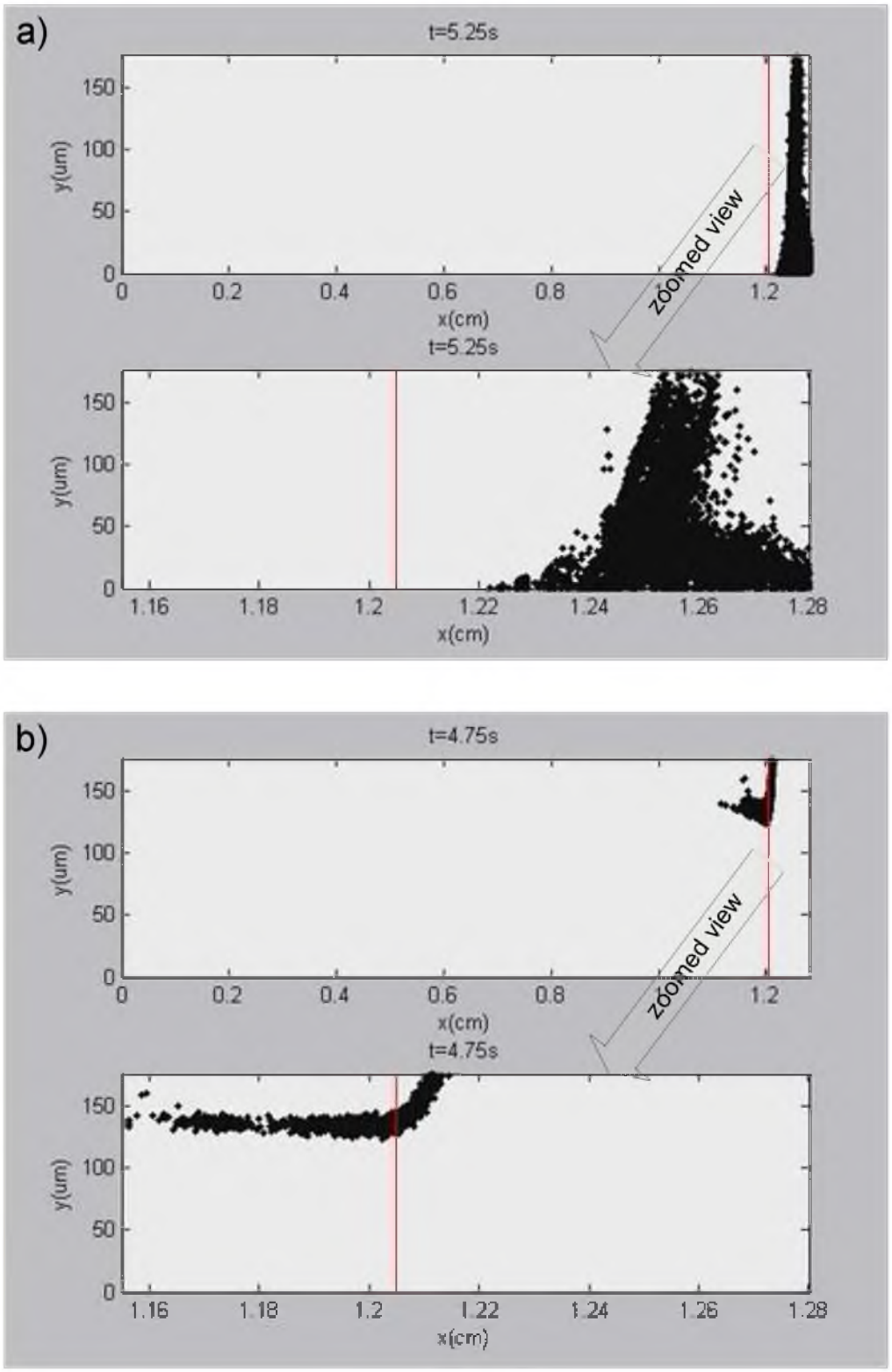

Figure 2.8. Particle simulations at the outlet of the channel. a) bottom wall is selected as the accumulation wall, b) top wall is selected as the accumulation wall.

continue to oscillate at the end of the channel, and it takes almost 2 minutes for all the particles to leave the channel. On the other hand, when the top channel wall is selected as the accumulation wall, particles that reach the end of the channel easily go through the outlet, without losing time in the channel. In Figure 2.8b, at t=5.25, all the particles have left the channel, whereas at the same time instant most of the particles still remain inside the channel (Figure 2.8a).

Figure 2.9 shows the UV fractogram corresponding to the selection of bottom wall as the accumulation wall. As can be seen, instead of a Gaussian shape peak, a peak with a long tail is observed. This also explains the tailing behavior witnessed in the experimental result shown in Figure 2.7a. According to this simulation, to achieve Gaussian shaped peaks in the fractograms, accumulation wall should be selected as the wall in which the outlet is located. Since in all of the current ElFFF systems the outlet is located on the top channel wall, the accumulation wall should be selected as the top wall to get rid of the tails in the UV fractograms.

As stated in the methods section, in all of the previous CyElFFF studies, 50% duty cycle voltage waveforms were used, with one exception, where Lao and coworkers applied unsymmetrical square waveforms in their system[5]. Since no rule of thumb exists for the selection of the duty cycle parameter, we decided to investigate the particle behavior for input voltages with different duty cycles. Mainly, we made the simulations with 50 and 70% duty cycle waveforms. Results can be seen in Figure 2.10.

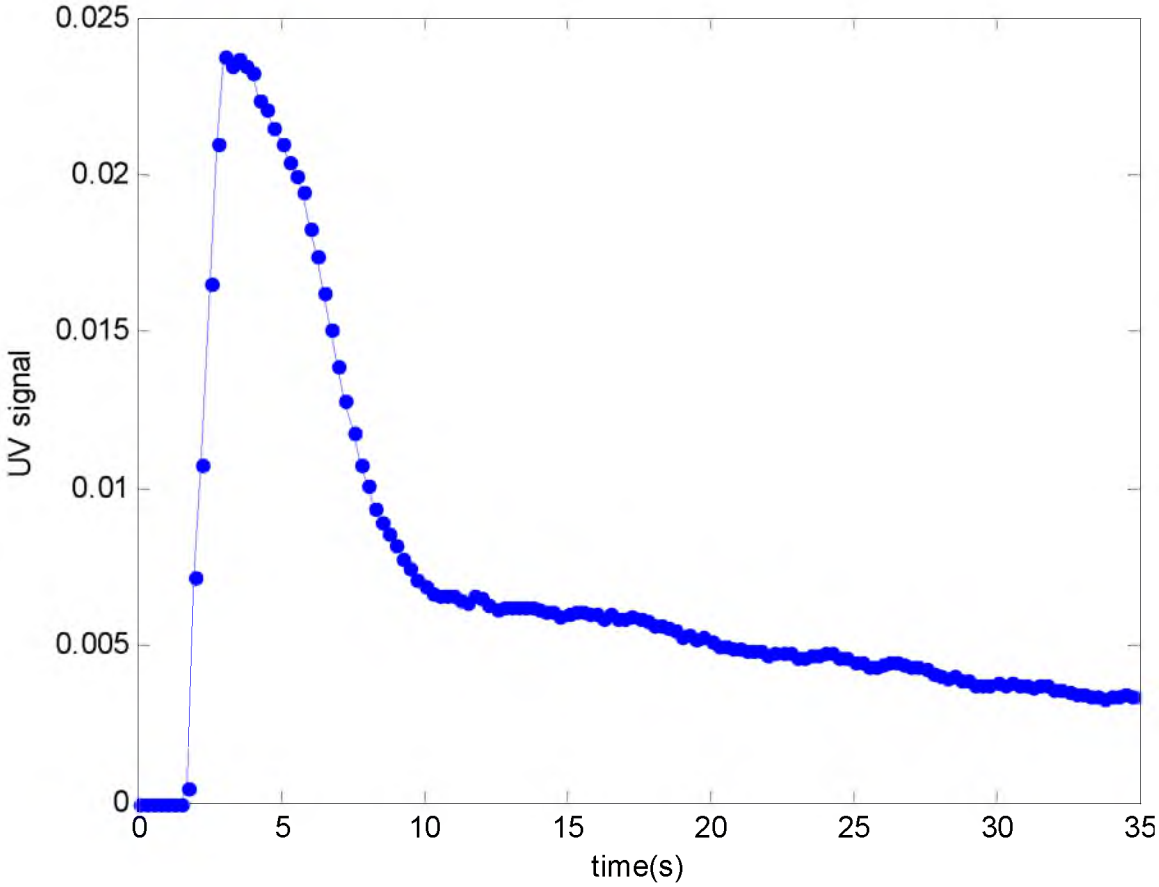

Figure 2.9. Simulated UV fractogram for 10nm gold nanoparticles when the bottom wall is selected as the accumulation wall. A significant tailing is observed in the peak. The input voltage used in the simulation had a 8.4Vpp magnitude and 1Hz frequency.

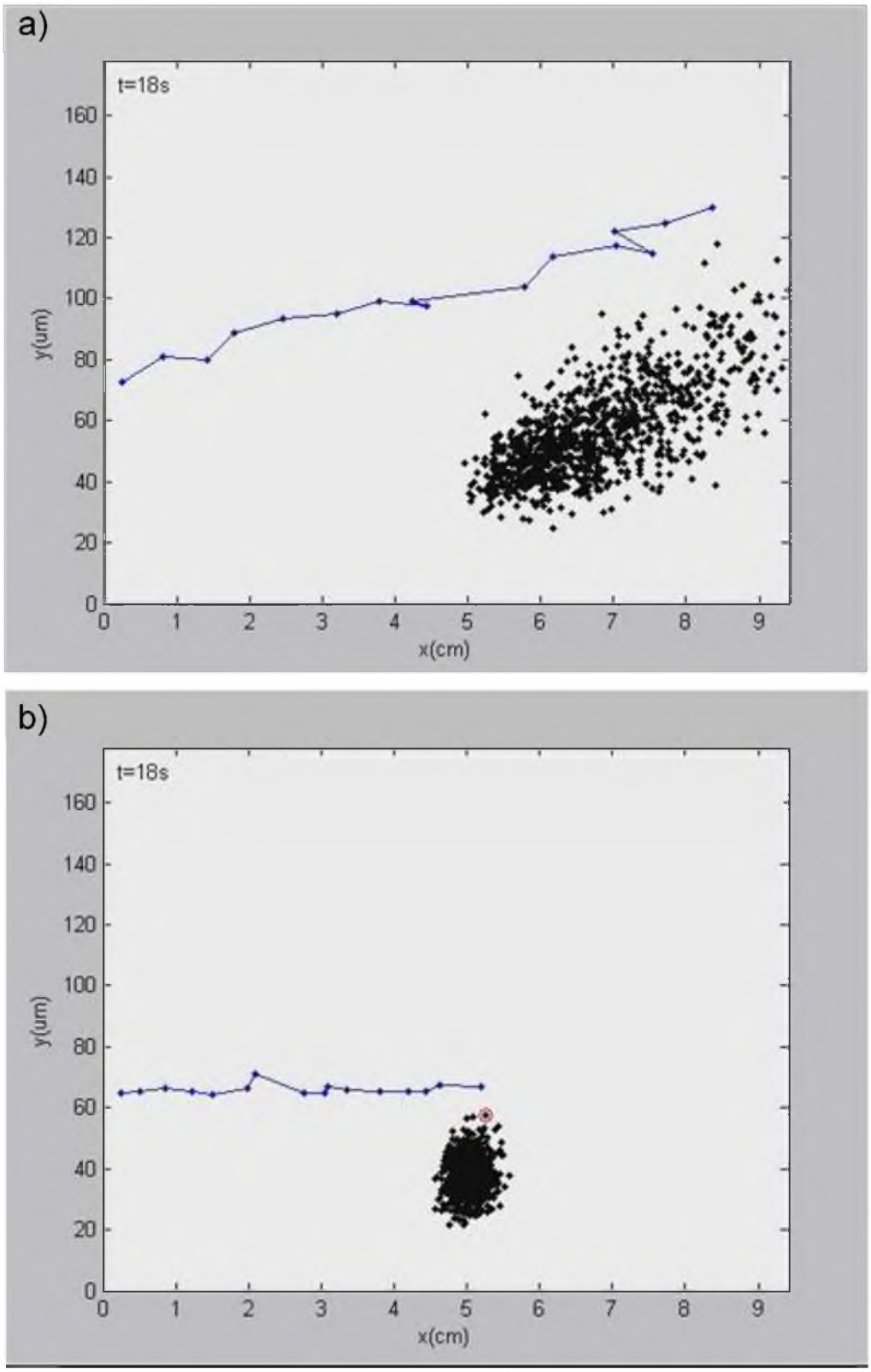

Figure 2.10. Particle simulations done with a) 50% duty cycle waveform, b) 70% duty cycle waveform. Remaining voltage parameters were Vamp=4Vpp and f=1Hz.

Figure 2.10 shows the particle behaviors in the first 9.25cm of the channel. Figure 2.10a corresponds to the situation where 50% duty cycle voltage is applied. In this simulation, at the end of each negative cycle, the x and y coordinates of the highest particle in the channel is picked and marked by a blue dot. As shown in Figure 2.10a, in each cycle, particles gain higher y-positions, and accordingly they move faster and faster throughout the channel. The particle cloud becomes more spread and eventually particle retention times in the channel drop drastically. When we check the result of the 70% duty cycle condition (Figure 2.10b), we observe that in each cycle, particles keep their y locations and their migration velocity remains almost constant. Consequently, particles spend more time inside the channel and they acquire much longer retention times compared to the 50% duty cycle case. As we look at Figure 2.10 again, we see that both plots are corresponding to the time instant of 18 seconds. While the particles in the top plot start to leave the channel, the particles in the bottom plot are still in the middle of the channel (around x=5cm). This simulation demonstrates that, to achieve high retention times, high duty cycle voltage waveforms are mandatory. High duty cycle voltages help the particles to return back to the channel wall at the end of each cycle. Thus, particles maintain their x velocity and gain high retention times inside the channel.

It has been shown that high duty cycle waveforms lead to high retention times in the channel. To see the effect of the high duty cycle voltages on the separation efficiency, separation simulations have been done with two different particles having electrophoretic mobilities of -3μmcm/Vs and -4μmcm/Vs. Particles used in the simulation were same sized particles with the diameter of 10nm. Particle simulations visualized in the first 3.25 cm of the channel can be seen in Figure 2.11.

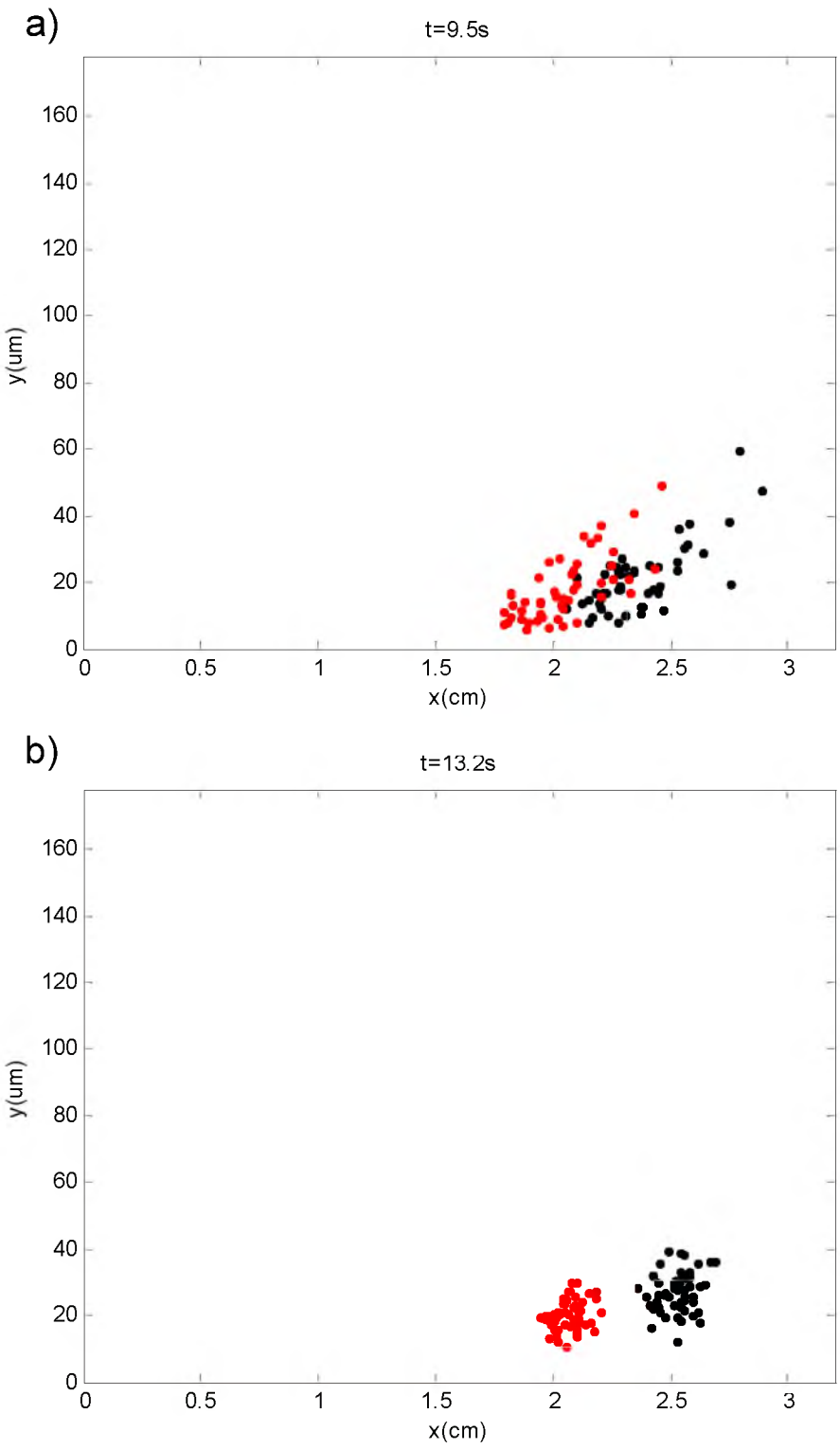

Figure 2.11. Particle separation simulations done with a) 50% duty cycle waveform, b) 70% duty cycle waveform. Remaining voltage parameters were Vamp=4Vpp and f=1Hz.

As shown in Figure 2.11a, when we use 50% duty cycle waveforms, particle clouds cannot be separated and particles spread in the channel. On the contrary, when we use 70% duty cycle voltages (Figure 2.11b), particles are completely separated. In addition, particle clouds maintain their forms without spreading in the channel. The resulting UV fractograms of the separation simulations are presented in Figure 2.12.

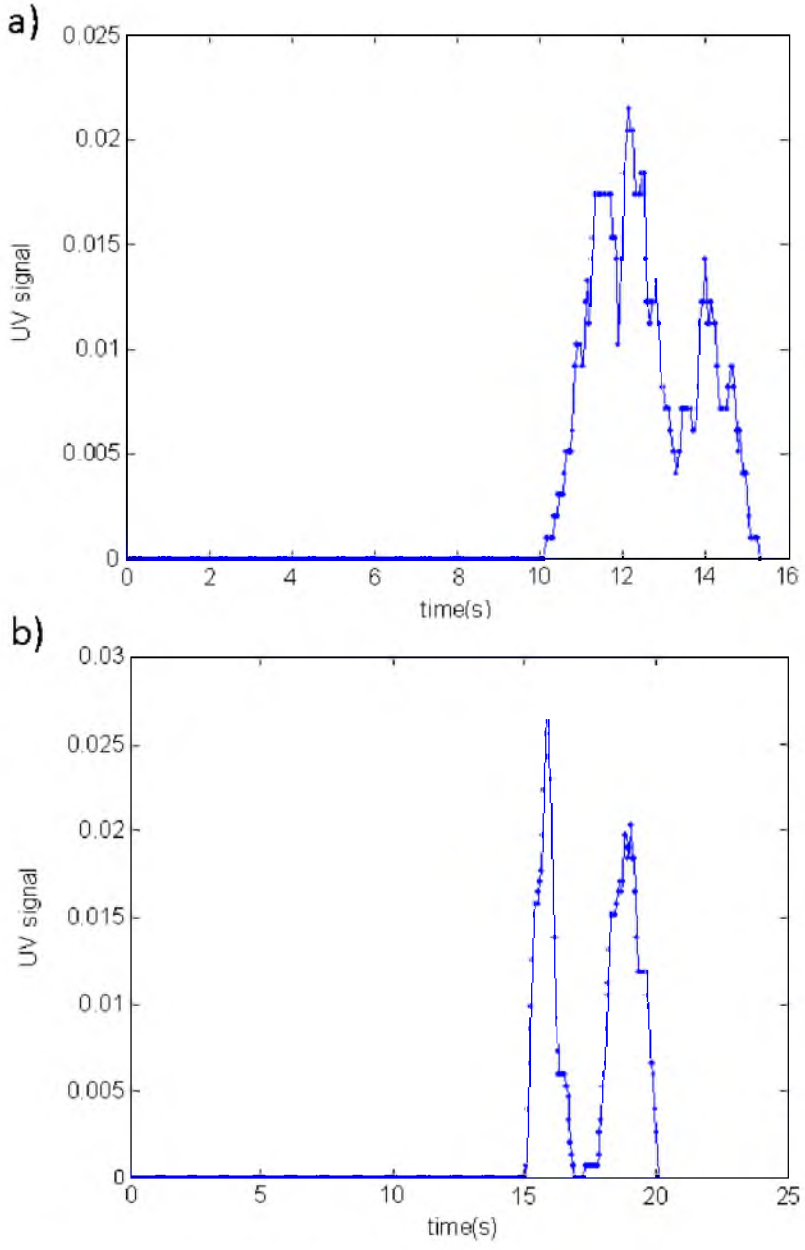

Figure 2.12, Simulated UV fractograms of the particles obtained for the application of a) 50% duty cycle waveform, b) 70% duty cycle waveform. Vamp=4Vpp and f=1Hz.

As shown in Figure 2.12a, no separation is observed in the UV fractogram for the 50% duty cycle case (peaks are combined). In contrast, a baseline separation is achieved in the 70% duty cycle case (Figure 2.12a). The UV fractograms of Figure 2.12 also reveal the retention times of the particles. For 50% duty cycle condition, all the particles are eluted before 16 seconds, whereas, for the 70% duty cycle condition, particles are eluted between 15 and 20 seconds, verifying that both particles achieved higher retention times with the application of higher duty cycle waveforms.

For the experimental verification of the separation simulations, two experiments were done with 10 and 40 nm gold nanoparticles. In the experiments, 10Vpp, 10Hz voltages were applied and two different duty cycles were tested, which were 50% and 80%. The carrier flow speed used in this experiment was 2ml/min. Figure 2.13 shows the UV fractograms obtained from the separation experiments.

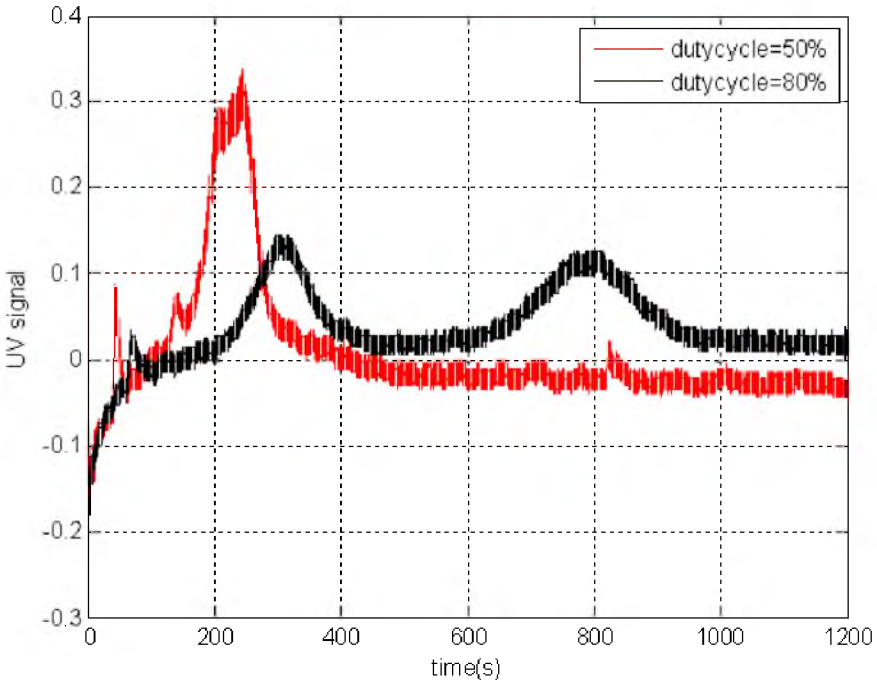

Figure 2.13 UV fractograms of 10 and 40 nm gold particles obtained for 50% and 80% duty cycle voltages. Vamp=10Vpp, f=10Hz, flow speed=2ml/min.

As clearly shown in Figure 2.13, baseline separation of the particles was achieved for the 80% duty cycle case. For the 50% duty cycle condition, no separation was achieved and all the particles were eluted before 300 seconds. By the help of this experiment, the outcomes of the separation simulations were verified. It has been experimentally and theoretically shown that high duty cycle waveforms produce much higher resolutions in the CyElFFF separations.

Conclusion

In this study, first particle based modeling of Electrical Field Flow Fractionation systems is achieved. The generated simulation code creates movie files which show the motions of individual particles in the channel. Particle visualization is very beneficial for understanding the effects of different operating conditions on the movements of the particles. It has been shown that the simulation code is capable of estimating the outcomes of the experiments both made by Normal and Cyclical ElFFF techniques. The UV fractograms obtained in the experiments have shown high agreement with the UV fractograms obtained from the simulations. In addition, by the accurate modeling of the channel outlet, it is demonstrated that the selection of the top channel wall as the accumulation wall gives higher quality peaks in the ElFFF systems. Furthermore, the behavior of the particles was simulated for 50% and higher duty cycle input voltages. It is verified by both simulations and experiments that high duty cycle voltages are necessary to get high retention times in the channel and to achieve high resolution separations in the CyElFFF systems.

The particle based simulation code created for the ElFFF systems is a powerful tool to estimate the outcomes of the separation experiments. Moreover, this tool can also be used to design systems with new geometries which may lead to further improvements in the separation efficiencies of the ElFFF systems.

References

[1] J. C. Giddings, "A new separation concept based on a coupling of concentration and flow nonuniformities," *Separation Science,* vol. 1, pp. 123-125, 1966.

[2] K. D. Caldwell, L. F. Kesner, M. N. Myers, and J. C. Giddings, "Electrical field-flow fractionation of proteins," *Science,* vol. 176, pp. 296-298, 1972.

[3] K. D. Caldwell and Y. S. Gao, "Electrical field-flow fractionation in particle separation. 1. Monodisperse standards," *Analytical Chemistry,* vol. 65, pp. 1764-1772, 1993.

[4] B. K. Gale and M. Srinivas, "Cyclical electrical field flow fractionation," *Electrophoresis*, vol. 26, pp. 1623-32, May 2005.

[5] A. I. Lao, D. Trau, and I.-M. Hsing, "Miniaturized flow fractionation device assisted by a pulsed electric field for nanoparticle separation," *Analytical Chemistry,* vol. 74, pp. 5364-5369, 2002.

[6] S. A. Palkar and M. R. Schure, "Mechanistic study of electrical field flow fractionation. 1. Nature of the internal field," *Analytical Chemistry,* vol. 69, pp. 3223-3229, 1997.

[7] J. J. Biernacki, P. M. Mellacheruvu, and S. M. Mahajan, "Electric circuit model for electrical field flow fractionation," *Analytical Chemistry,* vol. 78, pp. 4998-5005, 2006.

[8] Z. Chen and A. Chauhan, "Electrochemical response and separation in cyclic electric field-flow fractionation," *Electrophoresis*, vol. 28, pp. 724-739, 2007.

[9] B. K. Gale, K. D. Caldwell, and A. B. Frazier, "Geometric scaling effects in electrical field flow fractionation. 1. Theoretical analysis," *Analytical Chemistry,* vol. 73, pp. 2345-2352, 2001.

[10] J. J. Biernacki and N. Vyas, "A one-dimensional transient model of electrical field flow fractionation," *Electrophoresis*, vol. 26, pp. 18-27, 2005.

[11] Z. Chen and A. Chauhan, "Separation of charged colloids by a combination of pulsating lateral electric fields and poiseuille flow in a 2D channel," J*ournal of Colloid and Interface Science*, vol. 282, pp. 212-222, 2005.

[12] A. Kantak, S. Merugu, and B. K. Gale, "Improved theory of cyclical electrical field flow fractionation," *Electrophoresis*, vol. 27, pp. 2833-43, Jul 2006.

[13] J. Gigault, B. K. Gale, I. Le Hecho, and G. t. Lespes, "Nanoparticle characterization by cyclical electrical field-flow fractionation," *Analytical Chemistry,* vol. 83, pp. 6565-6572, 2011.

[14] A. Kantak, M. Srinivas, and B. Gale, "Characterization of a microscale cyclical electrical field flow fractionation system," *Lab Chip*, vol. 6, pp. 645-54, May 2006.

[15] A. S. Kantak, M. Srinivas, and B. K. Gale, "Effect of carrier ionic strength in microscale cyclical electrical field-flow fractionation," *Analytical Chemistry,* vol. 78, pp. 2557-2564, 2006.

[16] H. J. Sant and B. K. Gale, "Microscale field-flow fractionation: theory and practice," in *Microfluidic Technologies for Miniaturized Analysis Systems*, ed: Springer, 2007, pp. 471-521.

[17] W. Somchue, A. Siripinyanond, and B. K. Gale, "Electrical field-flow fractionation for metal nanoparticle characterization," *Analytical Chemistry,* vol. 84, pp. 4993-4998, 2012.

[18] M. Srinivas, H. J. Sant, and B. K. Gale, "Optimization of cyclical electrical field flow fractionation," *Electrophoresis*, vol. 31, pp. 3372-9, Oct 2010.

[19] W. Sutherland, "LXXV. A dynamical theory of diffusion for non-electrolytes and the molecular mass of albumin," *Philosophical Magazine Series* 6, vol. 9, pp. 781-785, 1905.

[20] S. Merugu, H. J. Sant, and B. K. Gale, "A novel method for effective field measurements in electrical field-flow fractionation," *Electrophoresis*, vol. 33, pp. 1040-1047, 2012.

[21] H. J. Sant, S. Chakravarty, S. Merugu, C. G. Ferguson, and B. K. Gale, "Characterization of polymerized liposomes using a combination of dc and cyclical electrical field-flow fractionation," *Analytical Chemistry,* vol. 84, pp. 8323-8329, 2012.

CHAPTER 3

UTILIZATION OF HIGH DUTY CYCLE VOLTAGE WAVEFORMS FOR HIGH RESOLUTION ELECTRICAL FIELD FLOW FRACTIONATION

Introduction

The ability to generate and characterize monodisperse nanoparticles is key to their rapidly developing applications in medicine, biology, chemistry, electronics, physics, energy, and other fileds[1]. As the applications for a wide variety of nanoparticles increase, finding analytical techniques useful in their characterization and separation becomes crucial. Methods such as chromatography[2, 3], electrophoresis[4, 5], and ultracentrifugation[6, 7] rely on high fields and are often damaging to the samples without providing the high resolution separations desired. A less well-known technique, field flow fractionation (FFF)[8], is a powerful method for the separation and characterization of nanoparticles and is rapidly gaining acceptance for nanoparticle analysis.

A strength of FFF is that the separation field is applied perpendicular to the carrier flow while particles migrate at different speeds down a channel based on their interaction level with that field. Thus, a relatively weak field can be used to generate substantial

separation and characterization information, including full distributions of particle properties and not just curve-fit estimates[9]. Based on the type of the separation field applied, different FFF methods have been established, such as electrical[10-12] magnetic[13-15], gravitational[16, 17], thermal[18, 19] and flow[20, 21] FFF.

Electrical field flow fractionation (ElFFF) is a subtechnique of FFF in which the separation field (electric field) is generated by applying a potential difference across the top and bottom walls (electrodes) of the separation channel. In this method, particles are sorted according to the relationship between their sizes and electrical properties (i.e., electrophoretic mobility).

ElFFF has been used to characterize a variety of particles, but only limited results have been obtained using small nanoparticles[22]. Beacuse retention in ElFFF is sensitive to surface charge and surface coatings, as well as particle size, ElFFF offers the ability to more thoroughly characterize electrical and surface properties of nanoparticles relative to other FFF methods and nanoparticle characterization techniques. Also, ElFFF channels can be fabricated fairly easily compared to other FFF instruments[10].

One major challenge in ElFFF is the reduced electrical field in the channel that results from the electrical double layer (EDL) formation on the channel walls. In traditional ElFFF, static voltages are applied to the channel walls, and typically the EDL is fully formed on the surface of the channel walls within approximately one minute[23]. As a consequence of the EDL, the electric field inside the channel drops to 3% or less of its initial value[24]. This major drawback gives rise to a considerable reduction in the separation efficiency of the ElFFF technique. To help overcome this limitation, researchers recently developed cyclical electrical field flow fractionation (CyElFFF)[23],

which is based on the general concept of cyclical FFF[25, 26]. In CyElFFF, cyclical (AC) voltages are used rather than a constant (DC) voltage. Since the polarities of the electrodes are changing in each cycle, insufficient time exists for the EDL to fully form at the electrode surface. As a result, much higher electric fields are achieved inside the channel, resulting in potentially improving separation efficiency. CyElFFF also has significant operational advantages over other techniques, including FFF techniques, because separations and retention in CyElFFF can be readily tuned and optimized by varying the magnitude, frequency and/or the shape of the applied voltage[9].

A typical cyclical ElFFF system is composed of top and bottom electrodes as shown in Figure 3.1. The flow inside the CyElFFF channel is laminar with a parabolic flow profile. A cyclical voltage is applied on the channel walls (electrodes), which causes the particles to move back and forth between the walls. In Figure 3.1, the trajectories of two particles having different electrophoretic mobilities are presented for three cycles of an applied square wave voltage. In each cycle, the particle having a higher electrophoretic mobility reaches distances farther into the middle of the channel, thereby attaining greater down-channel fluid velocities relative to the particle having a lower electrophoretic mobility, which stays relatively close to the channel wall. Consequently, the lower mobility particle moves much slower in the z-direction and elutes later than the higher mobility particle.

Several previous particle separation studies have used CyElFFF with a variety of nanoparticle types[23, 27-31]. However, separations using this technique have been reported only for particles larger than 100 nm. As an example of separations, Lao et al.[27] showed a baseline separation of 105 and 450 nm polystyrene particles. Since

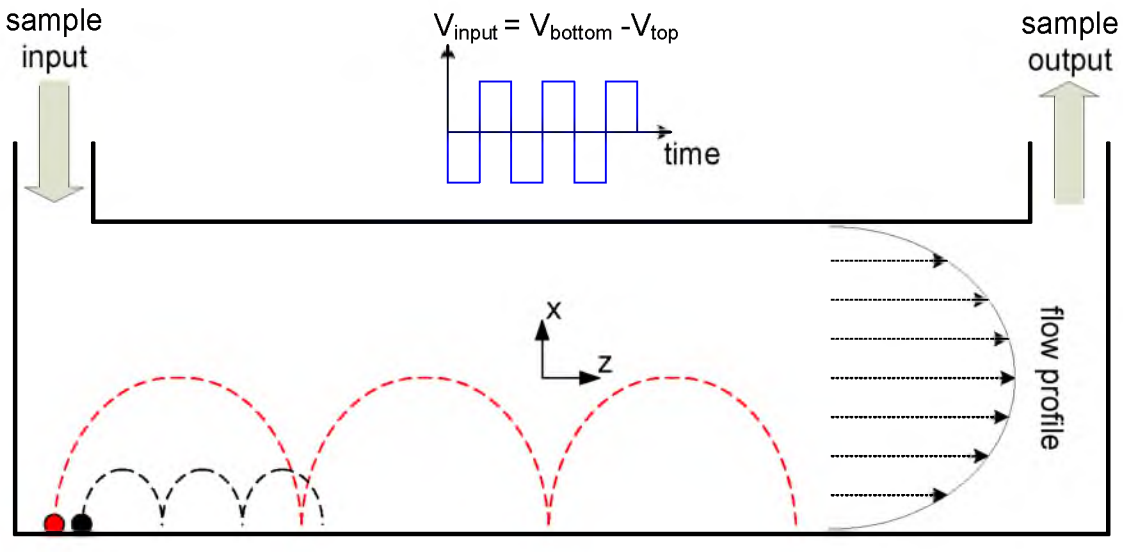

Figure 3.1 Operational principle of a typical CyElFFF system. The dashed lines show the motion of two particles (having different electrophoretic mobilities) for 3 cycles of an applied square wave voltage. (Figure is not to scale, it is rescaled for better visualization of particle motions. In ElFFF systems, the channel length is at least 1000 times longer than the channel height)

particle diffusion is much larger for smaller particles, diffusion limits fractionation of sub 100 nm particles in previously-reported CyElFFF studies.

In this work, we address the diffusion-induced limitation on nanoparticle separation by implementing fields designed to counteract diffusion by re-setting particle positions at the channel wall. We refer to this approach to CyElFFF as *biased* Cyclical Electrical Field Flow Fractionation (BCyElFFF), and the primary method used to accomplish this bias is an unequal duty cycle waveform, which is similar to Mode 4 as described by Lee, et al.[26]. In this work, bias in the voltage waveform is achieved using duty cycles greater than 50%, such that the positive cycle of the applied voltage has a longer duration than the negative cycle. Using this BCyElFFF technique, we have achieved high-resolution separations of 15 and 40 nm gold nanoparticles and we have provided a theoretical analysis to accomplish these separations. Biased cyclical electrical

field flow fractionation extends cyclical electrical FFF to sub 50 nm nanoparticles, and provides a new complement to flow- and sedimentation-FFF nanoparticle separation techniques, as well as other nanoparticle separation techniques[2-5].

Results and Discussion

To examine the effect of applying high duty cycle waveforms and to investigate the fractionation efficiency for different operating conditions (i.e., for different duty cycles, frequencies, and voltage amplitudes), a series of separation experiments have been conducted. In all the experiments, a mixture of 15 and 40 nm spherical gold nanoparticles were used.

Dut C cle ffect

Duty cycle (bias) values were varied to determine those that produced the highest-resolution separation. Square wave voltages with duty cycles ranging from 50% to 80% were applied. The frequency and amplitude of the applied voltages were 10Hz and 10Vpp respectively (f=10Hz, V_{amp}=10Vpp).

For the application of a 50% duty cycle waveform, retention time was less than 5 minutes and no separation occurred (Figure 3.2). Furthermore, no separation occurred in response to the superposition of a DC offset voltage on the 50% duty cycle AC voltage, although the retention time was slightly increased to more than 5 minutes. Notably, application of an offset voltage superimposed with a 50% duty cycle square wave was suggested to yield optimal separation in earlier CyElFFF work[23, 27-31]. However, the results presented in these papers were limited by the buildup of the electric double layer,

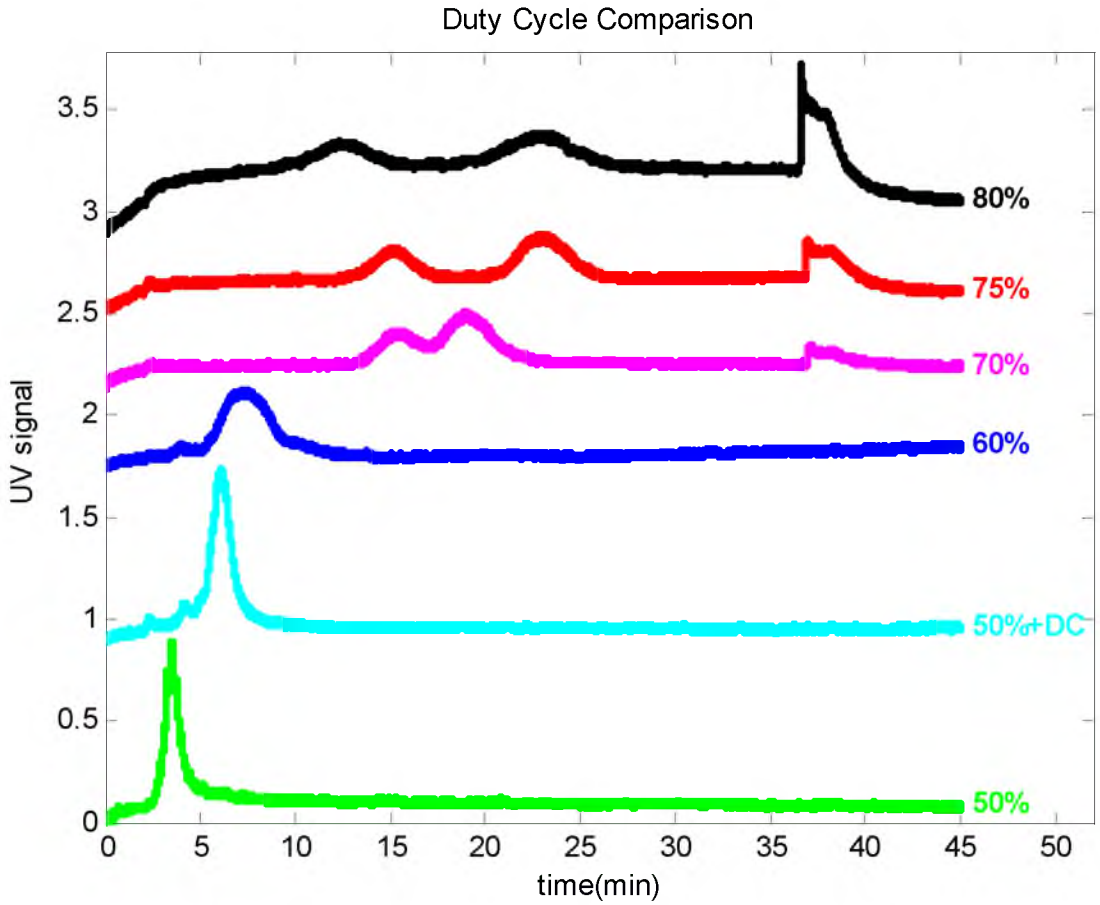

Figure 3.2. UV fractograms for the duty cycle comparison experiments. Electrical parameters were *f*=10Hz, *Vamp*=10Vpp.

which generated a rapid decay of the applied offset voltage such that the diminished field was overcome by the robust diffusion of nano-range particles.

Increased bias in the applied voltage (increased duty cycle from 60% to 75%) yielded a significant increase in retention time and initiation of baseline separation of the 15 nm and 40 nm particles, the latter having the longer retention time (Figure 3.2), as described further below. As duty cycle was further increased to 80%, peaks widened, and the resolution of the separation decreased. Among all experiments, the highest–resolution separation was achieved for the 75% duty cycle, and this duty cycle (*dc**) was used for all remaining experiments.

The results observed in Figure 3.2 show that duty cycles greater than 50% are essential to achieve high-resolution separations of nanoparticles. To our knowledge, the separations presented here are the first reported separations of sub 50 nm particles using CyElFFF.

Figure 3.2 also shows that for duty cycles larger than 60%, there is a "power-off" peak in the UV fractogram (i.e., after the power was turned off at t=37min). The peak seems likely to consist of particles previously immobilized on the electrodes (walls), that are released upon removal of the field. It is evident that for higher duty cycles, the power-off response also becomes larger. Notably, when the voltage is removed, a significant "reverse" current is observed, possibly driving the immobilized particles off the channel walls.

Experiments in which the 15 nm and 40 nm particles were injected individually (f=10Hz, *Vamp*=10Vpp and $dc = dc^*$) show elution of 15-nm particles at approximately 14 minutes, and 40nm particles at approximately 22 minutes (Figure 3.3). This result is in qualitative agreement with the electrophoretic mobilities of the particles, which are greater for the 15 nm particles relative to the 40 nm particles (Table 3.3). The separation occurs in Mode I according to Lee et al.[26], the higher electrophoretic mobility particles move closer to the middle of the channel, and therefore elute earlier.

Voltage Amplitude Effects

Voltage amplitudes ranging from 4Vpp to 11Vpp were applied with the constant conditions of f=10Hz and dc=dc^*. The maximum possible voltage to be applied was

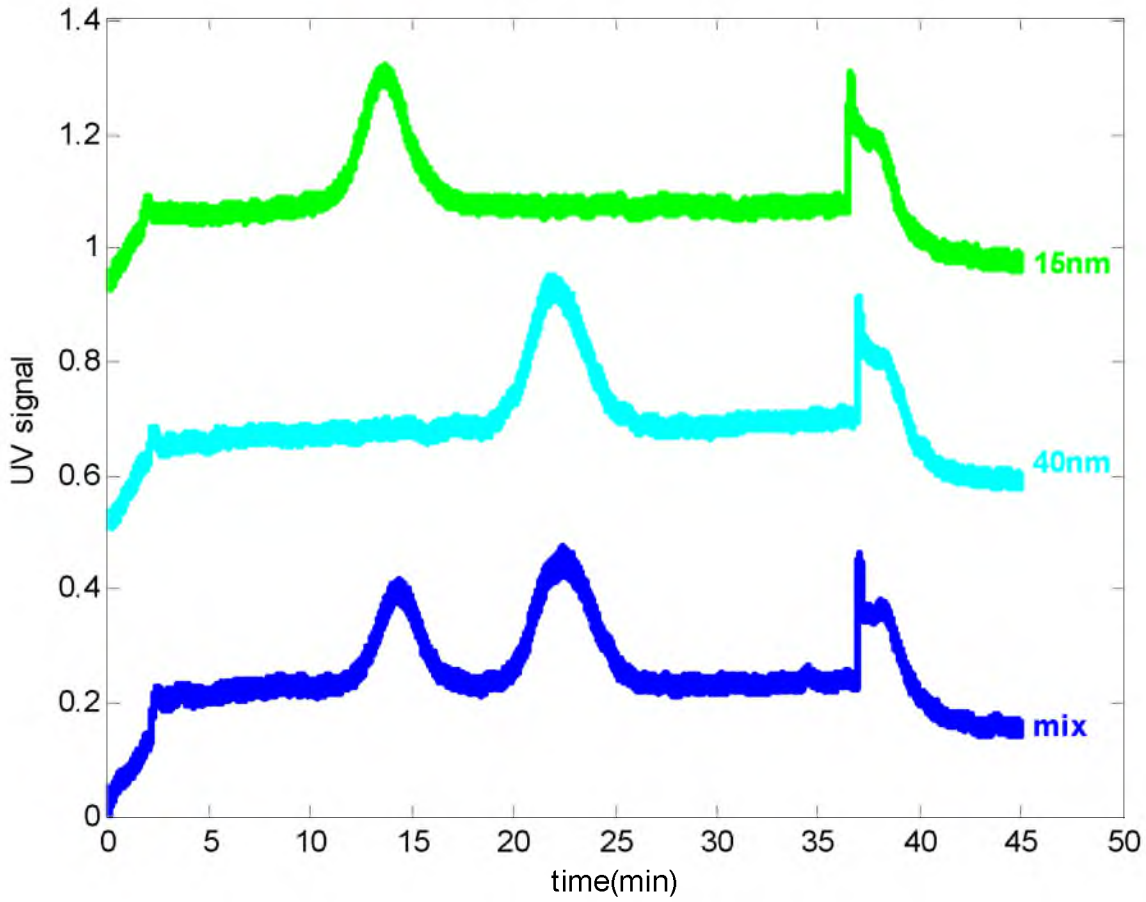

Figure 3.3. UV fractograms obtained for the individual injections of the particles. Electrical parameters were *f*=10Hz, *Vamp*=10Vpp, *dc*=75%.

11Vpp, since for voltages higher than 11Vpp, electrolysis of the carrier begins in the channel and air bubbles are created, which disturb the separation process.

For low voltage amplitudes, such as 4Vpp, the efficiency of the separation was very low (Figure 3.4) and particles were negligibly separated. The resolution of the separation increased as we raised the applied voltage from 4Vpp to 10Vpp, and the highest resolution was obtained for the 10Vpp case. For the 11Vpp condition, peak widths became significantly larger and the resolution of the separation dropped.

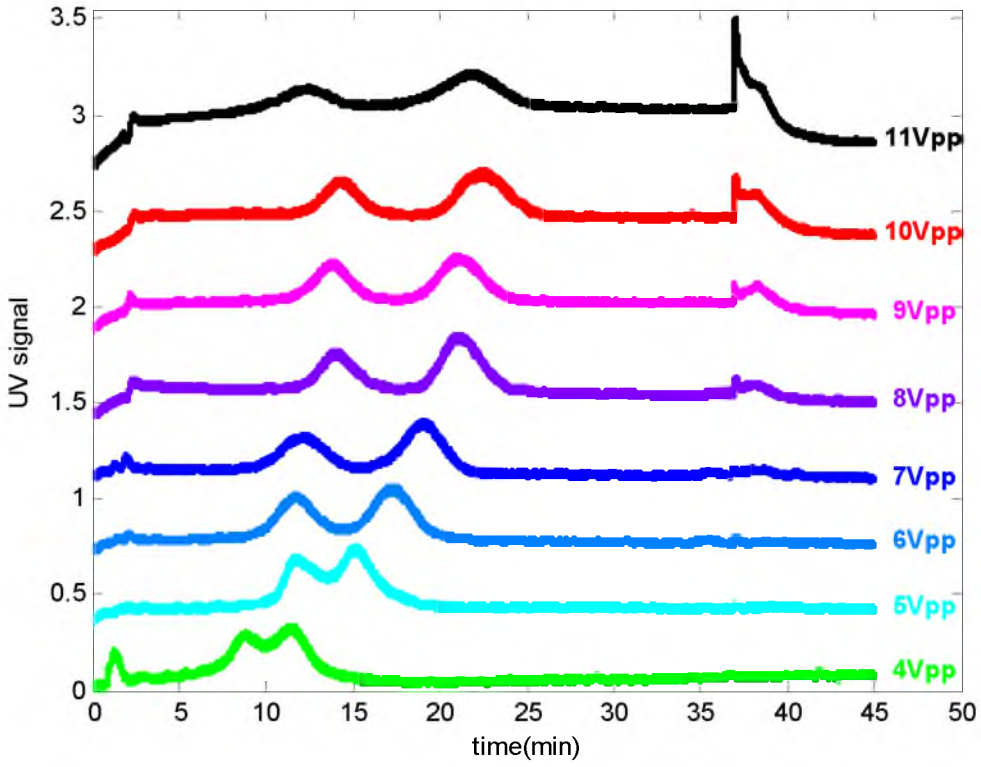

Figure 3.4. UV fractograms obtained at different voltage amplitudes. Electrical parameters were *f*=10Hz, *dc*=75%.

For voltages higher than 7Vpp (at t=37min), the power-off response (particle release) became significant. More particles were released as the voltage increased (Figure 3.4), with the largest increase corresponding to the 11Vpp case.

Frequency Effects

Frequencies ranging from 2Hz to 36 Hz were applied with the constant conditions of Vamp=10Vpp and dc=*dc**. Optimal separation results were obtained for mid-range frequencies (Figure 3.5), such as 8-14Hz. For the 2Hz condition, particles were poorly separated and the overall retention time was very low. As frequency was increased, both retention time and separation resolution increased (Figure 3.5). For frequencies above 14Hz, retention times dropped and separation resolutions decreased, though the peak

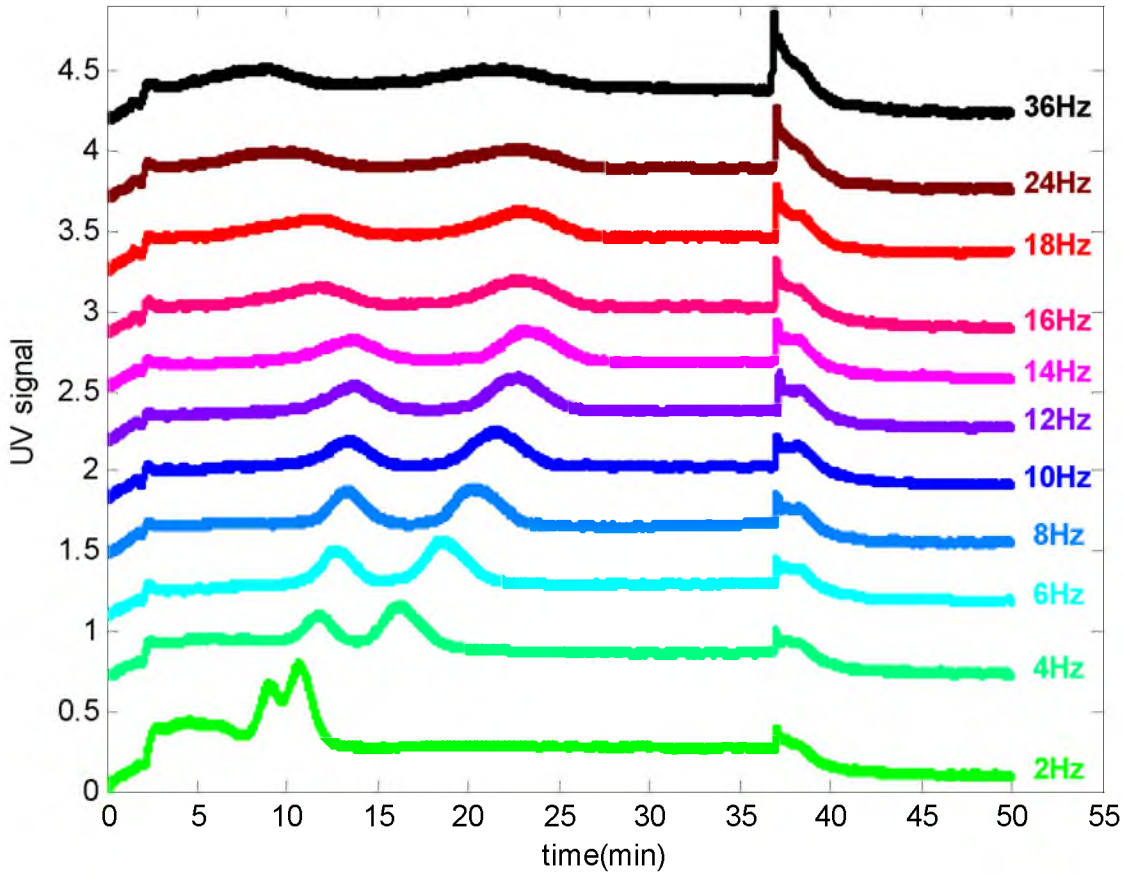

Figure 3.5. UV fractograms obtained at different frequencies. Electrical parameters were *Vamp*=10Vpp, *dc*=75%.

resolutions remain significantly improved relative to low frequencies. Power-off responses were greater at higher frequencies, which might suggest that the number of particle–surface (electrode) interaction events, which are directly proportional to the frequency of the applied field, cause particles to stick to the channel walls.

All fractograms clearly showed that application of a voltage bias via high duty cycle allows separation of sub-50 nm nanoparticles. Furthermore, separation efficiencies can be optimized via changes in the amplitude and frequency of the biased voltage. The mechanisms behind these influences are explored below.

The velocity (v_p) of a particle moving under the influence of a constant electric field is represented by

$$v_p = \mu_p \times E_{eff} \qquad \textbf{(3.1)}$$

where μ_p is the electrophoretic mobility of the particle $(m^2V^{-1}s^{-1})$ and E_{eff} (Vm^{-1}) is used to denote the effective electric field inside the BCyElFFF channel.

In addition to the electrically-driven motion, particle diffusion contributes significantly to its trajectory. The linear unidirectional diffusion length achieved by a particle is obtained from random walk theory as follows[33]

$$l_d = \sqrt{2Dt} \qquad \textbf{(3.2)}$$

where D (m^2s^{-1}) is the diffusion coefficient of the particle and t (s) is time. The diffusion coefficient of a spherical particle is calculated using the Stokes-Einstein equation[34].

$$D = \frac{Tk_b}{3\pi\eta d} \qquad \textbf{(3.3)}$$

where T (K) is temperature, k_b (JK^{-1}) is Boltzmann's constant, η (Pa·s) is the dynamic viscosity of the carrier liquid and d (m) is the particle diameter.

Since particle diffusion is inversely proportional to particle size (equation 3.3), attainment of significant retention times and high-resolution separations involves opposing the diffusion of nanoparticles away from the channel walls by applying suitable electrical fields.

The diffusion length of a particle in the x-direction, during one cycle of the electric field can be written as

$$l_{dx} = \sqrt{\frac{2D}{f}} \qquad \textbf{(3.4)}$$

Equation 3.4 is obtained from equation 3.2 by replacing t with the time length of 1 period of the cyclical voltage (f^{-1}).

A schematic trajectory of a negatively charged particle for a 50% duty cycle (dc) input voltage waveform is shown in Figure 3.6a. Here V_{input} is the voltage applied to the electrodes ($V_{input} = V_{bottom\text{-}electrode} - V_{top\text{-}electrode}$).

The distance traveled by the particle toward the opposite electrode due to the negative cycle of the input voltage is given by l_{e-}, and the per-cycle distance traveled in the same direction via diffusion is given by l_{dx}. Diffusion away from the channel wall has the greatest negative effect on resolution, since diffusion in the x-direction causes particles to spread across the large fluid velocity gradient, leading to a greater range of down-channel velocities among the particle population and peak broadening in the fractogram. In addition, if the particle is cycling in the bottom half of the channel (i.e., between the bottom channel wall and the middle of the channel) the diffusion occurring in the $+x$ direction (away from the channel wall) always results in higher particle velocities and lower retention times. Since particle diffusion away from the channel wall reduces both retention time and separation resolution, a method to counteract the diffusion, such as the application of biased-voltage waveforms, would be valuable.

With this basis, the scenarios in Figure 3.6 show that the unbiased electrical field (50% duty cycle) (Figure 3.6a) promotes the greatest particle diffusion away from the electrode (wall), since the net electrical displacement ($l_e = l_{e-} - l_{e+}$) is zero, and therefore smaller than the diffusion length ($l_e < l_{dx}$). As an outcome, the particle moves into the channel by $+l_{dx}$ during each cycle, yielding a decreased resolution and retention.

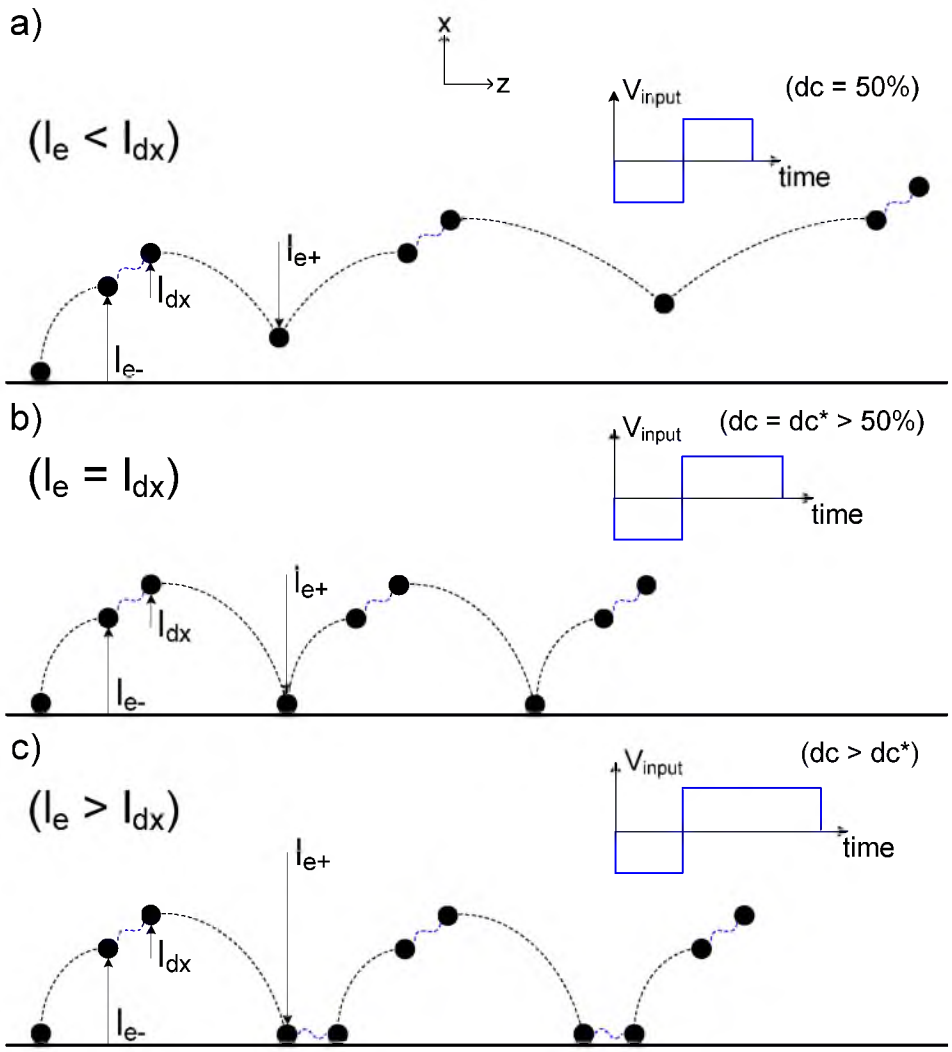

Figure 3.6. Particle trajectories for 3 different duty cycle (*dc*) conditions.
a) $dc = 50\%$, $(l_e < l_{dx})$; b) $dc = dc^* > 50\%$, $(l_e = l_{dx})$; c) $dc > dc^*$, $(l_e > l_{dx})$

To avoid resolution and retention loss resulting from diffusion, the electric field can be used to reset all particle locations to the channel wall. That is, l_{e+} must be greater than or equal to $l_{e-} + l_{dx}$ (Figure 3.6b,c), and this can be done by biasing the duration of the positive voltage relative to that of the negative voltage. Figure 3.6b shows the condition when the net electrical displacement is equal to the diffusion length ($l_e = l_{dx}$), such that the particle reaches to the channel wall at the end of each cycle. We refer to the duty cycle corresponding to this condition as dc* which is higher than a 50% duty cycle.

Increasing the duty cycle further ($dc>dc^*$) ultimately yields l_e greater than l_{dx} ($l_e > l_{dx}$), such that the particle resides on the electrode (wall) for a significant time during each cycle, allowing more time for diffusion to dominate (Figure 3.6c); this would lead to slightly increased band broadening and longer retention times in the resulting UV fractogram. Particles may also become immobilized on the electrode, yielding the observed "power off" signal in the fractogram (Figure 3.4).

In summary, based on the above analysis, we expect that among the three operating conditions ($l_e < l_{dx}$, $l_e = l_{dx}$ and $l_e > l_{dx}$) represented in Figure 3.6 the $l_e = l_{dx}$ operating condition is optimal to achieve high resolution separations.

Tabulating l_{dx} and l_e values for the 15 nm particles (Table 3.1 and Table 3.2), which have longer diffusion lengths than the 40 nm particles, shows that the best separation results were obtained for l_e/l_{dx} values closest to 1 (i.e., $l_e \approx l_{dx}$). For the experiments made with different voltage amplitudes, the highest separation resolution (Rs=1.69) was obtained for V_{amp}=10Vpp and the corresponding l_e/l_{dx} ratio was 1.05.

Results of the experiments made with different frequencies (Table 3.1) show that the best separation resolution (Rs=1.66) was achieved for f=8Hz, where the corresponding l_e/l_{dx} ratio was 0.96.

The tabulated l_e/l_{dx} ratios from Table 3.1 and 3.2 are also plotted in Figure 3.7, which shows that as the voltage was increased from 4Vpp to 10Vpp (Figure 3.7a), the l_e/l_{dx} ratio and resolution increased, and the highest resolution was obtained when l_e was nearly equal to l_{dx} (obtained for Vamp=10Vpp). As the voltage amplitude was further increased, l_e exceeded l_{dx} , and separation resolution decreased.

Table 3.1. Results of the amplitude variation experiments

Amplitude(Vpp)	$l_{e\text{-}}$(μm)	l_{dx}(μm)	l_e(μm)	l_e/l_{dx}	Resolution
4	10.49	3.12	0.75	0.24	0.65
5	11.18	3.12	1.02	0.33	0.79
6	12.21	3.12	1.56	0.50	1.12
7	12.5	3.12	2.18	0.70	1.37
8	13.87	3.12	2.53	0.81	1.54
9	13.45	3.12	2.49	0.80	1.56
10	**14.23**	**3.12**	**3.29**	**1.05**	**1.69**
11	14.95	3.12	3.92	1.25	1.25

Table 3.2. Results of the frequency variation experiments

Frequency(Hz)	$l_{e\text{-}}$(μm)	l_{dx}(μm)	l_e(μm)	l_e/l_{dx}	Resolution
2	78.28	6.98	18.39	2.63	0.70
4	37.91	4.94	8.23	1.67	1.03
6	25.3	4.03	5.21	1.30	1.39
8	**17.83**	**3.49**	**3.36**	**0.96**	**1.66**
10	13.94	3.12	2.5	0.81	1.61
12	11.55	2.85	2.26	0.79	1.59
14	9.89	2.64	1.97	0.75	1.56
16	8.37	2.47	1.69	0.68	1.44
18	7.29	2.33	1.53	0.66	1.39
24	5.31	2.02	1.19	0.59	1.23
36	3.32	1.65	0.81	0.49	1.14

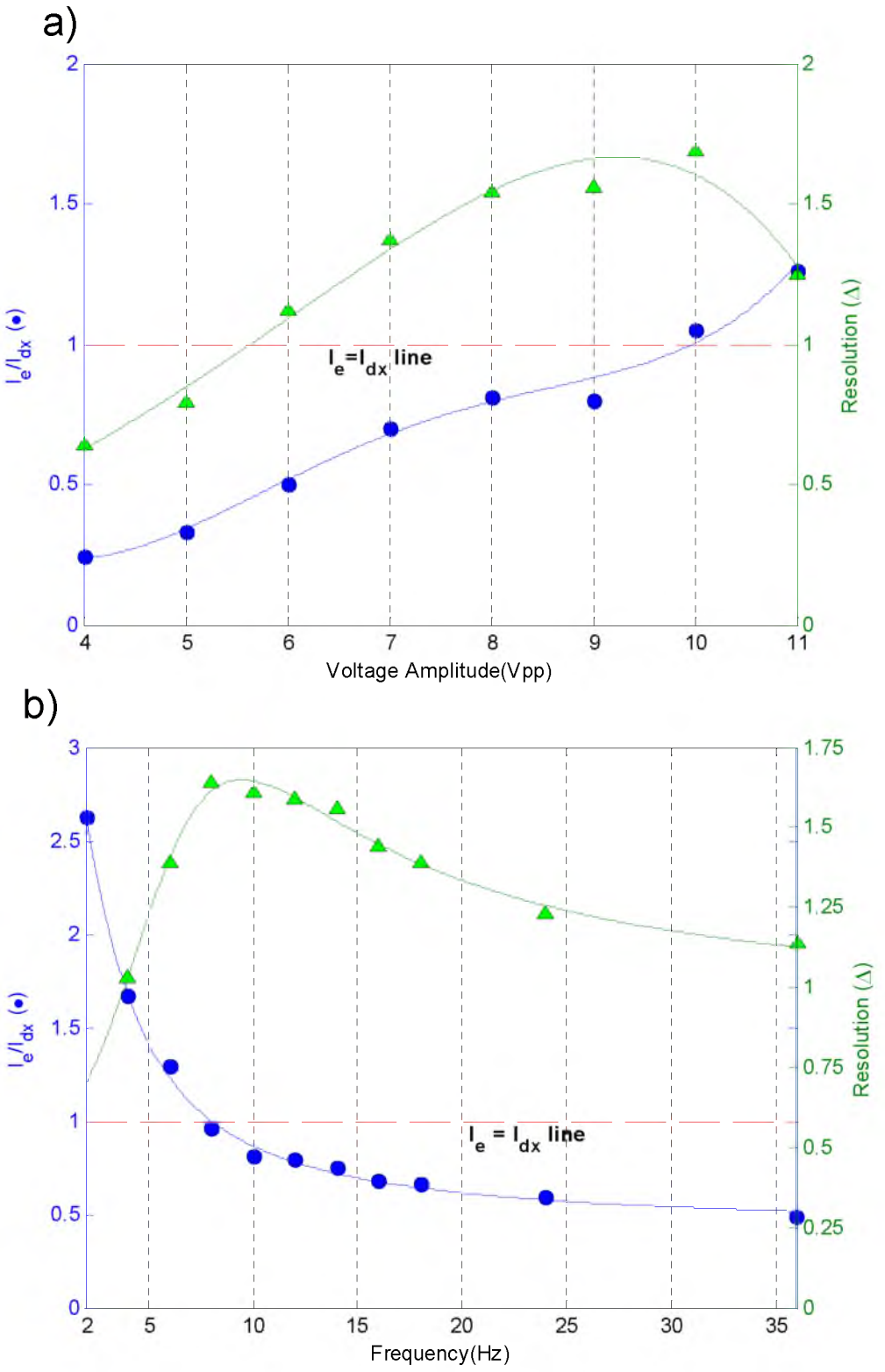

Figure 3.7. l_e/l_{dx} ratios and separation resolutions. a) Amplitude variation experiments b) Frequency variation experiments. Circle (o) represents l_e/l_{dx} and triangle (Δ) represents resolution.

For very low frequencies (Figure 3.7b), l_e was much higher than l_{dx}, and resolution was low. As frequency was increased, l_e approached l_{dx}, and the highest resolution was obtained for l_e approximately equal to l_{dx}, as was the case for f=8Hz. Further increases in frequency diminished l_e relative to l_{dx}, and resolution decreased.

The above analysis demonstrates that the highest resolution separation of sub 50 nm nanoparticles using BCyElFFF occurs when voltage parameters are such that the net per cycle electrical displacement (l_e) is equal to the per cycle diffusion length (l_{dx}). This condition ($l_e = l_{dx}$), made possible the high-resolution separation of 15 and 40 nm nanoparticles, as demonstrated above. For suboptimal conditions where $l_e < l_{dx}$, diffusion leads to net particle transport toward the channel center during each cycle, yielding decreased separation efficiency. Fields producing l_e greater than l_{dx} promote diffusion of particles on the channel wall, leading to band broadening in the UV fractogram.

For further examination of the $l_e = l_{dx}$ condition, this equality can be written in open form as shown below:

$$l_e = \mu_p \int_0^{1/f} E_{eff}(t)dt = \sqrt{\frac{2D}{f}} = l_{dx} \quad \textbf{(3.5)}$$

The net per cycle electrical displacement of the particle is calculated by taking the integral of the electric field inside the channel in one cycle. By collecting the particle related terms to the left side of the equation and electrical parameters to the right side, the following expression can be obtained.

$$\frac{\sqrt{2D}}{\mu_p} = \frac{1}{\sqrt{f}}\left[dc(E_{eff}^{+} + E_{eff}^{-}) - E_{eff}^{-} \right] \quad \textbf{(3.6)}$$

Here E_{eff}^{+} is the magnitude of the electric field in the positive cycle of the voltage and E_{eff}^{-} is the magnitude of the electric field during the negative cycle. The values of E_{eff}^{+} and E_{eff}^{-} depend on many parameters, such as the applied voltage amplitude, duty cycle, electrical properties of the electrode, ionic strength of the carrier solution and the channel height. Even if it is hard to estimate E_{eff}^{+} and E_{eff}^{-}, their values are increasing with the increased input voltage amplitude (V_{amp}), and decreasing with the decreased V_{amp}. For a dc of 50%, E_{eff}^{+} and E_{eff}^{-} becomes equal and the term in brackets turn outs to be 0. For increasing dc values (dc>50%), the bracketed term increases and similarly while dc is bigger than 50%, increasing V_{amp} also increases the value of the term in brackets.

Equation 3.7 can be effectively used for the determination of optimal operating conditions for the BCyElFFF system. This equation was satisfied for the 15nm gold particles of this study for V_{amp}=10Vpp, f=8Hz and dc=75%. For smaller particles(<15nm), D will become higher and to compensate it, f can be decreased or dc and/or V_{amp} can be increased. For a higher mobility particle, to satisfy the equation, frequency can be increased or dc and/or V_{amp} can be decreased.

While equation 3.7 can be used to reach the optimal operating conditions, it should be noted that there are limits to the range of voltages or frequencies that can be applied. High voltages and low frequencies can lead to particles crossing the middle of the channel, which is beyond the operating mode in which the optimal condition l_e=l_{dx} is valid. Thus, l_{e-} should also be checked and it should be validated that l_{e-} is less than the half of the channel height. Another limiting property of high voltages and low frequencies is that they tend to cause electrolysis and bubble formation in the channel, which can disturb particle retention and separation.

In summary, to operate the BCyElFFF system at optimal conditions, system should be run in the $l_e=l_{dx}$ state, and to ensure this condition, parameters can be selected according to equation 3.7 as explained in detail above.

Conclusion

High diffusivities of nanoparticles play a detrimental role in the fractionation capability of CyElFFF systems by reducing the fractionation efficiency significantly. In this study, some of the diffusion effects in CyEFFF systems are resolved by the implementation of a modified method called biased CyElFFF. In this technique biased voltages having duty cycles higher than 50% are used, and baseline separations of sub 50 nm particles are achieved for the first time. In addition, a theoretical analyses for determining the optimal operating conditions for BCyElFFF are provided and verified by the experiments. Highest separation resolutions are achieved when the net per cycle electrical displacement is close to the per cycle diffusion length ($l_e \approx l_{dx}$) and approaches to achieve this condition are discussed. Through the use of methods explained in this study, BCyEFFF can be used as a more powerful alternative to standard ElFFF, electrophoresis, and other nanoparticle separation and characterization techniques.

Methods

Separation experiments were made by using a mixture of 15 and 40 nm spherical gold nanoparticles (Nano-Composix, CA, USA). Gold nanoparticles were tannic acid stabilized and their mass concentration was 0.05 mg/mL. Particle sizes and

elecrophoretic mobilities were measured by using a Zetasizer Nano ZS instrument (Malvern Instruments Ltd., UK), and measurements are shown in Table 3.3.

For all of the experiments, de-ionized water (18.2 MΩ/cm) was used as the carrier, which was pumped at a flow rate of 1mL/min by an HPLC pump (Alltech model 426, Alltech Associates, Inc., IL, USA). For the application of AC and DC voltages, an Agilent signal generator (Model 33120A) and an Agilent DC power supply (Model E3640A) were used. The gold nanoparticles were detected by using a UV/Vis detector (ESA -Model 520) at the wavelength of 520 nm. The UV detector data, the electrical current flowing through the ElFFF system and potential difference between the channel walls were measured by using a LabView (National Instruments) data acquisition card.

The cyclical ElFFF system used in the experiments was the same as the one used in earlier works[10, 23]. The ElFFF channel had a length of 64 cm, a height of 178 μm and a width of 2 cm. In every experiment, 40 μL of a 15 & 40 nm gold nanoparticle mixture were injected using a 100 μL syringe.

Each experiment begins with injection of the sample into the ElFFF channel at t=0. Immediately following the injection, at $t=0^{+}$, the power supply is turned on to apply 1V DC for 1 minute. The reason of applying this constant voltage is to make sure that all the nanoparticles are positioned close to the channel wall. At t = 1 minute, we turn on an HPLC pump to start the flow. At the same time we also turn on the signal generator to apply the square wave voltage to the system. We continue applying the cyclical voltage for 37 minutes. This recipe was followed in all of the experiments conducted.

Table 3.3. Properties of the particles used in the separation experiments

	Particle #1	**Particle #2**
Material	Gold	Gold
Manufacturer size	15 nm	40 nm
Hydrodynamic diameter	17.6 ± 0.3 nm	45.1 ± 0.8 nm
Electrophoretic mobility	-3.55 x 1e^{-8} $m^2V^{-1}s^{-1}$	-3.41 x 1e^{-8} $m^2V^{-1}s^{-1}$

For each experiment, the resolution of the separation was calculated according to

$$Rs = \frac{t_2 - t_1}{2(\sigma_1 + \sigma_2)} \qquad \textbf{(3.7)}$$

where t_1 and t_2 are the positions of the peaks and σ_1 and σ_2 are the standard deviations of the peaks as they are approximated to a Gaussian curve.

For every experiment performed, the corresponding electric field (E_{eff}) inside the channel was calculated by using

$$E_{eff}(t) = \frac{I(t) \times R_{bulk}}{w} \qquad \textbf{(3.8)}$$

where, $I(t)$ is the measured current in Amperes, w (m) is the channel height and R_{bulk} (Ω) is the resistor representing the electrical resistance of the carrier liquid between the channel walls. R_{bulk} was calculated according to the methods explained by Srinivas et al.[23, 32]

Finally, for each experiment conducted, the net per cycle electrical displacement (l_e) of a particle was calculated using the following equation.

$$l_e = l_{e-} - l_{e+} = \mu_p \int_0^{1/f} E_{eff}(t)dt \qquad \textbf{(3.9)}$$

References

[1] C.-S. Wu, F.-K. Liu, and F.-H. Ko, "Potential role of gold nanoparticles for improved analytical methods: an introduction to characterizations and applications," *Analytical and Bioanalytical Chemistry,* vol. 399, pp. 103-118, 2011.

[2] J. C. Giddings, *Dynamics of Chromatography: Principles and Theory* vol. 1: CRC, 2002.

[3] Q. Wang and L. Zhang, "Review of research on quantitative structure-retention relationships in thin-layer chromatography," *Journal of Liquid Chromatography & Related Technologies,* vol. 22, pp. 1-14, 1999.

[4] C. C. Campos and C. Simpson, "Capillary electrophoresis," *Journal of Chromatographic Science,* vol. 30, pp. 53-58, 1992.

[5] B. Chankvetadze, *Capillary Electrophoresis in Chiral Analysis.* Chichester, Wiley, 1997.

[6] W. Mächtle and L. Börger, "Analytical ultracentrifugation of polymers and nanoparticles," *Springer, 2006.,* vol. 1, 2006.

[7] H. Cölfen, "Analytical ultracentrifugation of nanoparticles," *Polymer News,* vol. 29, pp. 101-116, 2004.

[8] J. C. Giddings, "A new separation concept based on a coupling of concentration and flow nonuniformities," *Separation Science,* vol. 1, pp. 123-125, 1966.

[9] H. Sant and B. Gale, "Microscale field-flow fractionation: theory and practice microfluidic technologies for miniaturized analysis systems," S. Hardt and F. Schönfeld, Eds., Springer US, 2007, pp. 471-521.

[10] K. D. Caldwell and Y. S. Gao, "Electrical field-flow fractionation in particle separation. 1. Monodisperse standards," *Analytical Chemistry,* vol. 65, pp. 1764-1772, 1993.

[11] K. D. Caldwell, L. F. Kesner, M. N. Myers, and J. C. Giddings, "Electrical field-flow fractionation of proteins," *Science,* vol. 176, pp. 296-298, 1972.

[12] T. Tasci, E. Manangon, D. Fernandez, W. Johnson, and B. Gale, "Separation of magnetic nanoparticles by cyclical electrical field flow fractionation," *Magnetics, IEEE Transactions on,* vol. 49, pp. 331-335, 2013.

[13] T. Schunk, J. Gorse, and M. Burke, "Parameters affecting magnetic field-flow fractionation of metal oxide particles," *Separation Science and Technology,* vol. 19, pp. 653-666, 1984.

[14] F. Carpino, L. R. Moore, M. Zborowski, J. J. Chalmers, and P. S. Williams, "Analysis of magnetic nanoparticles using quadrupole magnetic field-flow fractionation," *Journal of Magnetism and Magnetic Materials,* vol. 293, pp. 546-552, 2005.

[15] T. O. Tasci, W. P. Johnson, and B. K. Gale, "Cyclical magnetic field flow fractionation," *Journal of Applied Physics,* vol. 111, p. 07D128, 2012.

[16] J. C. Giddings, F. J. Yang, and M. N. Myers, "Sedimentation field-flow fractionation," *Analytical Chemistry,* vol. 46, pp. 1917-1924, 1974.

[17] K. D. Caldwell, G. Karaiskakis, and J. C. Giddings, "Characterization of liposomes by sedimentation field-flow fractionation," *Colloids and Surfaces,* vol. 3, pp. 233-238, 1981.

[18] G. H. Thompson, M. N. Myers, and J. C. Giddings, "Thermal field-flow fractionation of polystyrene samples," *Analytical Chemistry,* vol. 41, pp. 1219-1222, 1969.

[19] W. Cao, P. S. Williams, M. N. Myers, and J. C. Giddings, "Thermal field-flow fractionation universal calibration: Extension for consideration of variation of cold wall temperature," *Analytical Chemistry,* vol. 71, pp. 1597-1609, 1999.

[20] J. C. Giddings, F. J. Yang, and M. N. Myers, "Flow field-flow fractionation: new method for separating, purifying, and characterizing the diffusivity of viruses," *Journal of Virology,* vol. 21, pp. 131-138, 1977.

[21] W. Fraunhofer and G. Winter, "The use of asymmetrical flow field-flow fractionation in pharmaceutics and biopharmaceutics," *European Journal of Pharmaceutics and Biopharmaceutics,* vol. 58, pp. 369-383, 2004.

[22] W. Somchue, A. Siripinyanond, and B. K. Gale, "Electrical field-flow fractionation for metal nanoparticle characterization," *Analytical Chemistry,* vol. 84, pp. 4993-4998, 2012.

[23] B. K. Gale and M. Srinivas, "Cyclical electrical field flow fractionation," *Electrophoresis,* vol. 26, pp. 1623-32, May 2005.

[24] N. Tri, K. Caldwell, and R. Beckett, "Development of electrical field-flow fractionation," *Analytical Chemistry,* vol. 72, pp. 1823-1829, 2000.

[25] J. C. Giddings, "Cyclical-field field-flow fractionation: a new method based on transport rates," *Analytical Chemistry,* vol. 58, pp. 2052-2056, 1986.

[26] S. Lee, M. N. Myers, R. Beckett, and J. C. Giddings, "Particle separation and characterization by sedimentation/cyclical-field field-flow fractionation," *Analytical Chemistry,* vol. 60, pp. 1129-1135, 1988.

[27] A. I. Lao, D. Trau, and I.-M. Hsing, "Miniaturized flow fractionation device assisted by a pulsed electric field for nanoparticle separation," *Analytical Chemistry,* vol. 74, pp. 5364-5369, 2002.

[28] M. Srinivas, H. J. Sant, and B. K. Gale, "Optimization of cyclical electrical field flow fractionation," *Electrophoresis,* vol. 31, pp. 3372-9, Oct 2010.

[29] J. Gigault, B. K. Gale, I. Le Hecho, and G. t. Lespes, "Nanoparticle characterization by cyclical electrical field-flow fractionation," *Analytical Chemistry,* vol. 83, pp. 6565-6572, 2011.

[30] A. Kantak, M. Srinivas, and B. Gale, "Characterization of a microscale cyclical electrical field flow fractionation system," *Lab Chip,* vol. 6, pp. 645-54, May 2006.

[31] H. J. Sant, S. Chakravarty, S. Merugu, C. G. Ferguson, and B. K. Gale, "Characterization of polymerized liposomes using a combination of dc and cyclical electrical field-flow fractionation," *Analytical Chemistry,* vol. 84, pp. 8323-8329, 2012.

[32] S. Merugu, H. J. Sant, and B. K. Gale, "A novel method for effective field measurements in electrical field-flow fractionation," *Electrophoresis,* vol. 33, pp. 1040-1047, 2012.

[33] N. Wiener, "Differential space," *Journal of Mathematical Physics,* vol. 2, pp. 131-174, 1923.

[34] W. Sutherland, "LXXV. A dynamical theory of diffusion for non-electrolytes and the molecular mass of albumin," *Philosophical Magazine Series 6,* vol. 9, pp. 781-785, 1905.

CHAPTER 4

CIRCUIT MODIFICATION IN ELECTRICAL FIELD FLOW FRACTIONATION SYSTEMS FOR HIGH RESOLUTION SEPARATIONS OF NANOPARTICLES

Introduction

Nanotechnology and nanoscience are two of the fastest growing research fields, which involve production and use of substances at the nanoscale (i.e, between 1 and 100nm). Many nanotechnology-based consumer products are already available in the market, some of which are: cosmetics, nano-medicines, sunscreens, semiconductors, house cleaning items, paints and so forth. As the necessity of producing specialized nanoparticles increases, scientist have to use separation techniques which can sort particles according to their vast number of properties, such as size, shape, charge, internal structure, magnetic susceptibility and optical properties. Currently, several analytical methods are used to separate and characterize nanostructures. The three main separation techniques are chromatography, electrophoresis and field flow fractionation.

Field Flow Fractionation (FFF) is a powerful nanoparticle characterization and separation method first developed by Giddings in 1966 [1]. In FFF, separation occurs in a long, thin channel through which a carrier liquid passes. Carrier flow is laminar and has a

parabolic velocity profile. Perpendicular to this flow, a separation field is applied, which causes the particles to migrate to unique locations away from the channel walls, giving them different velocities down the channel length. Based on the interaction level of the particles with the separation field, migration rates differ between the particles and the separation occurs.

Field Flow Fractionation has several subtechniques, which differ based on the type of separation field applied. The major subtechniques are electrical FFF [2], magnetic FFF [3], thermal FFF [4], gravitational FFF [5], and flow FFF [6]. In electrical field flow fractionation (ElFFF), the separation field is produced by applying voltages to the top and bottom walls of an ElFFF channel. In this method, particles are separated according to their size and electrophoretic mobility [7].

ElFFF has also a submethod called cyclical electrical field flow fractionation (CyElFFF) [8]. In CyElFFF, alternating (cyclical) voltages are used rather than a static (constant) voltage. Cyclical voltages help to alleviate the challenges caused by electrical double layer formation (EDL) on the channel walls. When static voltages are applied in the traditional ElFFF method, an EDL is formed that negates the majority of the applied field and electric field inside the channel drops to 3% of its initial value [9]. In CyElFFF, since polarization changes with each cycle, insufficient time exists for the EDL to be formed completely and most of the applied electric field is preserved.

Compared to other subtechniques of FFF, CyElFFF is a fairly new method [10-13] that is still being improved. In previously reported CyElFFF studies, separations have been achieved only for particles bigger than 100nm [11, 12]. For particles smaller than 100nm, diffusion rates become very high, resulting in severe reductions in CyElFFF

separation efficiency. Essentially, particles in the CyElFFF channel begin to diffuse away from the channel walls over time, leading to lower retention times and particle dispersion, which reduces separation resolution. To help negate the effects of diffusion, in this work a novel approach that modifies the electrical circuitry to produce a consistent electrical field in the ElFFF channel was implemented. In all earlier ElFFF efforts [2, 7-20], electrical power sources have been directly connected to the ElFFF channel walls and no alterations have been made in the electrical circuitry of the system, other than minor changes to enable measurement of the electric field in the channel [17]. In this work, by using lumped electrical components, such as resistors and diodes, we alter the electrical circuitry of the system to allow the generation of an overall bias and to improve the effective electric field inside the separation channel so that high resolution separations become possible.

The primary approach in this work uses a diode and additional resistors to make a traditional DC offset voltage, which is often applied in addition to the cyclical voltage, thereby improving separation performance. In previous CyElFFF efforts, researchers used offset voltages to improve the particle relaxation process and in this manner prevented the elution of particles in the void or early peak. In recent work, Srinivas et al. [13] showed that offset voltages can also be used to help obtain higher retention times in a CyElFFF channel. In this work, we demonstrate that offset voltages implemented with circuits including diodes can be used not only for improving the retention time, but can also be used to achieve significant separation resolutions when using CyElFFF.

Normally, when an offset voltage is applied in CyElFFF, the EDL begins to form in response to the DC field. As the EDL forms, it begins to cancel out the effect of the

offset voltage, just as occurs in normal ElFFF, leading to an effective offset voltage of less than 3% of the applied DC field after only a few minutes. The effect of the diode in the circuit is to cause current to flow preferentially in one direction, creating an electric field bias in the channel and essentially "draining" the charge in that direction. This electrically generated bias has the overall effect of suppressing nanoparticle diffusion, which allows baseline separation of sub 50nm particles. Taken as a whole, the improvements implemented in this work can be used to make CyElFFF a more effective tool in the separation and characterization of nanoparticles and macromolecules.

Theory and Methods

A cyclical ElFFF system can be fabricated by locating a thin Mylar spacer (defining the channel) between two electrodes. The flow inside the CyElFFF channel is laminar with a parabolic velocity profile. As a cyclical voltage is applied on the channel walls (electrodes), particles susceptible to the electric field oscillate back and forth between the electrodes. In each electrical cycle, depending on their electrophoretic mobilities, particles spend more or less time in the faster fluid regions, which are near the center of the flow channel. Essentially, particles that spend more time close to middle of the channel elute earlier, whereas particles that spend more time close to the channel wall elute later.

The operational principle of CyElFFF is shown in Figure 4.1. Therein, the trajectories of particles having two different electrophoretic mobilities are presented for three cycles of an applied square wave voltage. In each cycle, the particle having a higher electrophoretic mobility comes closer to the middle of the channel. As a result, that

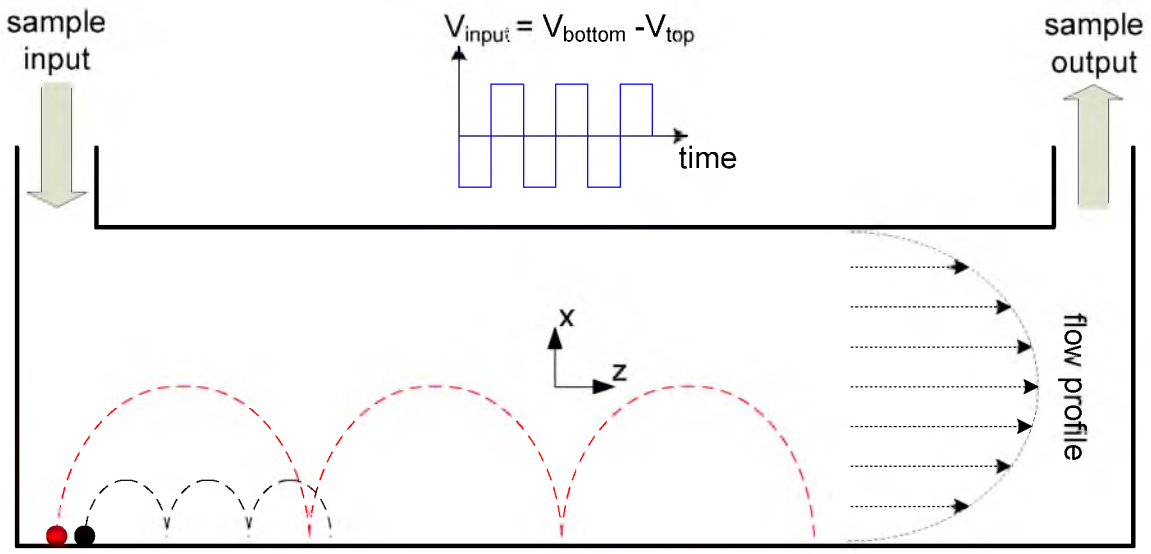

Figure 4.1. Operational principle of a typical CyElFFF system. The drawing shows the motion of two particles having different electrophoretic mobilities for three cycles of an applied square wave voltage. (Figure is not to scale. It is rescaled for better visualization of particle motions. In ElFFF systems, the channel length is usually at least 1000 times longer than the channel height)

particle moves faster through the channel (in the *z*-direction). The particle having the lower electrophoretic mobility stays closer to the channel walls and the slow flow regions. As a result, it moves more slowly in the *z*-direction and elutes later than the higher mobility particle.

The velocity of a nanoparticle under the influence of an electric field can be represented by the equation 4.1.

$$v_p = \mu_p \times E_{eff} \qquad \textbf{(4.1)}$$

Where $v_p(m/s)$ is the velocity of the particle, $\mu_p\ (m^2Vs)$ is the electrophoretic mobility of the particle, and $E_{eff}(V/m)$ is the effective electric field inside the channel. As shown in equation 4.1, to increase the electrically driven velocity of a nanoparticle, the effective electric field (E_{eff}) should be increased.

As noted earlier, nanoparticles also move as a result of diffusion (Brownian motion). The average diffusion length traveled by a particle in a given time is given by

$$l_d = \sqrt{2Dt} \quad \textbf{(4.2)}$$

where D (m^2/s) is the diffusion coefficient of the particle and t *(s)* is time. The diffusion coefficient of a spherical particle can be calculated using the Stokes-Einstein equation [21]

$$D = \frac{Tk_b}{3\pi\eta d} \quad \textbf{(4.3)}$$

where T (K) is temperature, K_b *(J/K)* is Boltzmann's constant, η (Pa·s) is the dynamic viscosity of the carrier liquid, and *d (m)* is the particle diameter.

Examination of equation 4.3 shows that the particle diffusion rate is higher for smaller particles. Particle diffusion is a significant limitation in CyElFFF. Diffusion occurring in the $+x$ direction has an especially negative effect on separation efficiency, retention time, and resolution. The reason for this negative effect is indicated in Figure 4.2a, which represents the particle trajectory in a typical CyElFFF system for 2.5 cycles of a square wave. As a consequence of the particle diffusion in the $+x$ direction, a particle moves away from the channel wall during each cycle, gaining a faster average velocity. When a particle moves faster and faster along the channel length, its retention time significantly drops and separation efficiency reduces drastically.

To reduce the detrimental effect of particle diffusion on the separation efficiency, diffusion in the $+x$ direction should be countered. This can be achieved by applying DC offset voltages along with the cyclical square wave voltages. Figure 4.2b represents this

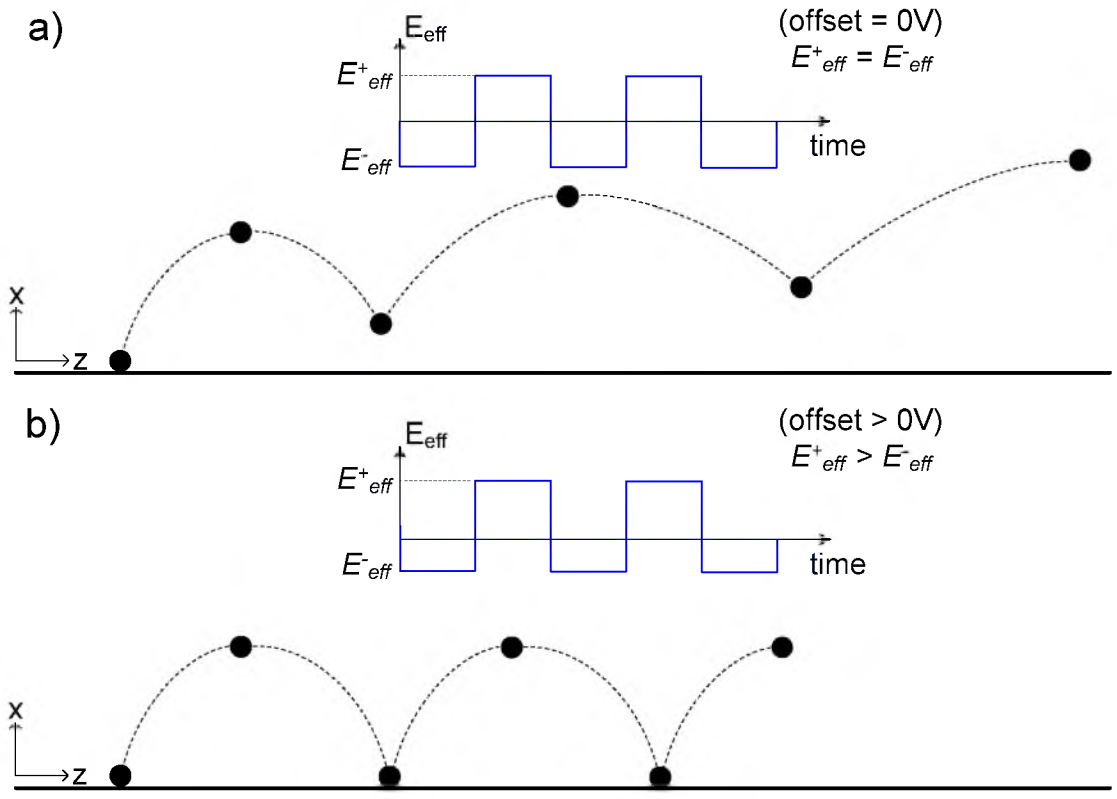

Figure 4.2. Particle trajectories in a CyElFFF system, for 2.5 cycles of a square AC voltage. a) No offset condition. Diffusion occurring in the positive x-direction causes the particle to move away from the channel wall. As a result, the particle gains a higher z-velocity and moves faster during each cycle, reducing the retention time. b) Positive offset condition. Diffusion in the x-direction is controlled. Since E^{+}_{eff} is bigger than the E^{-}_{eff}, over each cycle, particles are attracted to the channel wall, and higher retention times can be obtained.

situation. By applying offset voltages, the electric field inside the channel is modified such that the positive component of the electric field E^{+}_{eff} becomes higher than the negative component E^{-}_{eff} (i.e., electric field profile shifts up). As a result, even though the particle diffuses in the $+x$ direction, the relatively high E^{+}_{eff} forces the particle to return back to the channel wall (x=0) at the end of the cycle, effectively countering the effect of diffusion. In this way, particle keeps its longitudinal velocity (z-velocity) during each cycle consistent (and lower), and much longer retention times can be obtained compared to the no offset condition.

While the application of offset voltages seems reasonable for controlling diffusion, it is not always sufficient. As noted previously, the effect of any DC field applied across the CyElFFF channel eventually decays to less than 3% of its initial value [9]. This small effective DC field is usually insufficient to control the diffusion of small nanoparticles (smaller than 100nm). Consequently, another method is needed to overcome the diffusion problem in CyElFFF.

Figure 4.3.a represents the electrical circuitry of a regular CyElFFF system. The part surrounded by a red square is the electrical circuit equivalent of the ElFFF channel [22]. C_{dl} is the capacitance representing the electric double layer at the channel walls. R_{dl} is the resistance of the electrical double layer, and R_{bulk} symbolizes the resistance of the carrier between the channel walls. The resistance R_{s1} is connected in series to the ElFFF system to monitor the current flowing through the channel. By measuring the voltage on R_{s1}, and dividing it by its resistance value, one can easily obtain the current flowing through the system.

Among the circuit components in Figure 4.3a, R_{bulk} is of crucial importance, since the effective field (E_{eff}) is directly proportional to the R_{bulk} value as shown in

$$E_{eff}(t) = \frac{I_{EFFF}(t) \times R_{bulk}}{w} \qquad \textbf{(4.4)}$$

E_{eff} can be found by multiplying the R_{bulk} resistor with the current flowing through the channel (I_{ElFFF}), and dividing the result by the channel height *w (m)*. Again from equation 4.4, it is clear that effective field is also proportional to the current flowing through the channel (I_{ElFFF}), which suggests that one can modify with the current I_{ElFFF} to alter the effective field inside the channel.

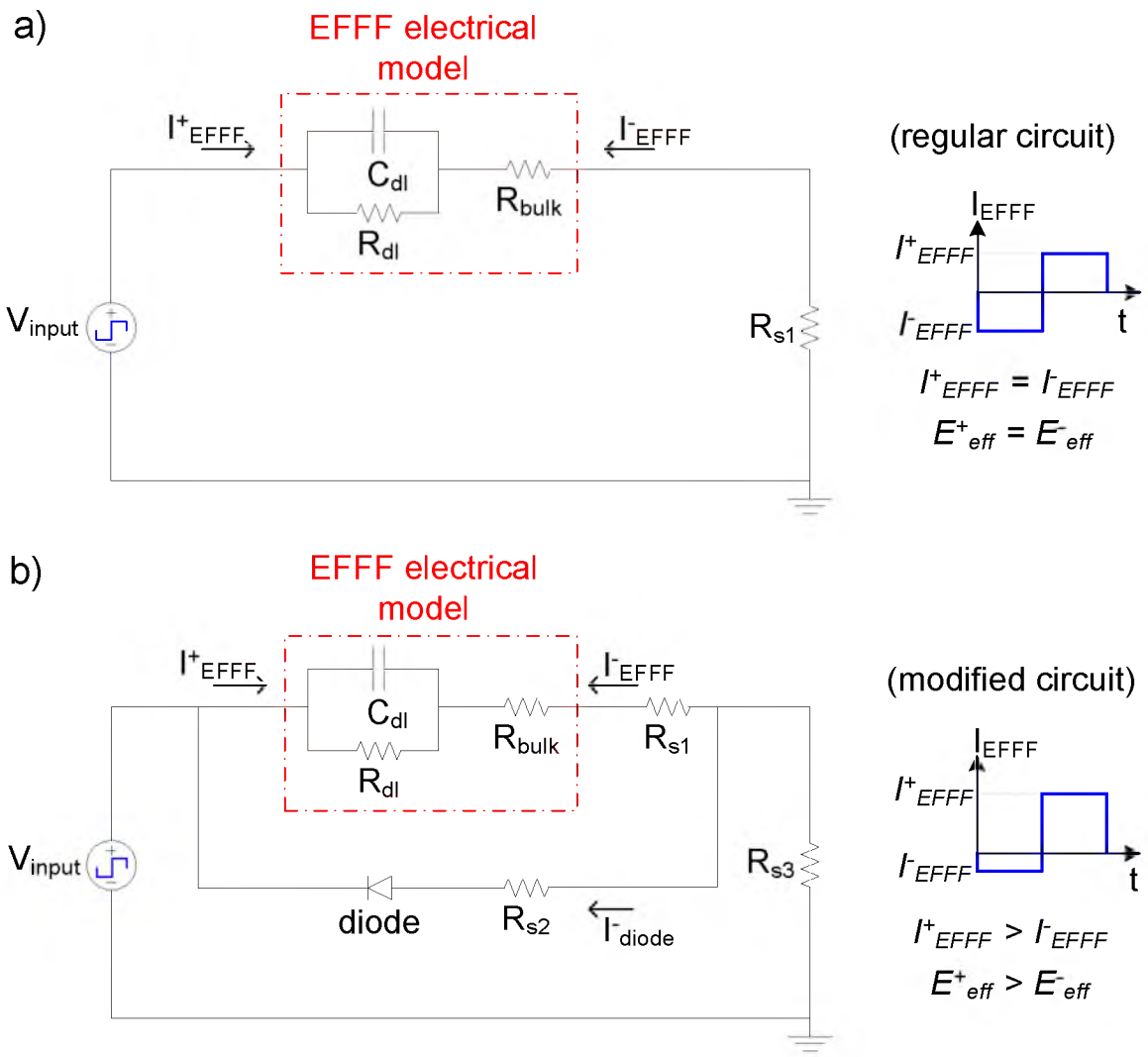

Figure 4.3. Electrical circuitry of **a)** A regular CyElFFF system **b)** The modified CyElFFF system.

The electrical circuitry of a regular CyElFFF system can be modified by using a diode and additional resistors to achieve an imbalance between E^{+}_{eff} and E^{-}_{eff}. As shown in Figure 4.3b, a diode is connected in parallel to the ElFFF channel. A diode operates such that it allows the current to flow in only one direction. As a consequence, when the input voltage is positive, the current only flows through the channel. When the input voltage is negative, current flows through both the channel and the diode. Thus, during

the negative cycle of the voltage input, current divides between the channel and diode and the resulting I^{-}_{ElFFF} becomes smaller than I^{+}_{ElFFF}. Using this circuit modification, even if the voltage input does not include any offset voltage, one can achieve an offset in the I_{ElFFF} profile. Accordingly, the necessary positive shift in the E_{eff} profile (i.e., $E^{+}_{eff} > E^{-}_{eff}$) can be obtained and countering the particle diffusion in the $+x$ direction becomes possible.

The remaining circuit elements in Figure 4.3b, R_{s1} and R_{s2} are small resistors to monitor the current flowing through the ElFFF and diode branches. A small resistor R_{s3} (on the order of 1Ω) should be added in series to the parallel ElFFF-diode network. If it is not connected, then diode will have no effect on the I_{ElFFF} current, since it would be directly connected between the power source and the ground. Preferably, all the resistors R_{s1}, R_{s2} and R_{s3} should be selected with low values ($1\Omega < R_s < 10\Omega$), because the effective field inside the channel decreases as the magnitude of these resistors increases.

In order to test the circuit modification and offset voltage application methods, several retention and separation experiments were conducted. A mixture of 15 and 40 nm spherical gold nanoparticles (Nano-Composix, CA, USA) were used as the samples to be separated. Particles were tannic acid stabilized and their mass concentration was 0.05 mg/mL. Particle sizes and elecrophoretic mobilities were measured by using a Zetasizer Nano ZS instrument (Malvern Instruments Ltd., UK), and tabulated in Table 4.1.

Table 4.1. Properties of the particles used in the separation experiments

	Particle #1	**Particle #2**
Material	Gold	Gold
Manufacturer size	15nm	40nm
Hydrodynamic diameter	17.6 ± 0.3 nm	45.1 ± 0.8 nm
Electrophoretic mobility	-3.55 μmcm/Vs	-3.41 μmcm/Vs

De-ionized water (18.2 MΩ/cm) was used as the carrier in all the experiments. The carrier liquid was pumped at a flow rate of 1ml/min by an HPLC pump (Alltech model 426, Alltech Associates, Inc., IL, USA). Application of AC and DC voltages was done using an Agilent signal generator (Model 33120A) and Agilent DC power supply (Model E3640A). For the detection of the nanoparticles, a UV/Vis detector (ESA -Model 520) was used at the wavelength of 520nm. The UV detector data, the electrical current flowing through the ElFFF system, and the potential difference between the channel walls, were measured and collected using a LabView (National Instruments) data acquisition card. To measure the currents flowing through the branches, voltages on the $R_{s1,}$ R_{s2} and R_{s3} resistors were monitored. The values for these resistors were selected as 5.4Ω, 5.4Ω and 1.0Ω respectively.

The ElFFF channel used in the experiments was the same as the one used in earlier reports [7, 8, 13]. The channel has a length of 64cm, height of 178μm and a width of 2cm. In every experiment, 40μL of a 15nm and 40nm gold nanoparticle mixture was injected by a 100 μL Hamilton microliter syringe.

Each experiment began with injection of the sample into the ElFFF channel at t=0. Immediately following the injection, at t=0^{+}, the power supply was turned on to apply 1V DC for 1 minute. This DC voltage serves as the particle relaxation step, which is used to attract all the particles to the channel wall. At t = 1 minute, the HPLC pump was turned on to start the carrier flow. At the same time the signal generator was turned on to apply the square wave voltage to the channel. The cyclical voltage was applied for 35 minutes (experiments 2-4) or 40 minutes (experiments 1, 5, 6) before being turned off.

This procedure was followed in all six sets of the experiments conducted. The modified CyElFFF circuit was used in all experiments, except where noted.

Experiment 1 - Comparison of Separation Performance Using the Regular and Modified Circuit in the Presence and Absence of an Offset Voltage

In this set of experiments, separations were made in the presence and absence of a 1.3V offset voltage. In addition, experiments were made with and without the modified circuit to investigate the effect of the circuit modification on the separation efficiency. For these experiments, the amplitude of the cyclical voltage was selected as 16Vpp and the frequency was chosen as 15 Hz (f = 15Hz, Vamp = 16Vpp).

Experiment 2 - Offset Voltage Comparison Experiments

The aim of these experiments was to explore the effect of the offset voltage on the separation efficiency of the CyElFFF system. Offset voltages from 0V to 2V were applied. 2V was the maximum voltage applied, because for the voltages higher than 2V, electrolysis of the carrier occurred and air bubbles were generated in the channel, which prevented any detectable particle separation. The remaining electrical parameters were V_{amp}=8Vpp and f=10Hz. At the end of these experiments, the offset voltage which produced the highest resolution was picked and denoted as V*.

Experiment 3 - Peak Determination Experiments

To reveal which particles (15 or 40 nm particle) correspond to the first and second peaks in the UV fractograms, experiments were conducted with injections of the

individual particles. The voltage parameters used in these experiments were as follows: V_{amp}=8Vpp, f = 10Hz, V_{offset} = V*.

Experiment 4 - Amplitude Comparison Experiments

The aim of these experiments was to find out how altering the voltage amplitude affects the resolution of the separations. Voltage amplitudes ranging from 2Vpp to 16Vpp were applied. The remaining electrical parameters were: f = 10Hz and V_{offset} = V*.

Experiment 5 - Frequency Comparison Experiments

In this set of experiments, the purpose was to see the effect of applying different frequencies on the separation efficiency. Frequencies ranging from 2Hz to 54 Hz were applied; a voltage amplitude of 8Vpp was used and the offset value was V*.

Experiment 6 - Frequency Comparison Experiments

In all the previous studies of CyElFFF, the shape of the voltage waveform was selected as a square wave. In this experiment, the effect of using voltages with different shapes, such as sinusoidal, triangular and sawtooth, was examined. The amplitudes used for the triangular, sawtooth, sinusaoidal and square wave voltages were 16Vpp, 16Vpp, 12.57Vpp and 8Vpp respectively. The reason for selecting different amplitudes was to obtain the same quantity of electric field during each cycle (i.e., the areas under the half period of the voltage waveforms became all the same). The other voltage parameters were f = 10Hz and V_{offset} = V*.

Finally, to compare the fractionation performance of each experiment, separation resolutions were calculated using

$$Rs = \frac{t_2 - t_1}{2(\sigma_1 + \sigma_2)} \qquad \textbf{(4.5)}$$

where t_1 and t_2 are the positions of the peaks and σ_1 and σ_2 are the standard deviations of the peaks as they are approximated by a Gaussian curve.

Results and Discussion

Figure 4.4 shows the UV fractograms obtained in experiment 1. The UV fractogram for the no offset condition with the regular circuit shows that there is hardly any separation between 15 and 40nm particles. In addition, the retention time for these particles is less than 10 minutes.

In contrast, for the no offset condition, but with the circuit modification, the 15 and 40 nm particles are well separated, with retention times being approximately 19 and 26 minutes. Clearly, even in the absence of any offset voltage, retention times are extensively increased with the circuit modification of the system. More importantly, baseline separation of the particles is achieved, which is the first reported baseline separation of sub 50nm particles with CyElFFF.

The fractogram for a 1.3V offset with the regular circuit shows that retention times are increased significantly as well, but separation of the 15 and 40 nm particles was not complete, demonstrating that the offset voltage application is a useful method for obtaining higher retention times, but it does not produce baseline separation of sub 50nm particles.

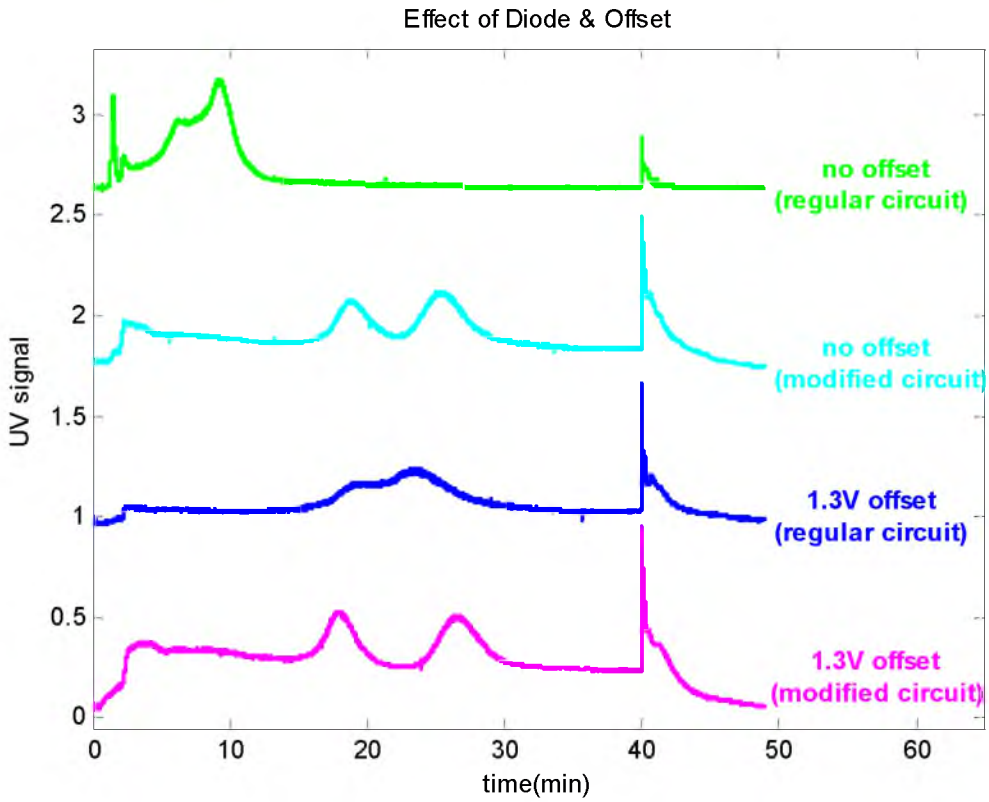

Figure 4.4. UV fractograms for the experiments made with the regular and modified circuits, in the presence and absence of the offset voltage. Electrical parameters were f=15Hz, V_{amp}=16Vpp.

The bottom fractogram of the Figure 4.4 shows the result when the circuit modification and a voltage offset are applied together. As shown, by combining these two methods, high resolution separation of 15 and 40nm particles becomes possible, which is a significant improvement over previously existing CyElFFF methods.

As shown in the UV fractograms of Figure 4.4, the response at t=40 minute is the instant that the power is turned off. The power-off response is very low for the no offset condition with the regular circuit. A comparably higher response in the other fractograms indicates that as offset voltages are applied, or the circuit is modified, some of the particles are trapped in the channel and they are released upon elimination of the electrical field.

Results for the offset comparison experiments (experiment 2) are presented in Figure 4.4. The UV fractogram on the bottom of Figure 4.4 corresponds to the no offset condition and the one on the top is for the 2V offset condition.

The fractogram for 0V offset case reveals that in the absence of the offset voltage, relatively high retention times (around 13 min) can be obtained, but to achieve a complete separation, the offset voltage should be increased. As shown in Figure 4.5 for offset voltages bigger than or equal to 1.0V, baseline separations are obtained. At the highest offset voltage of 2V, the separation resolution starts to drop and peaks become wider. The highest resolution was obtained for the offset voltage of 1.4 V and this offset value was denoted as V^* and used in the remaining experiments. The outcome of experiment 2 clearly demonstrates that offset voltage helps to achieve higher resolutions and it should be used in combination with the circuit modification method.

For the power-off responses at t=35 (Figure 4.5), it can be seen that the power-off response grows with the increasing offset voltage, indicating that more particles are trapped in the channel with higher offset application, but it does not appear to have a noticeable effect on the quality of the separation.

Experiment 3 was conducted to determine which particles corresponded to the first and second peaks in the UV-fractograms. As can be seen in Figure 4.6, for individual injections of 15nm particles, a peak around 15 minutes is observed. For the individual injection of 40nm particles, the peak was located around 23 minutes. This result is in agreement with the electrophoretic mobilities of the particles (see Table 4.1). Since 15nm particles have a higher mobility, they move further away from the channel wall during each cycle and therefore elute earlier than the 40nm particles.

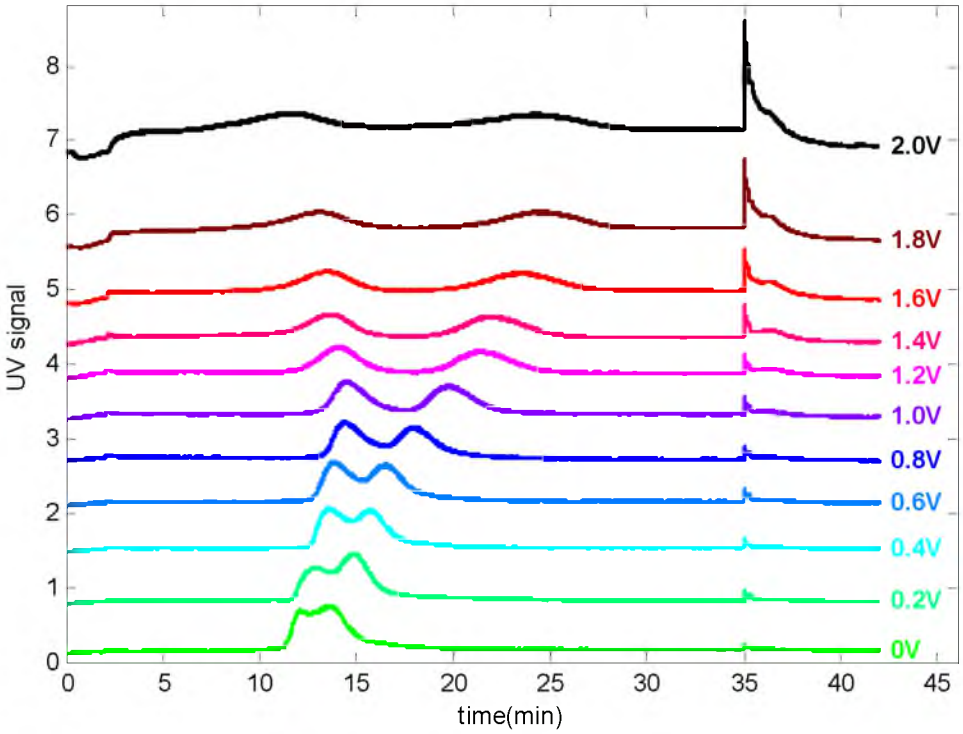

Figure 4.5. UV fractograms for the offset comparison experiments. Electrical parameters were f=10Hz, Vamp=8Vpp.

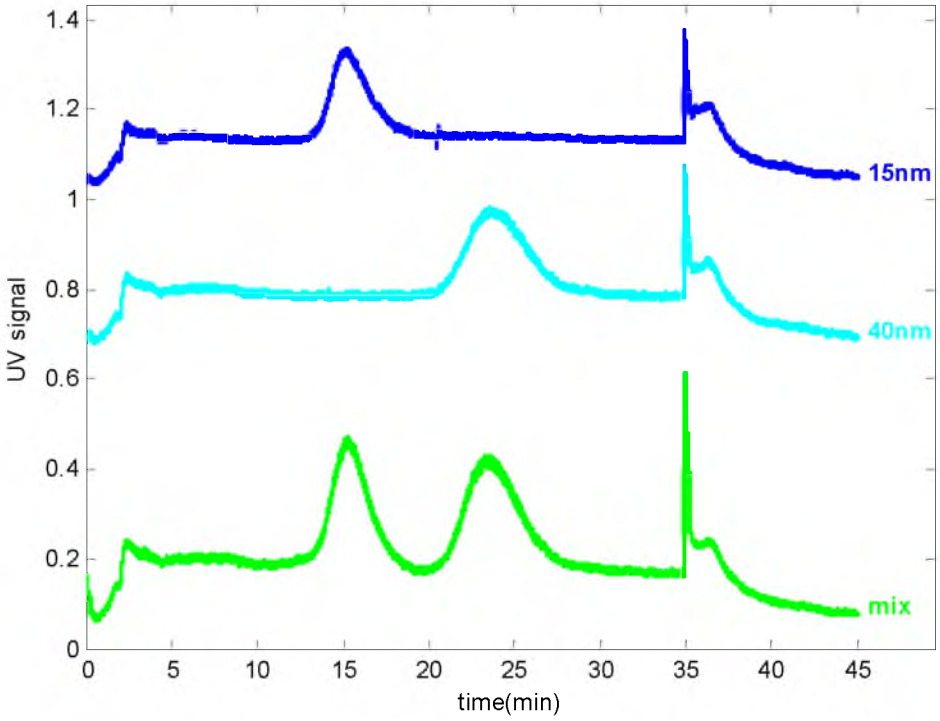

Figure 4.6. UV fractograms for the peak determination experiments. Electrical parameters were f=10Hz, V_{amp}=8Vpp, V_{offset}=1.4V.

The outcome of the voltage amplitude experiments are presented in Figure 4.7. Experiments were done with square wave voltages of different amplitudes, while the frequency and offset were fixed at 10Hz and 1.4V respectively. As clearly shown in Figure 4.7, in terms of the resolutions of the separations, there is no significant difference between the experiments, while the highest resolution corresponds to the 10Vpp condition. As we go down from 16Vpp to 2Vpp, the peaks become more separated but at the same time, the peaks become wider. Consequently, resolutions for these separations do not differ significantly between the experiments. These experiments demonstrated that once a proper value for the offset voltage is selected, altering the voltage amplitude does not make a considerable difference in the separation performance of the system.

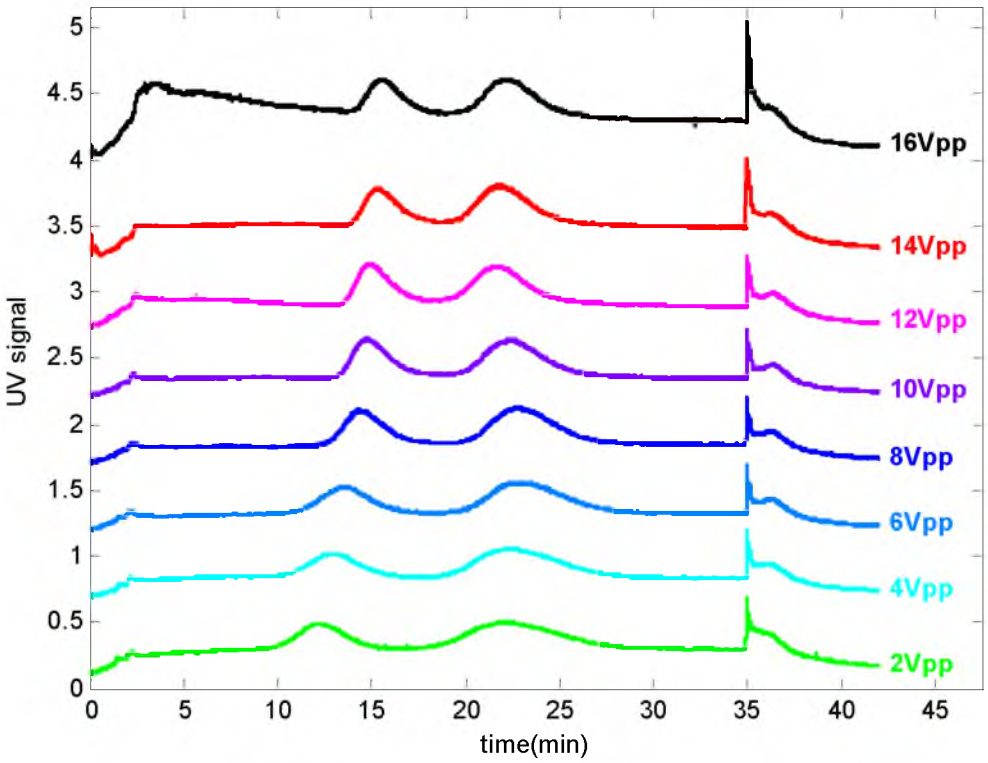

Figure 4.7. UV fractograms for the amplitude comparison experiments. Electrical parameters were f=10Hz, V_{offset} =1.4V.

Looking at the power-off responses, one can observe slightly more particle release for the 16Vpp condition, but again, it is not much different from the experiments done with lower amplitudes.

The effect of altering the frequency on the separation efficiency was investigated in experiment 5. In these experiments, a voltage amplitude of 8Vpp was used and the offset voltage was fixed at 1.4V. Different frequencies from 2Hz to 54 Hz were tested and the results are presented in Figure 4.8. For the frequency of 2Hz, retention time was less than 10 minutes. In addition, the resolution of the separation was low and baseline separation was not achieved. In comparison, for higher frequencies, 4Hz and above, baseline separations of particles are observed. For higher frequencies, peak separations were larger, but peak widths were wider. Thus, overall separation quality was not affected by the application of high frequency voltages, though the character of the results were changed somewhat.

In Figure 4.8, slightly larger power-off response for high frequencies can be observed. We suggest that these results are a consequence of the large number of particle-surface interactions at high frequencies.

In all the previous CyElFFF studies, square wave voltages were used as the cycling voltage. To investigate the separation performance with other voltage shapes, we made 4 different separation experiments with sinusoidal, triangular, sawtooth and square waves. Results are presented in Figure 4.9.

As clearly shown in Figure 4.9, there is no noticeable difference between the separation efficiencies of the experiments, which demonstrates that the shape of the voltage does not affect the separation resolution, if the integral of the applied voltage per

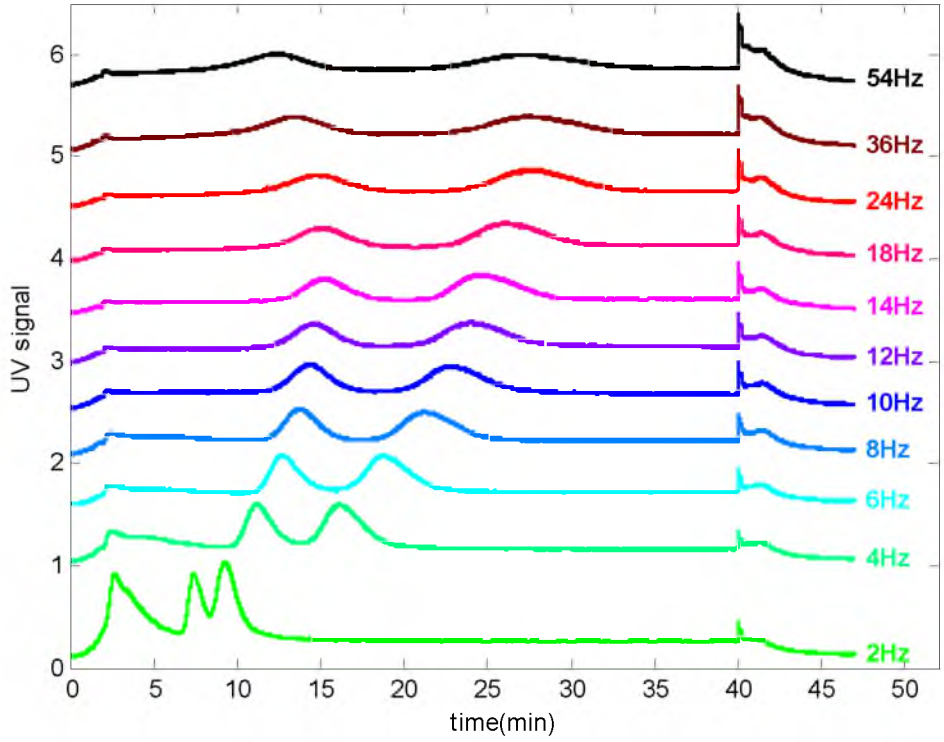

Figure 4.8. UV fractograms for the frequency comparison experiments. Electrical parameters were Vamp=8Vpp and Voffset =1.4V.

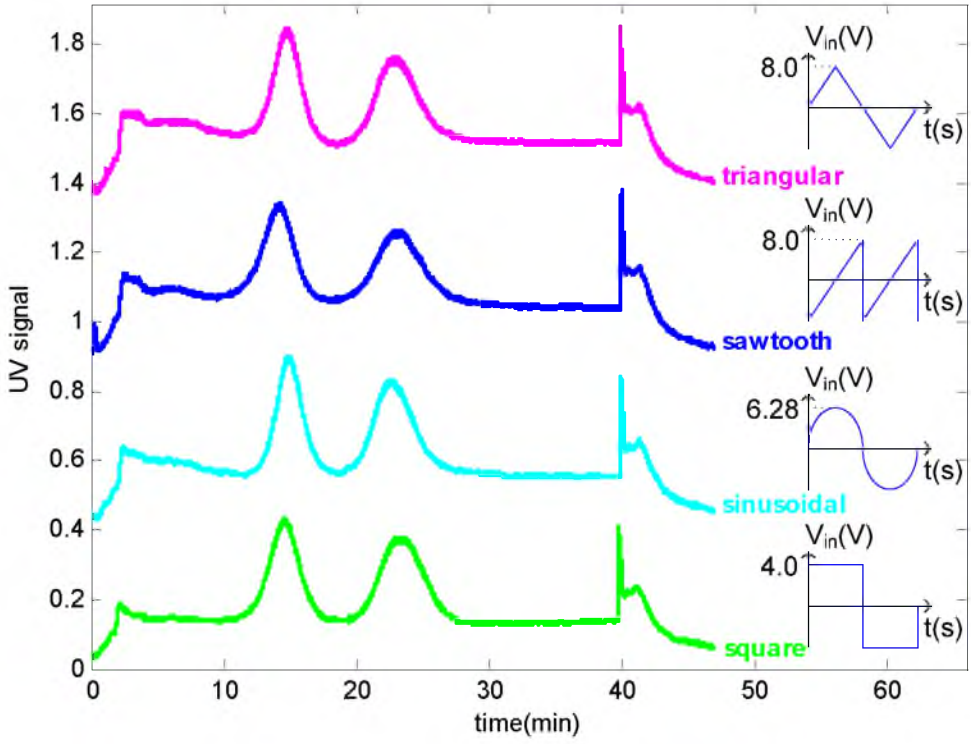

Figure 4.9. UV fractograms for the shape comparison experiments. Electrical parameters were f=10Hz and Voffset =1.4V. Applied voltage amplitudes were shown on the figure.

half cycle is equivalent between the experiments.

To summarize the results of the experiments, all the separation resolutions were calculated and tabulated in Table 4.2.

In reviewing the results of experiment 1, it can be seen that modifying the circuit causes a 4-fold improvement (from 0.3 to 1.19) in the resolution obtained with the regular circuit. In addition, the resolution obtained by the circuit modification method is about two times (0.59 to 1.19) the resolution obtained by the 1.3 V offset application. Finally, combination of the offset application and circuit modification methods gives the highest resolution of 1.69.

Table 4.2. Separation resolutions calculated for all separation experiments.

Experiment 1 (comparison of regular circuit and modified circuit in the presence and absence of the offset voltage)										
No offset (Regular Circuit)			No offset (Modified Circuit)			1.3V offset (Regular Circuit)			1.3V offset (Modified Circuit)	
0.30			**1.19**			**0.59**			**1.68**	
Experiment 2 (offset voltage comparison)										
0V	0.2V	0.4V	0.6V	0.8V	1.0V	1.2V	1.4V	1.6V	1.8V	2.0V
0.52	**0.64**	**0.71**	**0.74**	**0.91**	**1.27**	**1.55**	**1.62**	**1.61**	**1.59**	**1.30**
Experiment 4 (voltage amplitude comparison)										
2Vpp	4Vpp		6Vpp	8Vpp		10Vpp	12Vpp		14Vpp	16Vpp
1.39	**1.47**		**1.53**	**1.56**		**1.53**	**1.48**		**1.43**	**1.40**
Experiment 5 (frequency comparison)										
2Hz	4Hz	6Hz	8Hz	10Hz	12Hz	14Hz	18Hz	24Hz	36Hz	54Hz
0.90	**1.30**	**1.46**	**1.59**	**1.66**	**1.56**	**1.59**	**1.62**	**1.62**	**1.63**	**1.67**
Experiment 6 (voltage shape comparison)										
square			sinusoidal			sawtooth			triangular	
1.66			**1.65**			**1.60**			**1.69**	

To further explore the results of experiment 1, the DC component of I_{ElFFF} for each separation run has been calculated. For the no-offset experiment done with the regular circuit, the DC component was measured was 0A, which is an expected result, since the input voltage was a square wave without any offset. For the experiment done with the modified circuit in the no-offset condition, the DC component of I_{ElFFF} was measured as 19mA, which is an indication that the modified circuit helps to crate a positive shift in the current and accordingly in the effective field. The DC component measured for the 1.3V offset condition (with the regular circuit) was 17mA and finally, the DC component measured for the combination of the methods was 25mA. As explained in the methods section, as we obtain an increase in the effective field (i.e., $E^{+}_{eff} > E^{-}_{eff}$) high resolution separations become possible. Exp-1 verifies this hypothesis, since we obtained higher resolutions for the experiments with higher DC components.

For better visualization of the results, resolutions obtained from the offset, amplitude and frequency comparison experiments are plotted in Figure 4.10.

As shown in Figure 4.10a, for offset values smaller than 1V, baseline separation could not be achieved (i.e., resolutions were smaller than 1.0). For offset voltages between 1.2V and 1.8 V high resolution separations were achieved and finally, for offset values bigger than 1.8V, resolution started to drop.

Based on these results, offset values should be selected such that it is not too small or high (i.e., between 1.2 to 1.8V for this experiment) to achieve high resolutions.

Figure 4.10b shows resolutions obtained from the voltage amplitude comparison experiments. For all the voltage amplitudes (from 2Vpp to 16Vpp), baseline separations raging between 1.39 to 1.56 were acquired.

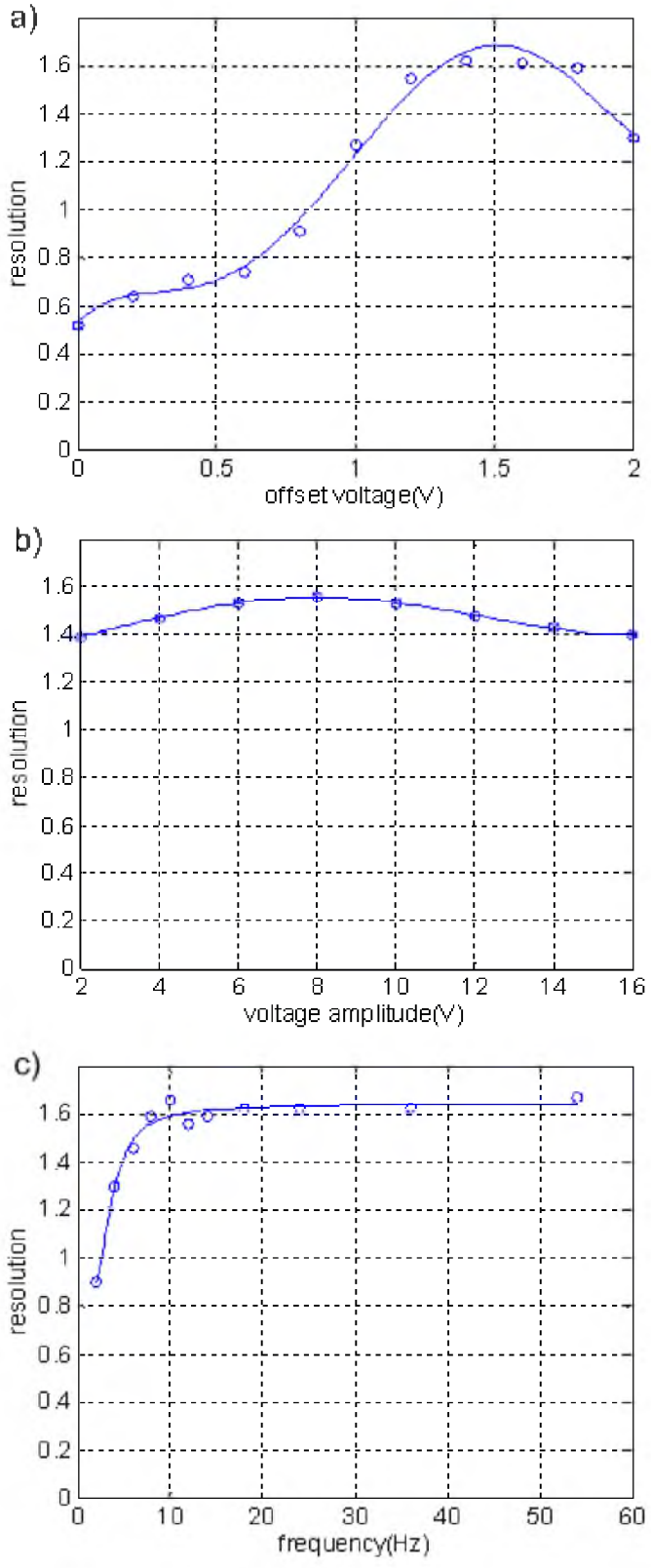

Figure 4.10. Separation resolutions for a) offset comparison b) amplitude comparison and c) frequency comparison experiments.

The voltage amplitude comparison experiment demonstrates that if a suitable offset voltage is selected (1.4V in his case), changing the voltage amplitude only produces a modest difference in the separation performance.

The outcome of frequency comparison experiments are summarized in Figure 4.10c. As can be seen, for frequencies larger than 6 Hz, separation resolutions were relatively high, around 1.6. Figure 4.10c demonstrates that by using the circuit modification and offset application methods, the utilization of high frequencies in CyElFFF become possible. In earlier works [8, 13], it has been stated that for high frequencies (even for frequencies larger than 10Hz), band broadening occurs and separation efficiency drops drastically. On the contrary, these results show that by applying optimized methods, high frequencies can be safely used in CyElFFF without significant reduction in the separation performance. Moreover, the availability of higher frequency voltages may lead to the fabrication of channels with shorter lengths, because there is less need for a longer channel when the number of cycles necessary to generate separation can be obtained in the shorter length channel with higher frequencies.

Finally, for the experiments made with different voltage waveform shapes, the separation performances are all very similar and resolutions are obtained between 1.60 and 1.69. The highest resolution was obtained for the triangular waveform (1.69), and the lowest one corresponds to the experiment done with the sawtooth waveform (1.60). Results indicate that if the right amplitude for the waveform is chosen, any shape of the voltage waveforms can be used in the CyElFFF separations.

Conclusion

For the first time in the electrical field flow fractionation literature, external circuit elements are used to modify the electrical circuitry of the system. By this modification, necessary improvement in the electric field is obtained, and baseline separations of sub 50nm nanoparticles are achieved. In addition, it has been shown that, offset voltages can be effectively used to get higher efficiencies in the separations. Furthermore, it is verified that circuit modification and offset voltage application methods can be combined to achieve high resolution separations of <50nm nanoparticles. The magnitude of the offset voltage is found to have the greatest effect on resolution. Moreover, the effects of applying different frequencies, amplitudes and voltage shapes are investigated and analyzed through experiments, with the effect of all being relatively modest. Using the techniques demonstrated in this study, cyclical electrical field flow fractionation becomes a more competent method for the fractionation of nanoparticles, which is now capable of separating particles even smaller than 50 nm.

References

[1] J. C. Giddings, "A new separation concept based on a coupling of concentration and flow nonuniformities," *Separation Science,* vol. 1, pp. 123-125, 1966.

[2] K. D. Caldwell, L. F. Kesner, M. N. Myers, and J. C. Giddings, "Electrical field-flow fractionation of proteins," *Science,* vol. 176, pp. 296-298, 1972.

[3] F. Carpino, L. R. Moore, M. Zborowski, J. J. Chalmers, and P. S. Williams, "Analysis of magnetic nanoparticles using quadrupole magnetic field-flow fractionation," *Journal of Magnetism and Magnetic Materials,* vol. 293, pp. 546-552, 2005.

[4] T. L. Edwards, B. K. Gale, and A. B. Frazier, "A microfabricated thermal field-flow fractionation system," *Analytical Chemistry,* vol. 74, pp. 1211-1216, 2002.

[5] M. R. Park, D. Y. Kang, J. Chmelik, N. Kang, J. S. Kim, and S. Lee, "Different elution modes and field programming in gravitational field-flow fractionation: Effect of channel angle," *Journal of Chromatography A,* vol. 1209, pp. 206-211, 2008.

[6] J. C. Giddings, F. J. Yang, and M. N. Myers, "Flow field-flow fractionation: new method for separating, purifying, and characterizing the diffusivity of viruses," *Journal of Virology,* vol. 21, pp. 131-138, January 1, 1977 1977.

[7] K. D. Caldwell and Y. S. Gao, "Electrical field-flow fractionation in particle separation. 1. Monodisperse standards," *Analytical Chemistry,* vol. 65, pp. 1764-1772, 1993.

[8] B. K. Gale and M. Srinivas, "Cyclical electrical field flow fractionation," *Electrophoresis,* vol. 26, pp. 1623-32, May 2005.

[9] Tri, N.; Caldwell, K.; Beckett, R., Development of Electrical Field-Flow Fractionation. *Analytical Chemistry* 2000, 72, 1823-1829.

[10] J. Gigault, B. K. Gale, I. Le Hecho, and G. t. Lespes, "Nanoparticle characterization by cyclical electrical field-flow fractionation," *Analytical Chemistry,* vol. 83, pp. 6565-6572, 2011.

[11] A. Kantak, M. Srinivas, and B. Gale, "Characterization of a microscale cyclical electrical field flow fractionation system," *Lab Chip,* vol. 6, pp. 645-54, May 2006.

[12] A. I. Lao, D. Trau, and I.-M. Hsing, "Miniaturized flow fractionation device assisted by a pulsed electric field for nanoparticle separation," *Analytical Chemistry,* vol. 74, pp. 5364-5369, 2002.

[13] M. Srinivas, H. J. Sant, and B. K. Gale, "Optimization of cyclical electrical field flow fractionation," *Electrophoresis,* vol. 31, pp. 3372-9, Oct 2010.

[14] Z. Chen and A. Chauhan, "Electrochemical response and separation in cyclic electric field-flow fractionation," *Electrophoresis,* vol. 28, pp. 724-739, 2007.

[15] A. Kantak, S. Merugu, and B. K. Gale, "Improved theory of cyclical electrical field flow fractionation," *Electrophoresis,* vol. 27, pp. 2833-43, Jul 2006.

[16] A. S. Kantak, M. Srinivas, and B. K. Gale, "Effect of carrier ionic strength in microscale cyclical electrical field-flow fractionation," *Analytical Chemistry,* vol. 78, pp. 2557-2564, 2006.

[17] S. Merugu, H. J. Sant, and B. K. Gale, "A novel method for effective field measurements in electrical field-flow fractionation," *Electrophoresis,* vol. 33, pp. 1040-1047, 2012.

[18] H. J. Sant, S. Chakravarty, S. Merugu, C. G. Ferguson, and B. K. Gale, "Characterization of polymerized liposomes using a combination of dc and cyclical electrical field-flow fractionation," *Analytical Chemistry,* vol. 84, pp. 8323-8329, 2012.

[19] H. J. Sant and B. K. Gale, "Geometric scaling effects on instrumental plate height in field flow fractionation," *Journal of Chromatography A,* vol. 1104, pp. 282-290, 2006.

[20] W. Somchue, A. Siripinyanond, and B. K. Gale, "Electrical field-flow fractionation for metal nanoparticle characterization," *Analytical Chemistry,* vol. 84, pp. 4993-4998, 2012.

[21] W. Sutherland, "LXXV. A dynamical theory of diffusion for non-electrolytes and the molecular mass of albumin," *Philosophical Magazine Series 6,* vol. 9, pp. 781-785, 1905.

[22] B. K. Gale, K. D. Caldwell, and A. B. Frazier, "Geometric scaling effects in electrical field flow fractionation. 1. Theoretical analysis," *Analytical Chemistry,* vol. 73, pp. 2345-2352, 2001.

CHAPTER 5

THE EFFECT OF THE CHANNEL HEIGHT ON THE SEPARATION EFFICIENCY OF AN ELECTRICAL FIELD FLOW FRACTIONATION SYSTEM

Abstract

In this study, the effect of the channel height on the separation efficiency of Electrical Field Flow Fractionation (ElFFF) systems was investigated. It has been shown for the first time that if optimum channel height and experimental parameters are selected, baseline separations of nanoparticles (with sizes less than 100nm) can be achieved by Cyclical Electrical Field Flow Fractionation. ElFFF channels with four different channel heights were fabricated and separation experiments were made with 15 and 40nm gold nanoparticles. Specifically, baseline separation of 15 and 40nm gold nanoparticles were achieved by using the system with a channel height of 125μm. We believe that by selecting the proper channel height and applying the appropriate voltage waveforms explained in this study, Cyclical Electrical Field Flow Fractionation will be a much more capable method for the fractionation of sub-100nm particles.

Introduction

Field Flow Fractionation (FFF) is a powerful method for the separation and characterization of macromolecular, colloidal and micron-sized particles [1]. Cyclical ElFFF (CyElFFF) is one of the subtechniques of FFF which separates the particles according to their size and electrical mobilities [2]. In CyElFFF, the separation channel is composed of bottom and top electrodes which are separated by a thin spacer. A typical schematic of a CyElFFF system can be seen in Figure 5.1.

In the literature, ElFFF systems have channel heights ranging from 30 to 200µm [3-5]. Until now, there were no studies investigating the different channel heights and their effect on the separation efficiency. In this work, we fabricated channels with 4 different heights and conducted separation experiments with each of them to determine the optimum channel geometry for the separation experiments.

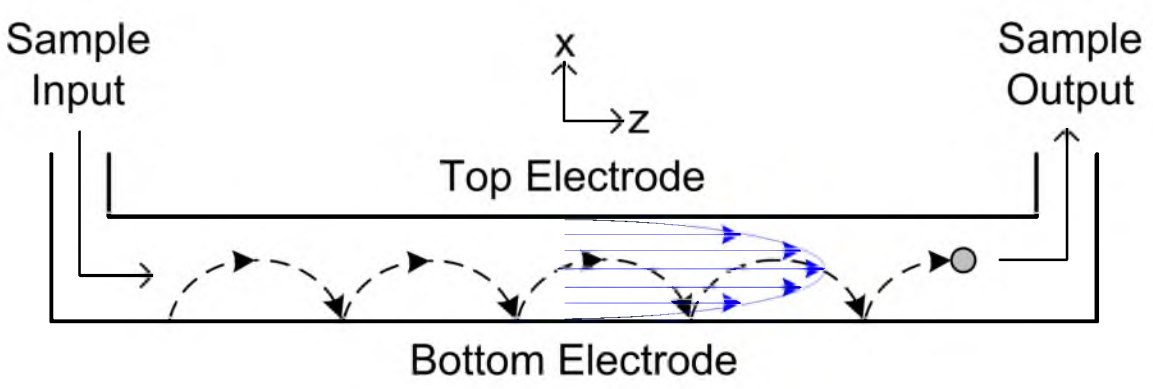

Figure 5.1. Cyclical ElFFF System. The dashed line shows a particle trajectory generated in response to the cyclical field. Oscillating square wave voltages are applied to the electrodes which result in a cyclical electric field inside the channel. As a result of the cyclical electric field, particles move back and forth between the electrodes. Particles with high electrophoretic mobilities move longer distances away from the channel walls and they spend more time in the faster fluid regions. As a consequence, they elute earlier than the lower mobility particles.

Methods

An ELFFF system (width: 2.4cm, length: 43cm) was fabricated by using graphite electrodes and a Mylar spacer as shown in Figure 5.2. Different channel heights were obtained by using spacers of different thicknesses (w=25, 75, 125 and 200μm).

We made separation experiments with a mixture of 15 and 40 nm mean diameter gold nanoparticles. In all experiments, the frequency of the applied square wave voltage was 20Hz and the peak flow velocity in the channel was kept at 4.9mm/s. In each experiment, de-ionized water (18.2 MΩcm−1) was used as the carrier. In most of the experiments, the electric field inside the channel was kept at 80kVpp/m, but we lowered the electric field for the 200um channel to prevent the electrolytic breakdown of water and bubble formation.

In addition to the separation experiments we also conducted I-V measurements to determine the electrical circuit parameters of the ElFFF systems. The electric circuit equivalent of the ElFFF system can be seen in Figure 5.3. We found all the equivalent circuit components for all of the different ElFFF channels.

Results and Discussion

Figure 5.4 shows the separation results for the 125μm channel. As can be seen from the figure, for the 80% duty cycle condition, we achieved a baseline separation. This is the first baseline separation demonstrated in the Cyclical ElFFF literature for sub 100nm nanoparticles.

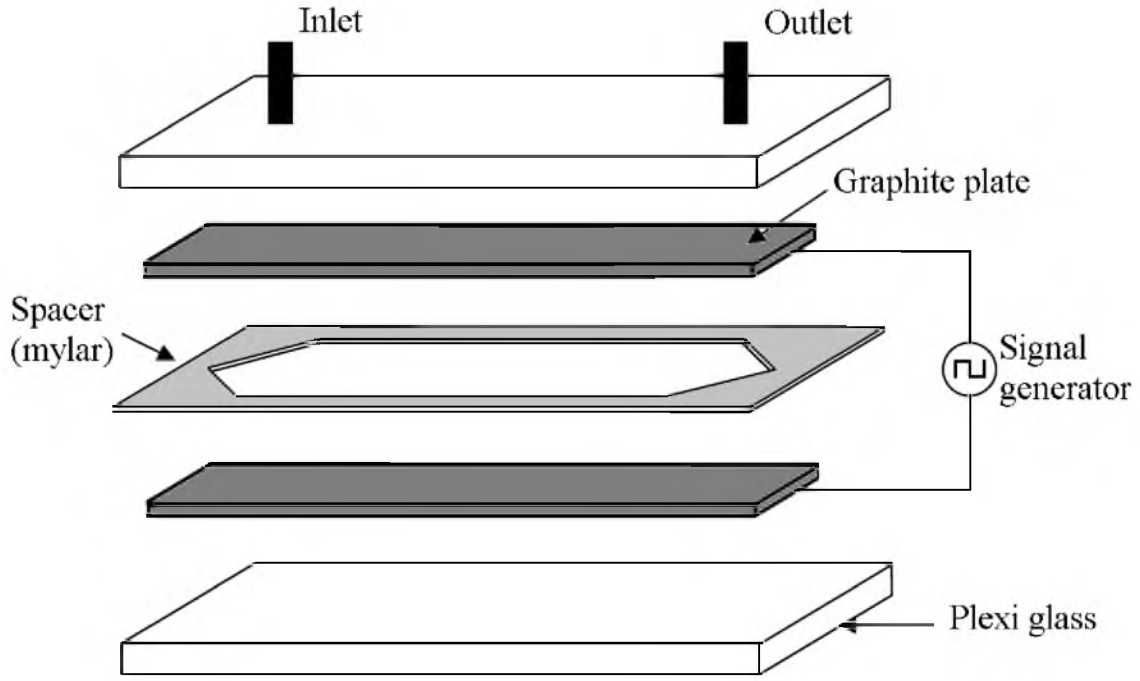

Figure 5.2. ElFFF system fabrication

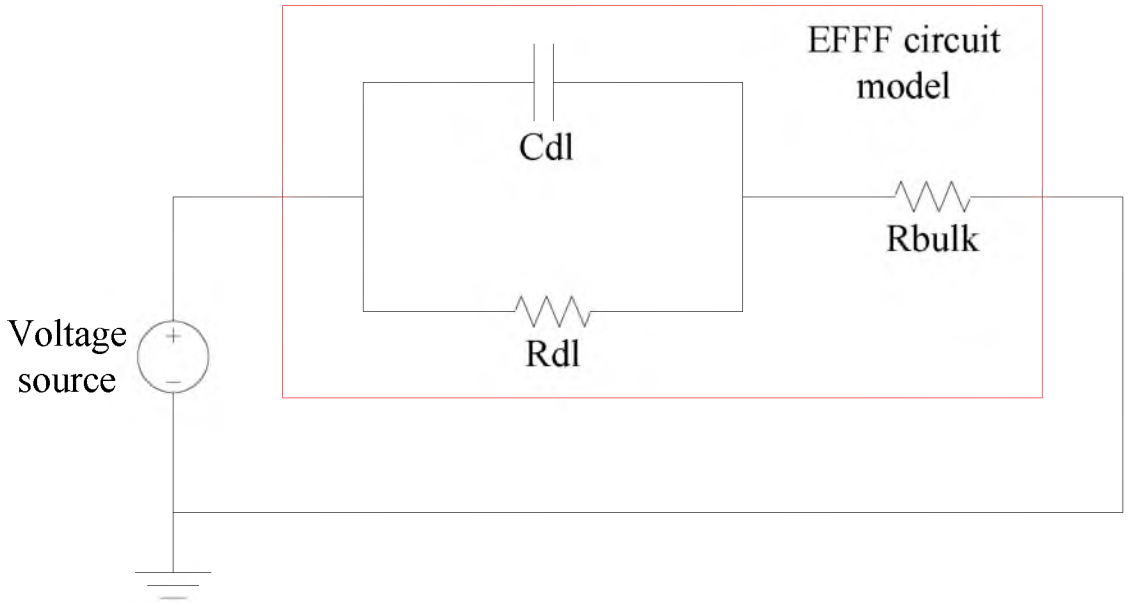

Figure 5.3. ElFFF electrical circuit model

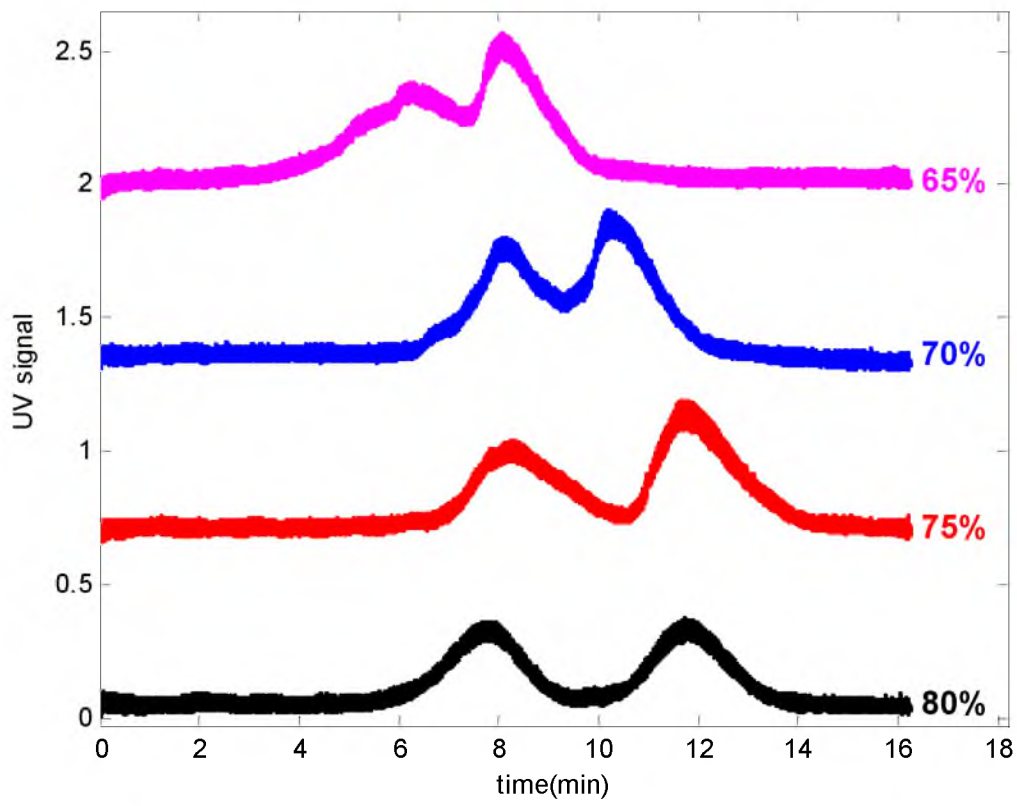

Figure 5.4. UV fractograms for the separation of 15 and 40 nm gold particles (channel height= 125 um) f=20Hz, flow=4.9mm/s, E-field=80kV/m.

As shown in Figure 5.4 as the duty cycle of the waveform increased much better separations were achieved. Since earlier CyElFFF related work used 50% duty cycle waveforms, none were capable of fractionating particles smaller than 100 nanometers.

Figure 5.5 shows the UV fractograms for individual injections of 15 and 40 nm gold nanoparticles, and a mixture. As can be seen in the figure, the first peak in the bottom fractogram corresponds to the 15nm gold nanoparticles and the second peak in the fractogram corresponds to the 40nm gold.

For each experiment, resolutions of the separations were calculated according to the equation 5.1. Where, R is the resolution, t1, t2 are the peak center times and pw1, pw2 are the peak width durations.

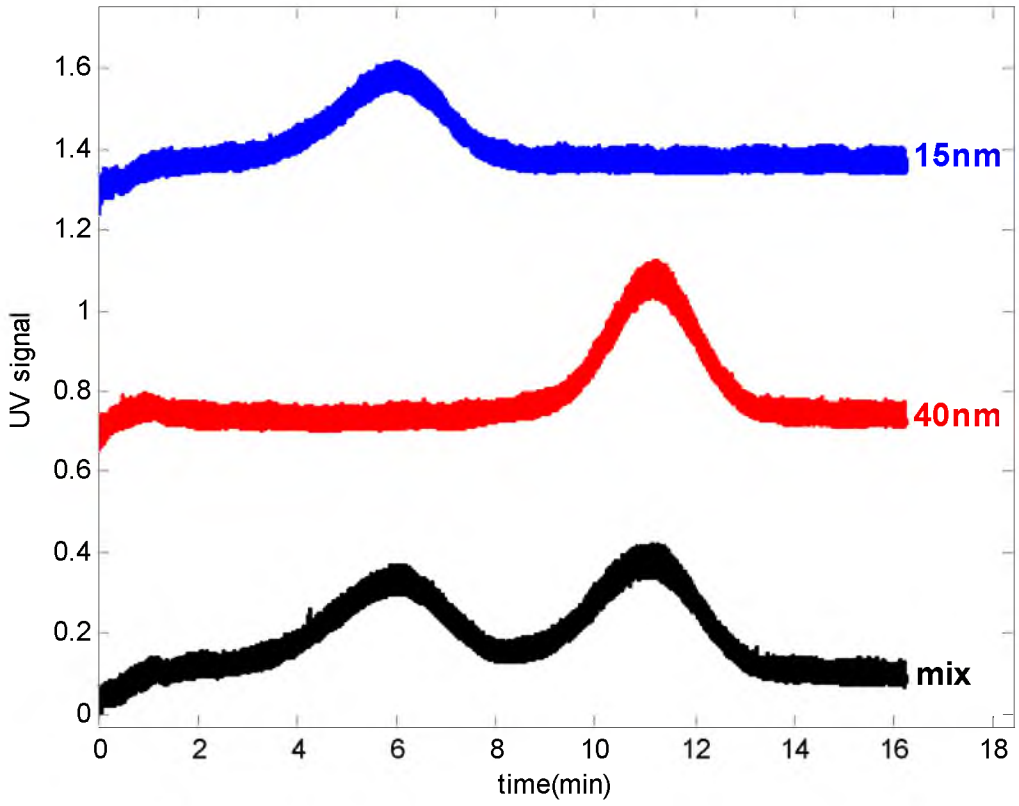

Figure 5.5. Fractograms corresponding to the injections of only 15 and 40 nm gold nanoparticles and their mixture. Experimental conditions were same as part a, and duty cycle is 80%.

$$R = \frac{2(t_2 - t_1)}{pw_2 - pw_1} \quad (5.1)$$

Highest resolution results were obtained for h=125µm as shown in Table 5.1. For the 25µm channel, no separation was observed. The reason for that was the electrical shortening of the top and bottom electrodes at the 25µm separation distance. In general, the best separation results were obtained for the 125µm channel, 75 and 200µm channels were less effective (Table 5.2, Table 5.3).

Electric circuit parameters found for each ElFFF channel were tabulated in Table 5.4. As expected, 75µm channel has the highest capacitance. Rbulk corresponding to the 125µm channel was found to be smallest among the others.

Table 5.1. Separation resolution results for channel height of 125µm.

w=125µm	*Electrical field(kVpp/m)*	*80*	*80*	*80*	*80*
	Duty cycle	*65%*	*70%*	*75%*	*80%*
	Resolution	*0.26*	*0.40*	*0.69*	*0.84*

Table 5.2. Separation resolution results for channel height of 200µm. (For the 200µm channel, bubble formation observed at 80kVpp/m E-field and we lowered the E-field magnitude to get rid of the bubbles.

w=200µm	*Electrical field(kVpp/m)*	*80*	*80*	*50*	*50*
	Duty cycle	*75%*	*80%*	*75%*	*80%*
	Resolution	*Bubble*	*Bubble*	*0.61*	*Bubble*

Table 5.3. Separation resolution results for channel height of 75µm.

w=75µm	*Electrical field(kVpp/m)*	*80*	*80*	*133*	*133*
	Duty cycle	*80%*	*90%*	*75%*	*80%*
	Resolution	*0.31*	*0.49*	*0.25*	*bubble*

Table 5.4. ElFFF electrical circuit parameters

Channel Height	Rdl (double layer resistance)	Cdl (double layer capacitance)	Rbulk (bulk resistance)
w=75µm	184 Ohm	5 mF	41 Ohm
w=125µm	206 Ohm	1.8 mF	23 Ohm
w=200µm	1033 Ohm	0.5 mF	51 Ohm

Conclusion

By this study, it has been shown that the selection of the proper channel height has a crucial importance to achieve separations of the nanoparticles. In addition, baseline separation of the sub-50nm particles was achieved for the first time with the Cyclical ElFFF method. This separation became possible by selecting the optimum channel height and by applying the optimum voltage waveforms with high duty cycles. In general, by the help of the methods explained in this study, Cyclical Electrical Field Flow Fractionation

now carries a great potential in the fractionation of nanoparticles with sizes even smaller than 50nm.

References

[1] J. C. Giddings, "A new separation concept based on a coupling of concentration and flow nonuniformities," *Separation Science,* vol. 1, pp. 123-125, 1966.

[2] K. D. Caldwell, L. F. Kesner, M. N. Myers, and J. C. Giddings, "Electrical field-flow fractionation of proteins," *Science,* vol. 176, pp. 296-298, 1972.

[3] A. I. Lao, D. Trau, and I.-M. Hsing, "Miniaturized flow fractionation device assisted by a pulsed electric field for nanoparticle separation," *Analytical Chemistry,* vol. 74, pp. 5364-5369, 2002.

[4] A. Kantak, M. Srinivas, and B. Gale, "Characterization of a microscale cyclical electrical field flow fractionation system," *Lab Chip,* vol. 6, pp. 645-54, May 2006.

[5] Z. Chen and A. Chauhan, "Electrochemical response and separation in cyclic electric field-flow fractionation," *Electrophoresis,* vol. 28, pp. 724-739, 2007.

CHAPTER 6

SEPARATION OF MAGNETIC NANOPARTICLES BY CYCLICAL ELECTRICAL FIELD FLOW FRACTIONATION

Abstract

In this study, the potential of Cyclical Electrical Field Flow Fractionation (CyElFFF) for the separation of magnetic nanoparticles is investigated. We demonstrated for the first time that by the application of appropriate voltage waveforms, one can separate gold nanoparticles with sizes less than 50nm. By using suitable voltage waveforms, the detrimental effect of the particle diffusion is suppressed and particles in the range of 10nms can be fractionated. In addition, it is shown that CyElFFF is capable of separating lipid and polystyrene sulfonate coated magnetite nanoparticles with the same hydrodynamic radius of 50nm.

Introduction

Field Flow Fractionation (FFF) is a powerful method for the separation and characterization of macromolecular, colloidal and micron-sized particles [1].

Cyclical Electrical Field Flow Fractionation (CyElFFF) is one of the subtechniques of FFF which separates the particles according to their sizes and electrical mobilities [2]. In

CyElFFF, the separation channel is composed of bottom and top electrodes which are separated by a thin spacer.

A typical schematic of the CyElFFF system can be seen in Figure 6.1. In this system, oscillating voltages are applied to the electrodes which result in a cyclical electric field inside the channel. As a result of the cyclical electric field, particles move back and forth between the electrodes. Particles with high electrophoretic mobilities will move longer distances away from the channel walls and they spend more time in the faster fluid regions. As a consequence, they elute earlier than the lower mobility particles.

Earlier studies showed that diffusion of the nanoparticles is a limiting factor in CyElFFF. It gives rise to band broadening in the UV fractogram and prevents the achievement of high resolution separations. We address and solve this problem by changing the shape of the applied voltage waveform. In the earlier works, researchers used square wave voltages with DC offset voltages. In this work, we do not apply any DC offset voltages but we use square wave voltages with higher duty cycles (i.e., the duration of the positive voltage is larger than the duration of the negative voltage).

In the literature, magnetic SPLITT and magnetic FFF systems have been used for the separation of magnetic nanoparticles [3, 4]. In a recent work, separation with alternating magnetic fields was investigated numerically [5]. Unlike those works, in this study, we use alternating electric fields for the fractionation of magnetic nanoparticles instead of magnetic fields.

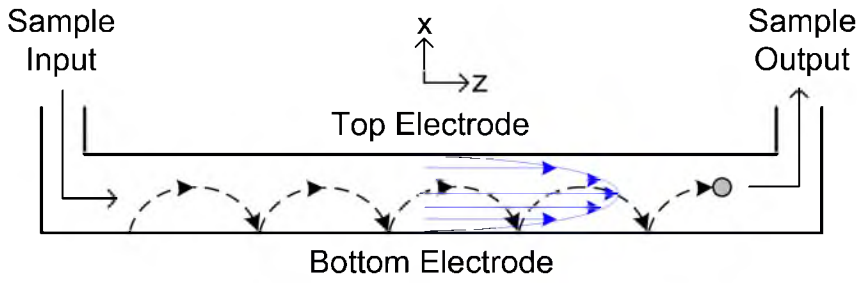

Figure 6.1. Cyclical ElFFF System. Dashed line shows the particle trajectory resulting from the cyclical field. (Operation principle: Oscillating square wave voltages are applied to the electrodes which result in a cyclical electric field inside the channel. As a result of the cyclical electric field, particles move back and forth between the electrodes. Particles with high electrophoretic mobilities move longer distances away from the channel walls and they spend more time at the faster fluid regions. As a consequence, they elute earlier than the lower mobility particles.)

Experimental Procedure

To investigate the separation capabilities of the CyElFFF system with the application of high duty cycle voltage waveforms, five experiments were done by using different types of nanoparticles. Nanoparticle types, particle coatings, hydrodynamic sizes and electrophoretic mobilities are summarized in Table 6.1.

The cyclical ElFFF channel used in the experiments was same as the one used in the earlier works [6-8]. The ElFFF channel had a length of 64cm, height of 178μm and a width of 2cm.

For all of the experiments, de-ionized water (18.2 MΩ/cm) was used as the carrier, which was pumped by the HPLC pump (Alltech model 426, Alltech Associates, Inc., IL, USA). The flow rate used in the experiments was 1ml/min, except for the experiment 3, in which the flow rate was 0.5 ml/min. Resulting void time in experiment 3 was 4.6 minute and void time for the remaining experiments was 2.3 minute.

Table 6.1. Properties of the particles used in the experiments. (For MACS particles, electrophoretic mobilities could not be obtained since zeta potential measurement didn't meet the quality criteria for those particles.)

	Exp1	Exp2	Exp3	Exp4	Exp5
Particle types	Gold (NanoComposix)	Magnetite (MACS)	Magnetite (MACS)	Magnetite (Chemicell)	Magnetite (Chemicell)
Average Size(s) (nm)	15 and 40	280	280	100	50
Coating	Tannic acid surfactant	antibody	antibody	Lipid / polystyrene sulfonate	Lipid / polystyrene sulfonate
Electrophoretic mobility (μmcm/Vs)	-3.7 -3.6	NA	NA	-2.6 -5.8	-3.2 -4.9

Application of AC and DC voltages was done by using Agilent signal generator (Model 33120A) and Agilent DC power supply (Model E3640A). For the detection of nanoparticles UV/Vis detector (ESA-Model 520) was used. The UV detector data, the electrical current flowing through the separation system and potential difference between the channel walls were measured by LabView (National Instruments) data acquisition card.

Each experiment began with the injection of the sample in to the ElFFF channel at t=0. Immediately following the injection, at t=0+, we turned on the power supply to apply 1V DC voltage for 1 minute. By the application of this constant voltage, we made sure that all the nanoparticles were attracted to the channel wall (accumulation wall). At t = 1 min, we turned on the HPLC pump to start the carrier flow. At the same time we also turned on the signal generator to apply the square wave voltage to the system. After observing the peaks in the UV detector, electrical power and pump were turned off. This recipe was followed in all of the experiments conducted. As a quick note, in this recipe, different from the earlier CyElFFF works [7-10], we only use the DC voltage in the first 1 min period, and after that, square wave voltages with high duty cycles are used alone.

In previous studies, researchers used DC offset voltages until the end of the separation experiments together with the 50% duty cycle square wave voltages.

Details of the separation experiments are given below.

Experiment 1

A mixture of 15 and 40nm mean diameter gold nanoparticles (NanoComposix, CA, USA) was used. Square wave voltages (10Hz, 10Vpp) with duty cycles ranging from 50% to 80% were applied.

Experiment 2

MACS anti-mouse IgG1 microbeads were used as the injected sample. Those are superparamagnetic particles which conjugated to epitope tag specific antibodies. Experimental conditions were the same as the experiment 1.

Experiment 3

Similar to experiment 2, MACS particles were injected. Applied voltage had amplitude of 10Vpp, frequency of 10Hz and a duty cycle of 60%. In this experiment, besides the UV detector, DAWN® HELEOS™ II light scattering detector was used to measure the rms radius of the particles.

Experiment 4

Lipid (fluidMAG-Lipid) and polystyrene sulfonate (fluidMAG-PS) coated 100nm (hydrodynamic size) magnetic nanoparticles were injected. Electrical parameters were

10 Vpp, 5Hz and 70% duty cycle.

Experiment 5

Lipid (fluidMAG-Lipid) and polystyrene sulfonate (fluidMAG-PS) coated 50nm (hydrodynamic size) magnetic nanoparticles were injected. Electrical parameters were 6Vpp, 10Hz and 75% duty cycle.

For each separation experiment, resolutions of the separations were calculated according to equation 6.1 below.

$$Rs = \frac{t_2 - t_1}{2(\sigma_1 + \sigma_2)} \qquad (6.1)$$

where t_1 and t_2 are the positions of the peaks and σ_1 and σ_2 are the standard deviations of the peaks as they are approximated to a Gaussian curve.

Finally, to determine the operation modes of all separation experiments, mean excursion distances of the particles were calculated. Mean excursion distance is the length traveled by the particle across the channel thickness during the negative cycle of the voltage. We denoted this length by l_{e-} which was calculated according to the equation 6.2. Where f (Hz) is the applied frequency, dc is the duty cycle of the voltage waveform, μ_p (m2/Vs) is the electrophoretic mobility of the particle and E_{eff} (V/m) is the effective electric field inside the channel.

$$l_{e-} = -\mu_p \int_{1/f*dc}^{1/f} E_{eff}(t)dt \qquad (6.2)$$

In equation 6.2, integral of the electric field inside the channel was calculated for the negative cycle of the applied voltage and this result was multiplied by the

electrophoretic mobility of the particle to obtain the length traveled by the particle.

The effective field represented in equation 6.2 was calculated by using equation 6.3 below.

$$E_{eff}(t) = \frac{I(t) \times R_{bulk}}{w} \qquad (6.3)$$

where, *I(t)* is the measured current in Amperes, *w (m)* is the channel height and R_{bulk} (Ω) is the resistor representing the electrical resistance of the carrier liquid between the channel walls. R_{bulk} value was calculated according to the methods explained by Srinivas et al [7].

Results and Discussion

UV fractograms obtained from experiments 1 and 2 can be seen in Figure 6.2. As shown in Figure 6.2a, as we increase the duty cycle of the applied voltage, we obtain 2 separate peaks, corresponding to 15 and 40 nm gold nanoparticles. The highest resolution was achieved at a duty cycle of 75%. As presented in Table 6.2, the resolution corresponding to 75% duty cycle condition is 1.71, which is much higher than the resolutions of other duty cycle experiments.

As we look at the electrophoretic mobilities of the 15 and 40nm particles, we observe that they are close to each other. This shows us that considerable amount of the separation is due to the diffusion coefficients of the particles.

Figure 6.2b is the experimental result obtained for MACS nanoparticles. It is clear that as the duty cycle of the applied voltage is increased, magnetic particles retained more in the channel. Maximum retention was obtained for 80% duty cycle case, but a small

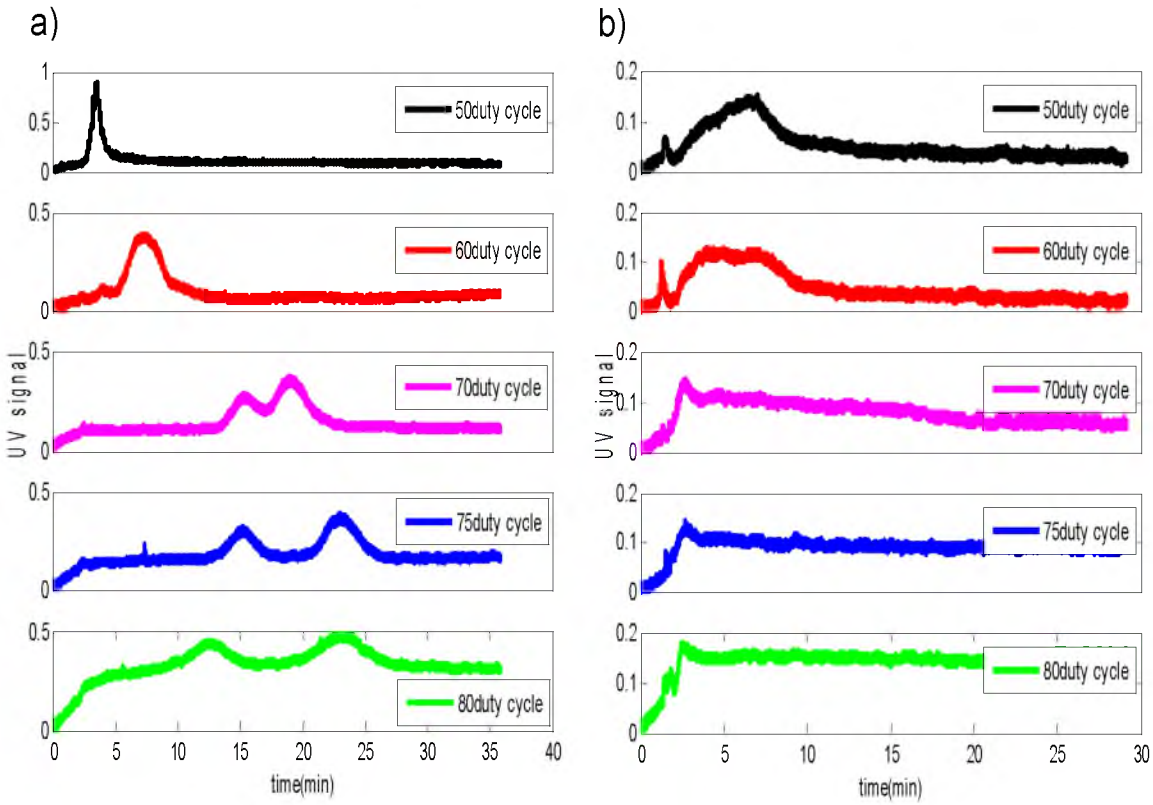

Figure 6.2. UV fractograms a) for 15 and 40nm gold nanoparticle mixture (exp1) b) for MACS magnetic particles (exp2)

separation was obtained for only the 60% duty cycle condition, with a separation resolution of 0.53 (Table 6.2, exp2).

Figure 6.3 shows the UV fractogram and light scattering data for exp3. Mean rms radius of the magnetic nanoparticles is measured as 140nm, and the particles eluted later have slightly less rms radiuses compared to the ones eluted earlier. According to Figure 6.3, MACS nanoparticles have an average rms radius of 140nm with a narrow range of ±10nm. In addition, these particles have broad range of electrophoretic mobilities (as determined from the wide range of retention times). We predict that high variation in the electrophoretic mobilities can be resulted from the difference in the number of attached antibodies to the nanoparticles.

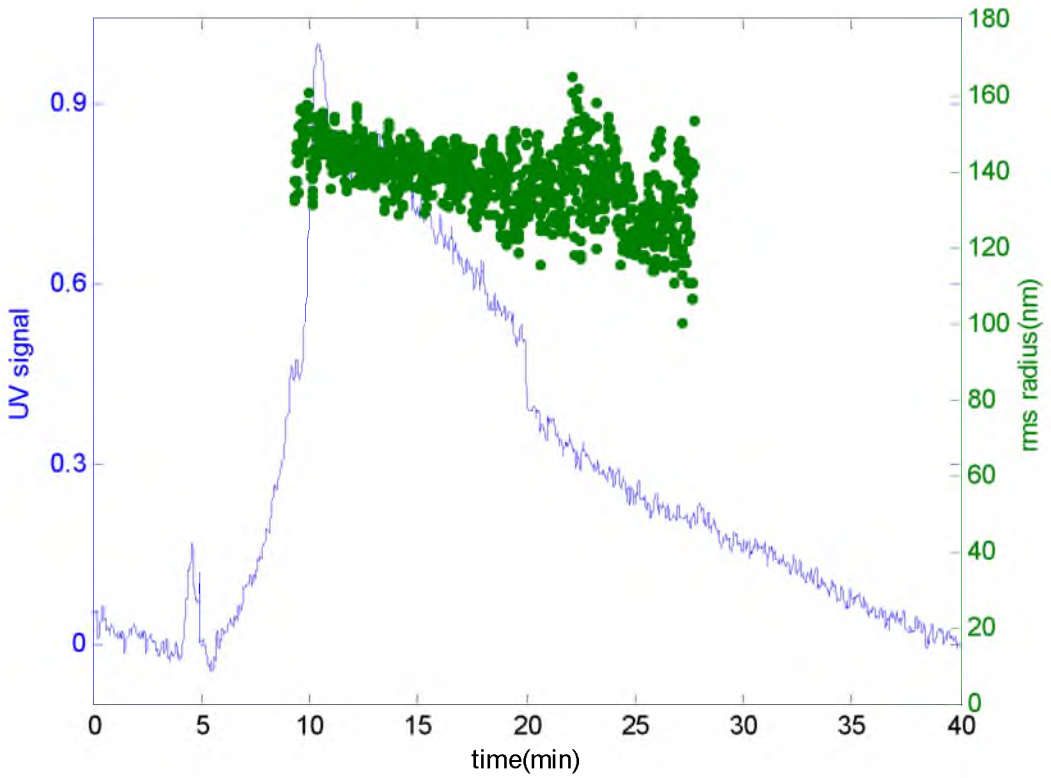

Figure 6.3. UV absorption fractogram and rms radius data of the MACS nanoparticles (exp3). Voltage: 10Vpp, 10Hz, 60% duty cycle. Flow: 0.5ml/min.

Result of experiment 4 can be seen in Figure 6.4. In this experiment, injection of lipid and polystyrene sulfonate (PS) coated 100nm magnetite particles were used. As shown, both PS and lipid coated particles have high retention times (more than 10 minutes). Since lipid coated magnetite particles have smaller average electrophoretic mobility (shown in Table 6.1), lipid coated particles have a higher retention time compared to the PS coated ones. The UV fractogram obtained for the mix shows that we couldn't get a separation at these operating conditions. We have a single and broader peak for the injection of the particle mixture. Electrical parameters used in this experiment were 10Vpp, 5Hz and 70% duty cycle. These parameters should be further optimized with more experiments to obtain separate peaks in the UV fractogram. In summary, in experiment 4, by high duty cycle (70%) application in CyElFFF, high

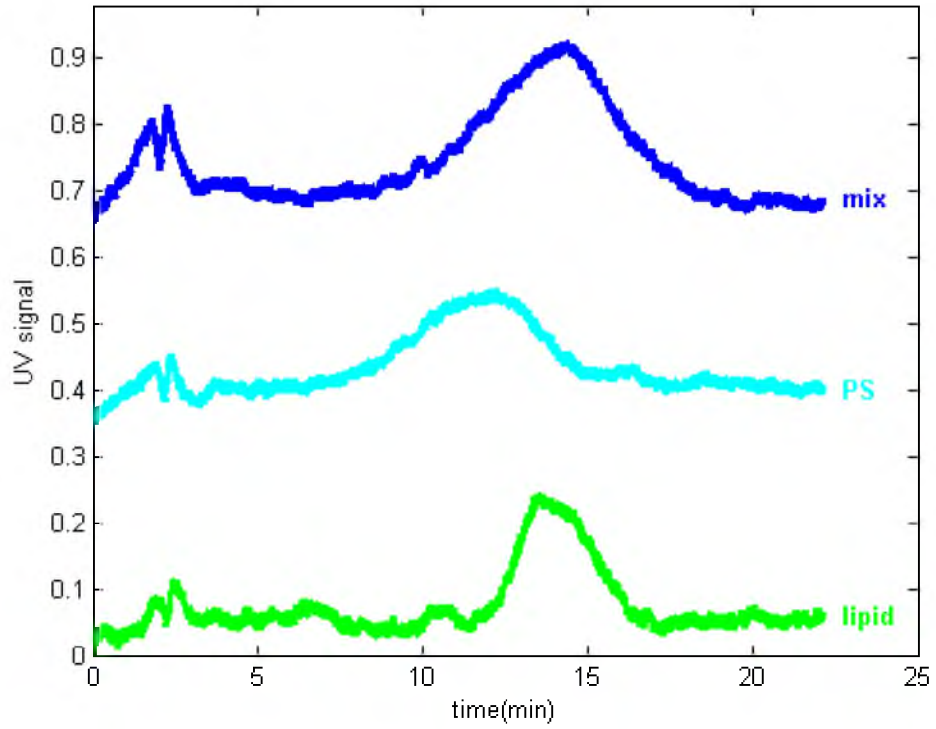

Figure 6.4. UV fractograms of 100nm lipid and polystyrene sulfonate (PS) coated magnetite nanoparticles (exp4). Voltage: 10Vpp, 5Hz, 70% duty cycle. Flow: 1ml/min.

retention times were obtained for both lipid and PS coated magnetite particles. Further experiments are needed to obtain a reasonable separation between those 100nm magnetite particles.

UV fractograms corresponding to experiment 5 can be seen in Figure 6.5. In this experiment, lipid and PS coated 50nm magnetite particles were used. As shown, similar to experiment 4, both PS and lipid coated particles had high retention times (again more than 10 minutes). As can be seen in the UV fractogram corresponding to the particle mixture, we can see two peaks instead of a single peak. The resolution of the separation was 0.67 as tabulated in Table 6.2. Thus, this result shows that Cyclical ElFFF is capable of separating same sized magnetic nanoparticles (50nm in this particular experiment) with different coatings such as lipid and polystyrene sulfonate.

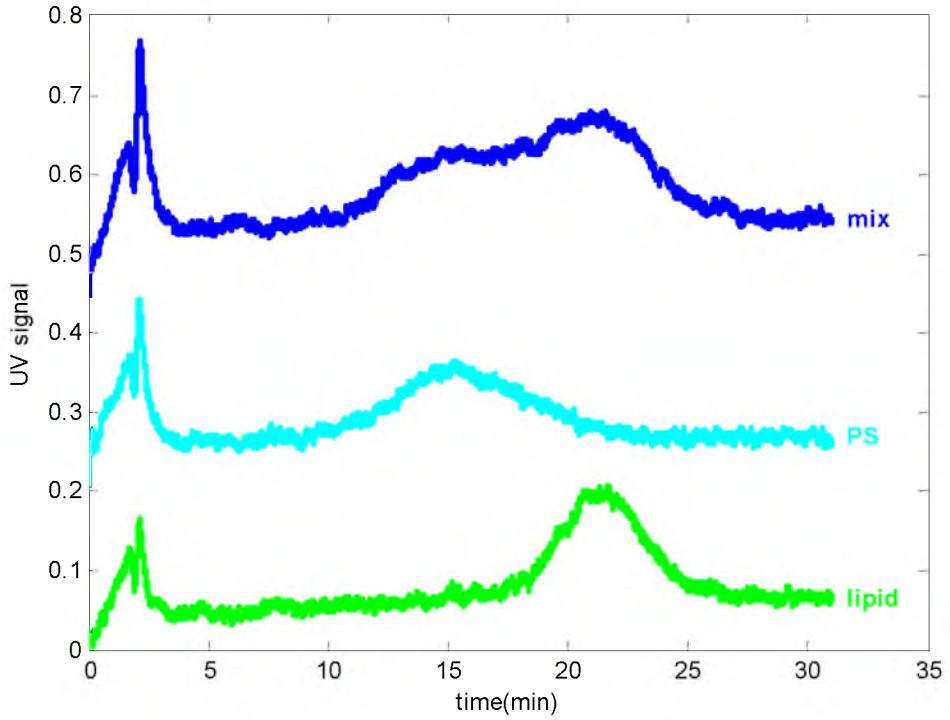

Figure 6.5. UV fractograms of 50nm lipid and polystyrene sulfonate (PS) coated magnetite nanoparticles (exp5). Voltage: 6Vpp, 10Hz, 75% duty cycle. Flow: 1ml/min

Table 6.2. Resolutions and mean excursion lengths calculated for the experiments.

	Exp1	Exp2	Exp3	Exp4	Exp5
Resolutions	dutycycle=50% 0.00	dutycycle=50% 0.00	0.00	0.00	**0.67**
	dutycycle=60% 0.00	dutycycle=60% **0.53**			
	dutycycle=70% 0.85	dutycycle=70% 0.00			
	dutycycle=75% **1.71**	dutycycle=75% 0.00			
	dutycycle=80% 1.19	dutycycle=80% 0.00			
Mean excursion lengths $l_{e^-}(\mu m)$	dutycycle=50% 45.5 (for 15nm) 44.3 (for 40nm)	NA	NA	32.2 (for lipid) 71.9 (for PS)	13.3 (for lipid) 20.4 (for PS)
	dutycycle=60% 38.5 (for 15nm) 37.5 (for 40nm)				
	dutycycle=70% 22.8 (for 15nm) 22.2 (for 40nm)				
	dutycycle=75% 16.3 (for 15nm) 15.9 (for 40nm)				
	dutycycle=80% 10.9 (for 15nm) 10.6 (for 40nm)				

Finally, as we looked at the mean excursion lengths (l_{e^-}) of the particles in Table 6.2, we see that all lengths are less than the channel thickness. As a result, in each experiment the operation mode of the FFF system was 'mode I'. Meaning that particles do not reach the opposite channel wall during each cycle of the voltage waveform. Different than mode I, in modes II and III of the FFF systems, particles reach the opposite channel wall in each cycle of the square wave voltage.

Conclusion

It has been shown for the first time that Cyclical Electrical Field Flow Fractionation can be used for the size and electrophoretic mobility analysis of the magnetic nanoparticles. As we increase the duty cycle of the applied voltage, magnetic nanoparticles gain higher retention times in the separation channel. By applying higher duty cycles, the detrimental effect of particle diffusion is suppressed and separations of particles less than 100nm could be possible. Mainly, separation of same sized (50nm) magnetite nanoparticles with different coatings is achieved. As a future work, Cyclical ElFFF experiments will be conducted with other various coating types and particle sizes.

References

[1] J. C. Giddings, "A new separation concept based on a coupling of concentration and flow nonuniformities," *Separation Science,* vol. 1, pp. 123-125, 1966.

[2] K. D. Caldwell, L. F. Kesner, M. N. Myers, and J. C. Giddings, "Electrical field-flow fractionation of proteins," *Science,* vol. 176, pp. 296-298, 1972.

[3] F. Carpino, L. R. Moore, M. Zborowski, J. J. Chalmers, and P. S. Williams, "Analysis of magnetic nanoparticles using quadrupole magnetic field-flow fractionation," *Journal of Magnetism and Magnetic Materials,* vol. 293, pp. 546-552, 2005.

[4] A. H. Latham, R. S. Freitas, P. Schiffer, and M. E. Williams, "Capillary magnetic field flow fractionation and analysis of magnetic nanoparticles," *Analytical Chemistry,* vol. 77, pp. 5055-5062, 2005.

[5] T. O. Tasci, W. P. Johnson, and B. K. Gale, "Cyclical magnetic field flow fractionation," *Journal of Applied Physics,* vol. 111, p. 07D128, 2012.

[6] K. D. Caldwell and Y. S. Gao, "Electrical field-flow fractionation in particle separation. 1. Monodisperse standards," *Analytical Chemistry,* vol. 65, pp. 1764-1772, 1993.

[7] B. K. Gale and M. Srinivas, "Cyclical electrical field flow fractionation," *Electrophoresis,* vol. 26, pp. 1623-32, May 2005.

[8] J. Gigault, B. K. Gale, I. Le Hecho, and G. t. Lespes, "Nanoparticle characterization by cyclical electrical field-flow fractionation," *Analytical Chemistry,* vol. 83, pp. 6565-6572, 2011.

[9] A. Kantak, M. Srinivas, and B. Gale, "Characterization of a microscale cyclical electrical field flow fractionation system," *Lab Chip,* vol. 6, pp. 645-54, May 2006.

[10] M. Srinivas, H. J. Sant, and B. K. Gale, "Optimization of cyclical electrical field flow fractionation," *Electrophoresis,* vol. 31, pp. 3372-9, Oct 2010.

CHAPTER 7

CYCLICAL MAGNETIC FIELD FLOW FRACTIONATION

Abstract

In this study, a new magnetic field flow fractionation system was designed and modeled by using finite element simulations. Other than current magnetic FFF systems, which use static magnetic fields, our system uses cyclical magnetic fields. Results of the simulations show that our cyclical magnetic FFF system can be used effectively for the separation of magnetic nanoparticles.

Cyclical Magnetic FFF system is composed of a microfluidic channel (length=5cm, height=30μm) and 2 coils. Square wave currents of 1Hz (with 90 degrees of phase difference) were applied to the coils. By using Comsol Multiphysics 3.5a, magnetic field profile and corresponding magnetic force exerted on the magnetite nanoparticles were calculated. The magnetic force data were exported from Comsol to Matlab. In Matlab, a parabolic flow profile with maximum flow speed of 0.4mL/h was defined. Particle trajectories were obtained by the calculation of the particle speeds resulted from both magnetic and hydrodynamic forces.

Particle trajectories of the particles with sizes ranging from 10nm to 50nm were simulated and elution times of the particles were calculated. Results show that there is a

significant difference between the elution times of the particles so that baseline separation of the particles can be obtained.

In this work, it is shown that by the application of cyclical magnetic fields, the separation of magnetic nanoparticles can be done efficiently.

Introduction

In this study, a novel magnetic field flow fractionation (FFF) system was designed and modeled by using finite element simulations. Other than current magnetic FFF systems [1, 2], which use static magnetic fields, our system uses cyclical magnetic fields for the separation of magnetic nanoparticles. In the cyclical magnetic FFF system, in addition to the magnetic field strength, frequency of the magnetic field can also be adjusted to achieve the best separation results. Simulation results show that cyclical magnetic FFF system can effectively be used for the separation of magnetic nanoparticles.

Theory and Methods

Cyclical Magnetic FFF system is composed of a microfluidic channel and two electromagnets, shown in Figure 7.1. A pressure driven flow is generated, resulting in a parabolic flow profile in the channel. After the stop flow relaxation of the particles, square wave currents with 90 degrees of phase difference are applied to the top and bottom electromagnets, so that the particles are driven away from the bottom channel wall. The particles with higher magnetophoretic mobilities will move longer distances

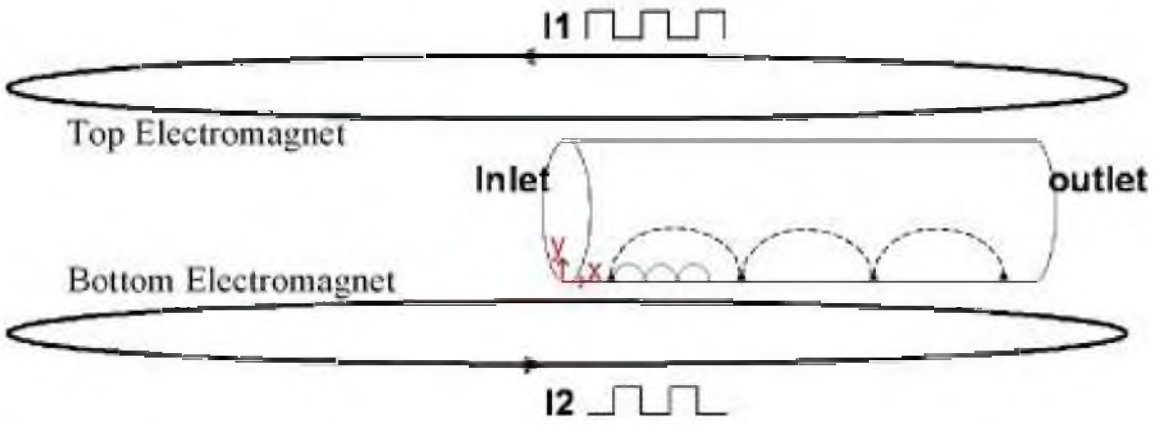

Figure 7.1. Cyclical Magnetic FFF System. Square pulses with pi/2 phase difference were applied to the electromagnets. Dashed line shows the particle trajectory for the particle with high magnetophoretic mobility . Solid line shows the particle trajectory for the low magnetophoretic mobility particle. (x=0 shows the inlet of the channel, y=0 is the bottom wall of the channel)

away from the channel walls. As a result, they stay in the faster fluid regions and elute earlier than the lower mobility particles.

A microfluidic channel (length=5cm, height=30μm) was modeled in Comsol Multiphysics. Square wave magnetic fields were generated by the electromagnets (B=0.8T, f=1Hz). An inlet velocity of 0.4mL/h was defined, resulting flow profile and magnetic field can be seen in Figure 7.2.

By using the magnetic field profile obtained from Comsol Multiphysics simulation, magnetic force acting on the magnetite (Fe_3O_4) nanoparticles was calculated according to eqn 7.1 (next page). Where $\mathbf{V_p}$ is the volume of the particle, $\boldsymbol{\chi_p}$ is the particle susceptibility, $\mathbf{B}$ is the magnetic flux density and $\boldsymbol{\mu_0}$ is the magnetic permeability of the free space. To obtain the volume magnetic susceptibility for different size magnetite particles at given magnetic fields, equations supplied by Rosensweig[3] was used.

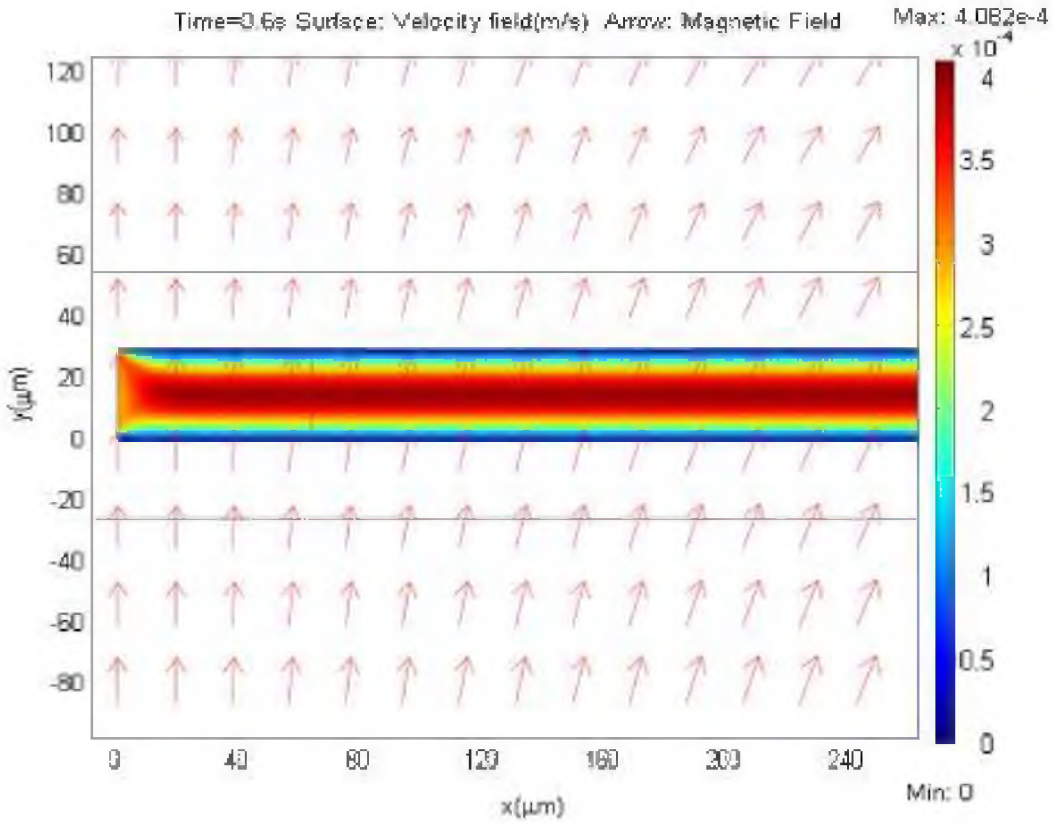

Figure 7.2. Comsol Simulation Plot. Surface plot shows the pressure driven fluid velocity. Arrows show the magnetic field vectors when the upper electromagnet is active.

$$F_{magx} = \frac{V_p \chi_p}{\mu_0}\left(B_x \frac{\partial B_x}{\partial x} + B_y \frac{\partial B_x}{\partial y}\right)$$

$$F_{magy} = \frac{V_p \chi_p}{\mu_0}\left(B_x \frac{\partial B_y}{\partial x} + B_y \frac{\partial B_y}{\partial y}\right) \qquad (7.1)$$

Hydrodynamic force acting on the nanoparticles was calculated by using Stokes drag law.

$$F_{drag} = 6\pi\eta r_p (v_f - v_p) \qquad (7.2)$$

where, η is the fluid viscosity, r_p is the particle radius, v_f is the velocity of the fluid resulting from the pressure driven flow, and v_p is the velocity of the particle.

By using eqn 7.1 and eqn 7.2 with Newton's second law, we obtain the following equation, where $\mathbf{m_p}$ is the particle mass.

$$m_p \frac{\partial v_p}{\partial t} = F_{mag} + F_{drag} \qquad (7.3)$$

Due to their very small particle sizes, nanoparticles reach their equilibrium velocity almost instantaneously and as a result we neglect the inertia term in the above equation, and obtain the particle velocity as below.

$$v_p = \frac{F_{mag}}{6\pi\eta r_p} + v_f \qquad (7.4)$$

To find the particle trajectories in the channel, a Matlab code was generated which solves the particle velocity equation, eqn 7.4.

Results

Particle trajectory of a 40nm magnetite particle inside the channel was calculated and shown in Figure 7.3. Figure 7.3a represents the particle motion in the absence of the pressure driven flow, so that only source of motion is the magnetic force. Figure 7.3b shows the motion of the particle, in the presence of the pressure driven flow. As can be seen in the figure, as the particle goes away from the bottom wall of the channel, it gains a higher x velocity and move along the channel.

Particle trajectories of 30 and 50nm magnetite particles were obtained for the first 3.6 seconds of fractionation (Figure 7.4). As shown in the figure, 50nm particle moves much faster throughout the channel.

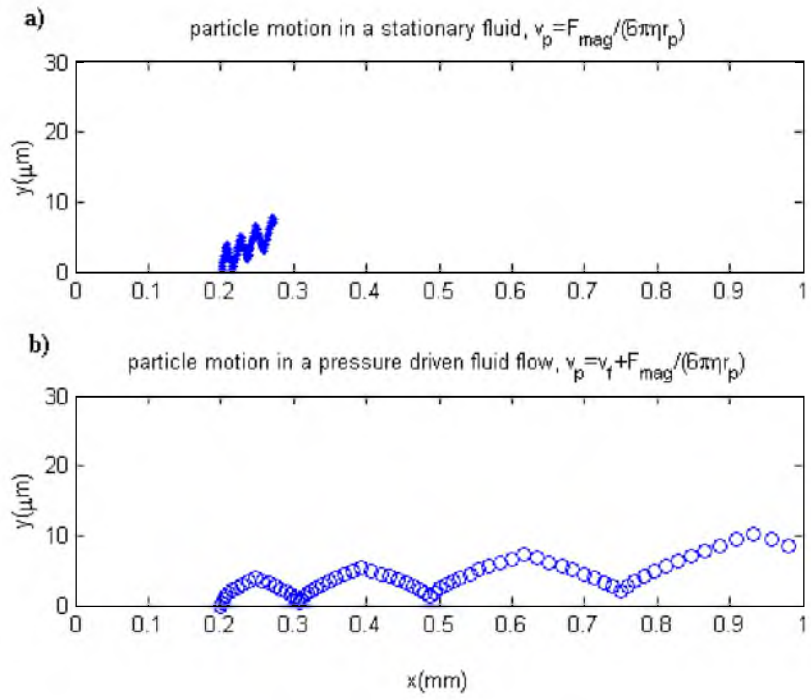

Figure 7.3. Particle motion of the 40nm magnetite particle inside the channel.
Y-axis shows the channel height, X-axis shows the 1mm portion of the channel. Initial position of the particle was chosen as x0=0.2mm, y0=0.
a) Particle trajectory in the absence of pressure driven flow.
b) Particle trajectory in the in the presence of pressure driven flow.

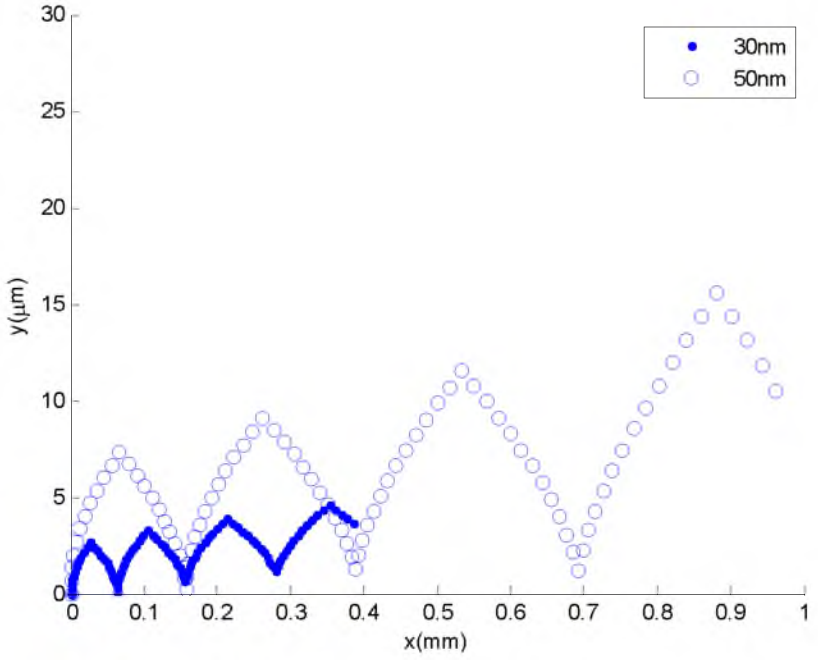

Figure 7.4. Particle trajectories of 30nm and 50nm particles, between t = 0 - 3.6s. (Y axis shows the channel height and X-axis shows the 1mm portion of the channel length)

The elution times of the particles ranging from 10nm to 50nm were calculated and plotted in Figure 7.5. Dots represent the resulting elution times for the applied frequency of 1Hz, circles represent the result for f=5Hz. As can be seen, for both of the frequencies there is a significant difference between the elution times of the different sized particles. In addition, for 1 Hz frequency, elution time differences between the particles are slightly larger compared to 5Hz condition, and we are getting a considerably better seperation for 1Hz field application. The realistic frequencies for this system are in the range of a few tens of Hz.

As observed in the earlier works [4-6], for a fixed magnetic field amplitude, as we increase the frequency to a much higher value, the distance travelled by the particle in one cycle becomes too low, and this will result in a very poor or no seperation. In terms of sychronization of the particle motion with the magnetic field, for low frequencies (f<50Hz) the motion of the particles are synchronized with the magnetic field [4-6].

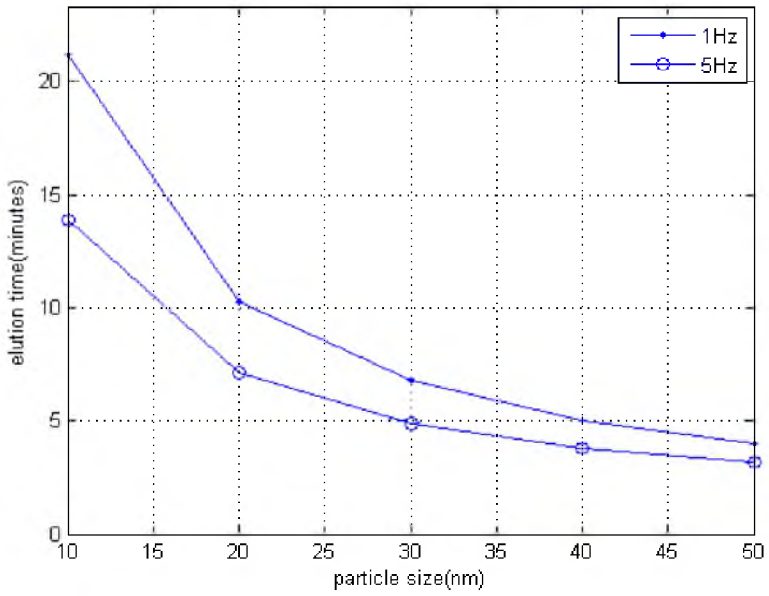

Figure 7.5. Elution time versus particle size graph for the spherical magnetite particles with sizes between 10nm & 50nm. Dots represent the result for f=1Hz, circles represent the result for f=5Hz.

Conclusion

In this work, a cyclical magnetic FFF system was modeled and it was shown that by the application of cyclical magnetic fields, the separation of magnetic nanoparticles can be done efficiently. Compared to the current magnetic FFF systems, this system can be easily adjusted for different types of particle samples, and it is done by just modifying the strength and frequency of the magnetic field. The future work will be the fabrication of the system and the comparison of the experiments with the theoretical data presented here.

References

[1] F. Carpino, L. R. Moore, M. Zborowski, J. J. Chalmers, and P. S. Williams, "Analysis of magnetic nanoparticles using quadrupole magnetic field-flow fractionation," *Journal of Magnetism and Magnetic Materials,* vol. 293, pp. 546-552, 2005.

[2] A. H. Latham, R. S. Freitas, P. Schiffer, and M. E. Williams, "Capillary magnetic field flow fractionation and analysis of magnetic nanoparticles," *Analytical Chemistry,* vol. 77, pp. 5055-5062, 2005.

[3] R. E. Rosensweig, "Heating magnetic fluid with alternating magnetic field," *Journal of Magnetism and Magnetic Materials,* vol. 252, pp. 370-374, 2002.

[4] Y. Wang, J. Zhe, B. Chung, and P. Dutta, "A rapid magnetic particle driven micromixer," *Microfluidics and Nanofluidics,* vol. 4, pp. 375-389, 2008.

[5] A. Munir, W. Jianlong, Z. Zanzan, and H. S. Zhou, "Mathematical modeling and analysis of a magnetic nanoparticle-enhanced mixing in a microfluidic system using time-dependent magnetic field," *Nanotechnology, IEEE Transactions on,* vol. 10, pp. 953-961, 2011.

[6] Y. K. S. T.N Le, S. Kang, "Efficient mixing in microchannel by using magnetic nanoparticles," *International Journal of Mathematical Models and Methods in Applied Sciences,* vol. 3, 2009.

CHAPTER 8

A FERROFLUIDIC MAGNETIC MICROMIXER

Introduction

In this study, a novel microfluidic mixer is designed and fabricated by using a permanent magnet, ferrofluid, and a serpentine microfluidic channel. Apart from other magnetic micromixers presented in the literature, this is a passive mixer and does not include any moving parts or electromagnets. It has been shown that mixing efficiency of a regular serpentine micromixer can be increased more than four-fold and mixing efficiencies up to 95% can be achieved. In addition to mixing two or more fluids, this microfluidic mixer can also be used for mixing of magnetic beads/nanoparticles with proteins and/or cells to achieve very high binding rates. We believe, with its simple fabrication and high mixing efficiency, ferrofluidic magnetic micromixer has a big potential to be used as a mixer tool for numerous microfluidic applications.

Background

Magnetic microfluidic mixers designed until now were all active micromixers, which used moving parts [1] or electrical actuation of electromagnets [2]. These active magnetic micromixers were produced through complex fabrication steps which prevented them to be widely used mixing tools [3, 4]. To our knowledge, the magnetic ferrofluidic

micromixer presented here is the first magnetic microfluidic mixer operated by passive actuation.

Methods

Operation principle of the micromixer can be seen in Figure 8.1. There are three inlets in the device. One is for the ferrofluid and the other two are for the fluids to be mixed. A permanent magnet is used to attract the ferrofluid. While magnetic force is pulling the ferrofluid downwards, ferrofluid deflects the flow paths of other fluids. Since flow paths of the fluids are intercepted by ferrofluid at each serpentine leg, efficient mixing of the fluids occurs in every leg of the serpentine. As shown, the micromixer has two outlets; the one close to the magnet is used to collect the ferrofluid, and the other one is used to collect the fluid mixture.

The mixer was fabricated from PDMS by using the process of Xurography [5]. The mold for the microfluidic channel was cut in tape (Gerber Instachange Removable Film, Gerber Scientific Products, Tolland, CT, USA) using a CO2 laser (VLS 3.60, Universal Laser Systems, AZ, USA). The channel was then transferred to a petri-dish using a transfer adhesive. PDMS (Sylgard 184, Dow Corning) at 10:1 base to curing agent ratio was poured into mold and was cured at 65 $^{\circ}$C for two hours. Finally, access holes were cored for inlets and outlets, and two PDMS layers were bonded by using corona discharge treatment.

Microfluidic channel had a width of 1.5mm and a height of 100 microns. The ferrofluid used in the mixer was a water based ferrofluid with an average magnetite

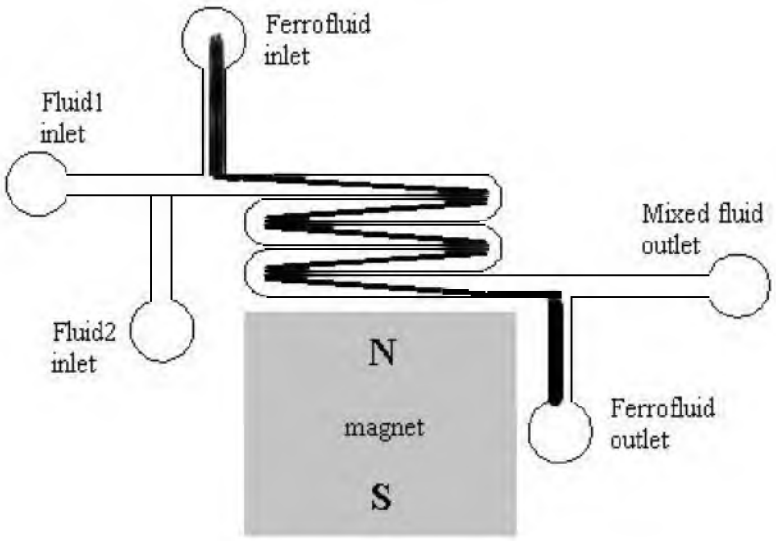

Figure 8.1. Micromixer operation principle. As a consequence of the magnetic force, ferrofluid tends to go downward and deflects the flow paths of fluid1 and 2, causing them to mix.

particle size of 10nm and a density of 60.5mg/ml. The permanent magnet used was a N40 grade neodymium magnet. Picture of the actual device can be seen in Figure 8.2.

Mixing experiments were conducted at flow rates of 0.01ml/min, 0.05ml/min, 0,1ml/min and 0.15ml/min, while the magnet was located 1 cm away from the bottom leg of the serpentine channel. Fluids to be mixed were chosen as blue and yellow fluids, which were prepared by mixing DI water with food coloring dyes. Photographs were taken at the inlet and outlet parts of the mixer by using microscope and camera. Pictures were investigated by ImageJ 1.44p software to calculate the mixing efficiencies according to the mixing efficiency equation shown on the next page.

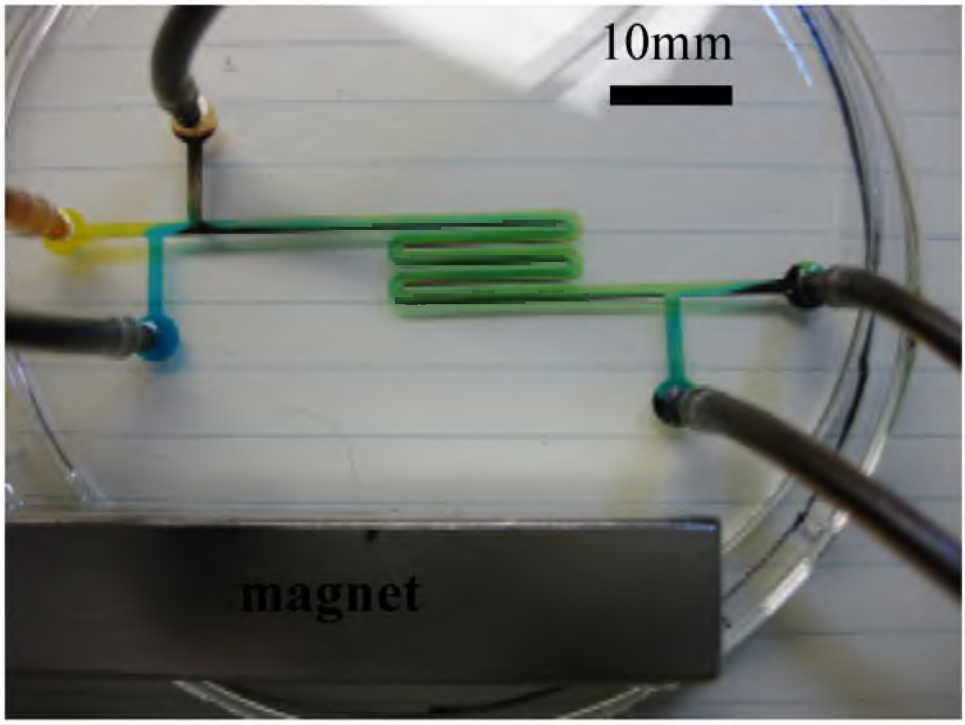

Figure 8.2. Actual picture of the micromixer device

$$MixingEfficiency = \frac{std(inputprofile) - std(outputprofile)}{std(inputprofile)} \times 100$$

Equation: Mixing efficiency equation, std (inputprofile) is the standard deviation of the color profile at the inlet and std (outputprofile) is the standard deviation of the outlet color profile.

Results

Figure 8.3 represents the mixing results at the serpentine portion of the mixer. The left column shows the result for "no magnet" condition and right column shows the result when the magnet is placed. As can be seen, presence of the magnet significantly improves mixing. As a consequence of mixing of yellow and blue fluids, green color was observed. It is clear that most efficient mixing was obtained for the lowest flow rate of 0.01ml/min and we see a totally green serpentine channel for this condition.

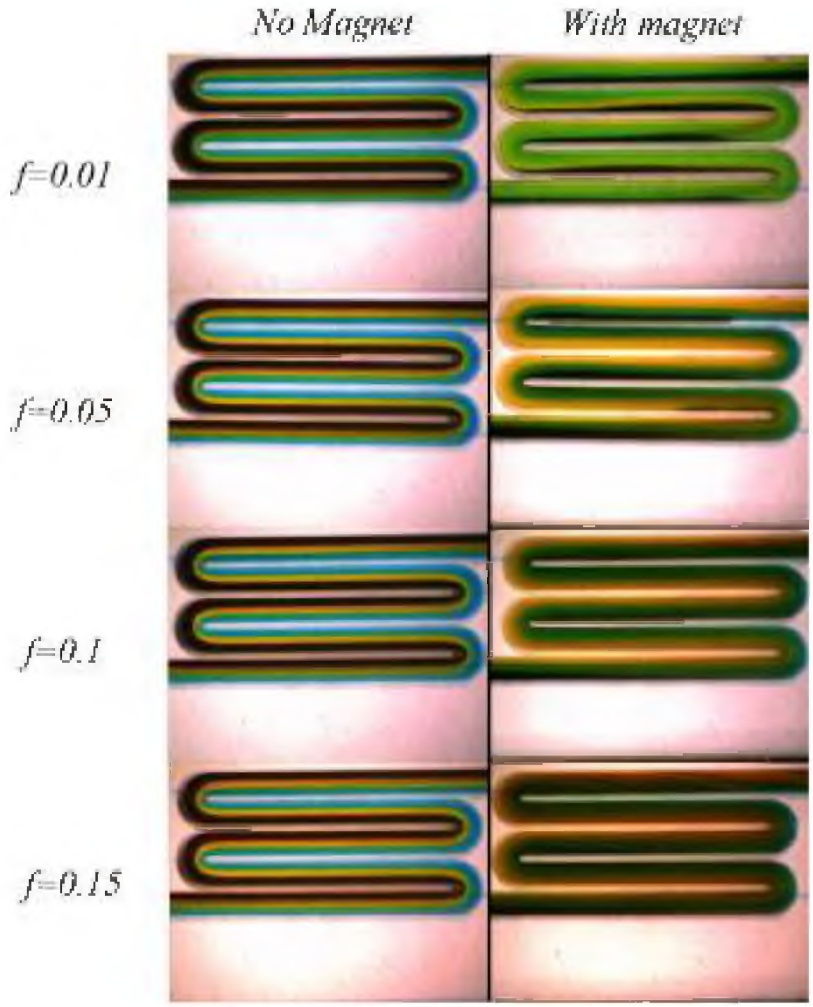

Figure 8.3. Mixing at the serpentine part of the micromixer. *f* is the flow rate in ml/min.

Figure 8.4 shows the outlet portion of the micromixer. Again maximum mixing was observed for the lowest flow rate case, and similarly uniform green color is observed at the outlet as well.

Mixing efficiencies of the mixers are tabulated in Table 8.1. As can be seen, for each flow rate, the mixing efficiency of the classical serpentine mixer was increased significantly by the presence of the magnet and ferrofluid. For the 0.15ml/min case, mixing efficiency of the serpentine mixer was increased by more than four-fold. The maximum mixing efficiency of 94% was obtained for 0.01ml/min flow rate.

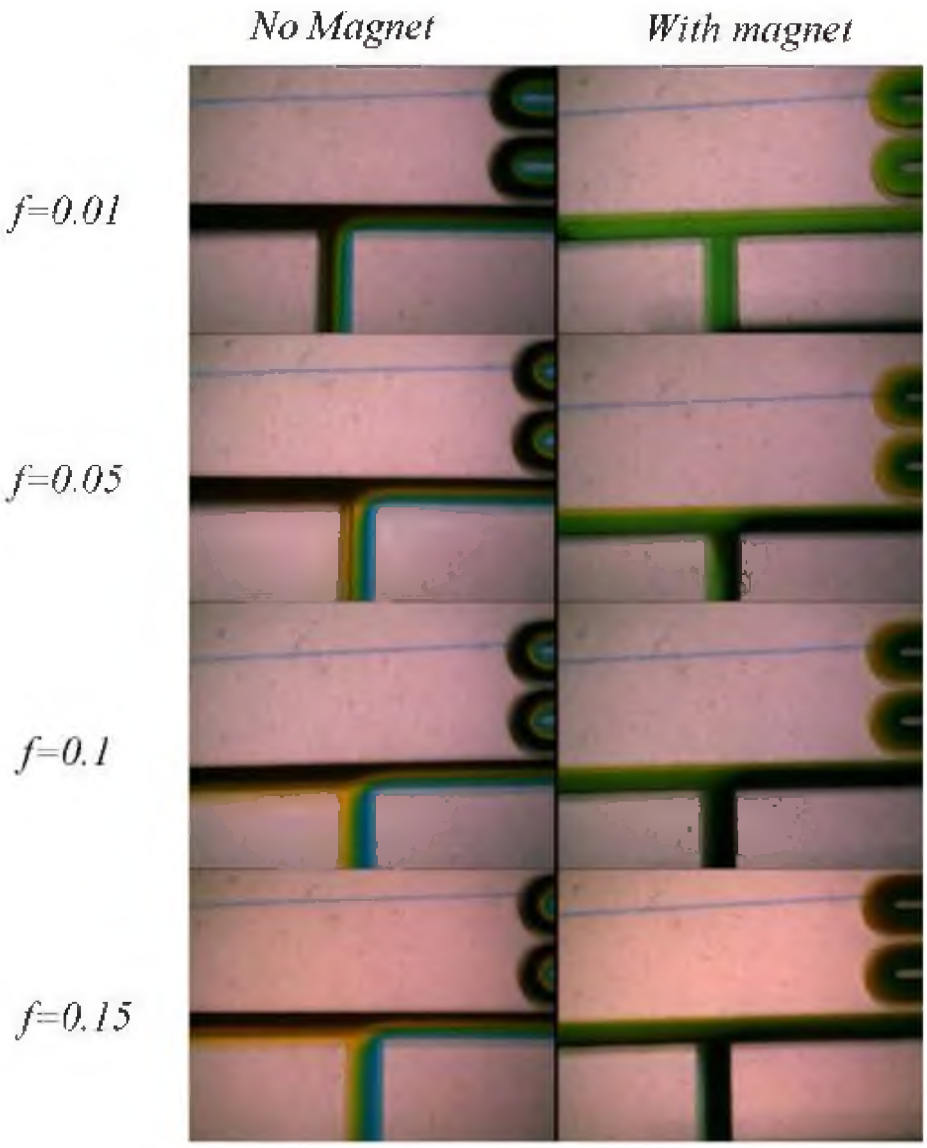

Figure 8.4. Mixing at the outlet part of the micromixer. *f* is the flow rate in ml/min.

Table 8.1. Mixing efficiencies for different flow rates at "no magnet" and "with magnet" conditions.

Mixing Efficiencies	**Flow rates (ml/min)**			
	$f = 0.15$	$f = 0.10$	$f = 0.05$	$f = 0.01$
Serpentine (No Magnet)	17 ± 8	24 ± 8	29 ± 7	37 ± 5
Serpentine (With Magnet)	76 ± 3	81 ± 2	86 ± 2	**94 ± 1**

Conclusion

A novel magnetic micromixer was fabricated by using a permanent magnet and ferrofluid. Results show that complete mixing of the fluids was achieved for flow speeds around 0.01ml/min. This system can also be used for mixing magnetic nanoparticles or microbeads with several biofluids, e.g., for tagging proteins and cells with magnetic particles. For this purpose, ferrofluid in the mixer can easily be replaced by magnetic nanoparticles or microbeads. As a future work, magnetic ferrofluidic micromixer will be tested with ferrofluids of various concentrations. In addition, mixing experiments will be conducted with magnetic microbeads and antibodies, and improvement in the binding efficiencies will be investigated.

References

[1] O. Dong-Wook, J. Jae Sik, C. Jai Hyun, K. Ho-Young, and L. Joon Sik, "A microfluidic chaotic mixer using ferrofluid," *Journal of Micromechanics and Microengineering,* vol. 17, p. 2077, 2007.

[2] C.-Y. Wen, C.-P. Yeh, C.-H. Tsai, and L.-M. Fu, "Rapid magnetic microfluidic mixer utilizing AC electromagnetic field," *Electrophoresis,* vol. 30, pp. 4179-4186, 2009.

[3] L. Chia-Yen, L. Gwo-Bin, L. Jr-Lung, H. Fu-Chun, and L. Chia-Sheng, "Integrated microfluidic systems for cell lysis, mixing/pumping and DNA amplification," *Journal of Micromechanics and Microengineering,* vol. 15, p. 1215, 2005.

[4] K. S. Ryu, K. Shaikh, E. Goluch, Z. Fan, and C. Liu, "Micro magnetic stir-bar mixer integrated with parylene microfluidic channels," *Lab Chip,* vol. 4, pp. 608-613, 2004.

[5] D. A. Bartholomeusz, R. W. Boutte, and J. D. Andrade, "Xurography: rapid prototyping of microstructures using a cutting plotter," *Microelectromechanical Systems, Journal of,* vol. 14, pp. 1364-1374, 2005.

CHAPTER 9

CONCLUSION

In this study, by addressing the main limitations of both Electrical and Magnetic Field Flow Fractionation systems, considerable improvements are achieved in these separation methods.

Basically, one order of magnitude improvement is obtained in the separation capability of the Cyclical ElFFF systems. Previously, this technique was only capable of fractionating particles bigger than 100 nanometers. Whereas, in this work, it is shown that, separation of particles on the order of 10 nanometers is now possible.

The diffusion drawback of CyElFFF systems is resolved by application of high duty cycle waveforms. In addition, optimum operating mode to achieve high resolution separations is presented theoretically, and verified through the separation experiments. While using high duty cycle voltages, by operating the CyElFFF systems in this explained (optimum) state, highest possible resolutions can be obtained.

Besides application of high duty cycle voltages, a completely new method is created to accomplish high resolution separations. In this method, the electrical circuitry of the ElFFF system is modified by addition of several electrical components. This

technique is verified via experiments, in which baseline separations of 15 and 40 nm gold nanoparticles are achieved.

In addition to the improvements gained in the experimental side, developments have been made in modeling side as well. The first particle based modeling of CyElFFF systems is done. The particle based simulation code generated is capable of visualizing individual particles inside the channel. By this visualization capability, operation mechanism of the ElFFF system is better understood. It is shown by simulations that high duty cycle voltage waveforms lead to longer retention times and higher separation resolutions. Furthermore, accurate modeling of the ElFFF channel outlet is made, by exporting the output of Comsol Multiphysics simulation into the particle based simulation code. In this way, it is revealed that selection of the top channel wall as the accumulation wall gives higher quality peaks in the ElFFF systems. Furthermore, it is demonstrated that simulations are capable of estimating the experimental UV fractograms. As a result, this simulation tool can be used to estimate the separation results without conducting the actual experiments, which mostly takes more time and effort.

Channel height is one of the important parameters affecting the separation efficiency of the ElFFF systems. To determine the optimum channel height, a new ElFFF system is fabricated and tested at four different channel heights. It is shown that 125μm channel produces much better results compared to the other heights of 25 μm, 75 μm, and 200μm.

It is shown for the first time that ElFFF can be used for the separation of magnetic nanoparticles as well. In previously reported studies, magnetic field driven techniques were used for the separation of magnetic particles. However, in this study, it is revealed

that an electrical field driven technique can also be used for the separation of magnetic particles.

Although magnetic nanoparticles are vastly used in biomedicine, still versatile methods do not exist to separate particles according to their specific properties such as magnetic susceptibility, magnetic anisotropy, magnetic core size and hydrodynamic size. Current magnetic separation systems use static magnetic fields for the separation, which leads to the entrapment of particles in the channel. To address this problem, a new separation method is designed which uses alternating magnetic fields instead of static magnetic fields. This system is tested through electromagnetic, and particle based simulations and shown that it is capable of separating magnetite particles of different sizes, such as 30nm and 50nm.

Apart from most of the studies conducted in this thesis, magnetic force is used to mix particles and/or fluids, rather than separating them. A novel magnetic mixer is designed, which uses a magnet, serpentine channel and ferrofluid to produce mixing in the microscale. It is shown that mixing efficiencies of a standard serpentine mixer can be enhanced three times by this new micromixer design.

Future Work

By the methods explained in this thesis, the capabilities of both electrical and magnetic field flow fractionation techniques are improved significantly. As a consequence of this improvement, new research topics have emerged, which need to be explored in future.

It has been shown that separation performance of CyElFFF systems extended significantly. This improved CyElFFF method should be tested by many other samples other than the gold and magnetite particles used in this study. Nanostructures such as carbon nanotubes and fullerenes can be good candidates for the CyElFFF separations. In addition, biological samples such as cells, viruses, proteins and peptides can be analyzed with the improved separation capability of the CyElFFF systems.

In this work, it is shown that baseline separations of spherical particles can be achieved. Besides spherical particles, particles with different shapes (i.e., rods, shells, cubes, or cages) should also be analyzed with the CyElFFF method.

Different samples may need carriers with various ionic strengths. In this work, DI water is used as the carrier. The performance of the system should also be tested with carriers having ionic strengths different from the DI water.

In this thesis, the detection of the separated samples is mostly achieved by UV detectors. As a future work, detectors such as DLS, MALS, ICP-MS should be incorporated with the ElFFF systems, which will result in a very powerful nanoparticle characterization strategy.

During the experiments conducted with the CyElFFF system, it has been observed that electrical properties of the system may change time to time. In addition, based on the conductivity of the carrier liquid, the effective field in the ElFFF channel may show big variances. Consequently, there is a high need of methods to control the effective field inside the channel. For this purpose, recording electrodes can be placed inside the channel to monitor the effective field. The readings of the electrodes can be fed back to

the power source to achieve the desired effective field in all of the separation experiments.

The ElFFF channel used in this study is composed of graphite electrodes. It has been witnessed that at high offset voltages or at high duty cycles, some of the graphite particles are released from the electrode surface. This unwanted release of graphite particles may cause noise in the separation fractogram. As a future work, electrode types different than graphite can be tested as candidates of ElFFF channel walls.

The particle based simulation code generated in this work has shown good agreement with the experimental fractograms obtained with 10nm gold nanoparticles. To test the prediction performance of the simulation code, simulations and experiments should be conducted with different types of materials and the results should be compared to determine the estimation capability of the simulation code. In addition, this simulation tool can be further developed by addition of particle-particle or particle-surface interaction equations into the code.

As an evident future work, the Cyclical Magnetic Field Flow Fractionation system designed in this study should be fabricated, and the performance of the system should be compared with the simulations used in the design and development of the system.

The mixing ability of the ferrofluidic magnetic micromixer presented in this work can be further tested with ferrofluids of different magnetite concentrations. Furthermore, this system can also be used for mixing magnetic beads with several biofluids. For instance, micromixer can be used to enhance the binding rates of magnetic beads with cells and/or antibodies. As a future work, this magnetic micromixer should be tested with

magnetic beads and biomolecules, afterwards, the improvement in the binding rates should be investigated.

Nanoparticle manufacturers always look for techniques that can separate small nanoparticles (mostly between 1-50nm). It has been shown that improved CyElFFF method can achieve baseline separations of particles smaller than 50nm. Since in FFF systems, a very small volume of sample is investigated, there is a high demand for a continuous, high throughput separation system which can produce fractions of sub 50nm particles. In future, the methods used in the improvement of the CyElFFF technique can be used to develop high performance SPLITT (split-flow lateral transport thin separation) systems to achieve high throughput separations of small nanoparticles.